

# **DEVELOPMENT AND EFFICIENCY STUDIES OF ORGANIC SOLAR CELLS**

**THESIS**

**Submitted to the Delhi Technological University  
For the award of the degree of**

*Doctor of Philosophy*

*By*

**SARITA S NAIR**



**Department of Applied Chemistry and Polymer Technology  
Delhi Technological University,  
Bawana Road, Delhi-110042  
India  
March 2015**

**Copyright© Delhi Technological University-2015**

**All rights reserved.**

# **DEVELOPMENT AND EFFICIENCY STUDIES OF ORGANIC SOLAR CELLS**

by

**SARITA S NAIR**

**Department of Applied Chemistry and Polymer Technology**

**Submitted**  
**in fulfilment of the requirements of the degree of**  
***Doctor of Philosophy***  
**to the**



**Delhi Technological University**  
**Bawana Road, Delhi-110042**  
**India**  
**March 2015**


## *CERTIFICATE*

This is to certify that the thesis titled “**DEVELOPMENT AND EFFICIENCY STUDIES OF ORGANIC SOLAR CELLS**” submitted to the Department of Applied Chemistry & Polymer Technology, Delhi Technological University, in fulfilment of the requirements for the award of degree of Doctor of Philosophy in Applied Chemistry embodies the original research work carried out by Miss Sarita S Nair under my supervision and this work has not been submitted in part or full for any degree or diploma of this or any other university. It is further certified that the scholar has devoted more than two years, the minimum stipulated period, for the completion of this work.

Miss Sarita S Nair has also satisfactorily completed the courses required for the Ph.D programme in Applied Chemistry.

**Prof. D. Kumar**  
Supervisor,  
HOD, Applied Chemistry & Polymer Technology,  
Delhi Technological University  
Bawana Road, Delhi-110042 India





*You may see me struggle  
but you won't see me fall.  
Regardless if I'm weak or not  
I'm going to stand tall.  
I'm going to wear the biggest smile  
even though I want to cry.  
I'm going to fight to live  
even though I'm destined to die.*

**By Joyce Alcantara...**

**-To my Parents who gave me strong roots and wings to fly high.....**

# ACKNOWLEDGEMENT

There is a long list of people who I owe a lot of thanks and gratitude to for their help and encouragement throughout the production of this thesis. As it would be impossible to list every person who has affected the outcome of this work in big or small ways so, I would attempt to make mention of those people most closely associated with this research. It has been an interesting, life questioning experience for me, and I have learnt a lot about myself and of course, also about the material described within this thesis!

First and foremost, I would like to thank my supervisor, Prof. D. Kumar, for his unending support both in my academic and personal life. In addition to being an excellent advisor, he has gone beyond the call of duty to help me. He has instilled confidence in me and has taught me lessons that extend beyond the lab. His support, guidance, and patience over the years have been unwavering. I appreciate all his contributions of time, ideas, useful insights and putting faith in me at the beginning of the project that helped in shaping my work into a cohesive dissertation. The joy and enthusiasm he has for his research was contagious and motivational for me, even during tough times in the Ph.D. pursuit. I am also thankful for the excellent example he has provided as a successful researcher and professor. I am very grateful for all the help that was provided to me by everyone in the department of chemistry; the professors for their constant encouragement, and the technical staff for their timely support.

I would also like to thank Dr. Amitava Majumdar (Vice president, Moserbaer India Ltd.) for his patient discussions and valuable insight on this work. He often provided insight into aspects of my research that would never have occurred to me. Thanks also go to the numerous people that I have worked with in various aspects of my PhD: Mr. Abhishek Sharma, Mrs. Radha Gahlot, Mr. Sujith Pillai and Mr. G Vignesh of the Moserbaer India Ltd. for their assistance in

*the fabrication and characterisation of OSCs; and Mr. Pinaki Ranjan for making sure all my laboratory needs were taken care of at Moserbaer.*

*I am highly appreciative of the good times shared with my colleagues and co-PhDs: Miss. Reetu Prabhakar, Dr. Sudha, Mr. Sujeet Kumar Mishra, Mr. Saurabh, Mr. A.V. Ullas, Mr. Nahid to name a few. I would like to thank them all for their active cooperation. I would also like to thank my seniors from the lab especially Dr. Irfan Ahmad Mir who has been generous with praise and continually pushing me to believe in my abilities and myself.*

*My time at DTU was made enjoyable in large part due to the many friends and groups that eventually became a part of my life. I am grateful for time spent with my roommates Lucky Krishnia and Alisha Singhal who have been a family away from the family. I would also like to extend my heartfelt thanks to my friends Deepika, Priyanka and Pooja for their awesome company.*

*Most importantly, I thank my family for their unwavering love and support. My parents, S. D. Nair and Indira S Nair, have been wonderful inspirations, teaching me the important lessons in life that have better prepared me for my path ahead. I appreciate all the hard work and sacrifice that they have endured to facilitate my future. I am indebted to my brother Sunil S Nair, who stood by me and backed my aspirations. I wish to thank my entire extended family for their wishes and support. My uncle Mr. Satish Kutty and My aunt Radha Kutty deserve a special mention.*

*Last, but certainly not least, these years have given me faith that there is a divine presence that helps us make sense of this world. I want to thank the almighty god for giving me strength to bypass every hurdle in the way.*

**(SARITA S NAIR)**

# Table of Contents

---

<i>List of Tables</i>	<i>i</i>
<i>List of Figures</i>	<i>ii-iv</i>
<i>List of Abbreviations</i>	<i>v</i>
<i>Preface</i>	<i>vi- viii</i>

## 1. Introduction

1.1	Importance of Solar Energy	2
1.2	Different Generations of Solar Cells	2
1.3	Organic Solar Cells	4
	1.3.1 Organic Semiconductor Materials	5
	1.3.2 Solar Cell Characteristics	11
1.4	Polymer Solar Cells	16
	1.4.1 Principle of Polymer Solar Cells	17
	1.4.2 Device Assembly	19
	1.4.3 Concept of a Heterojunction	22
	1.4.4 Morphology of the Polymer: Fullerene Photoactive Layer	27
	1.4.5 Approaches Used to Modify the Polymer: Fullerene Bulk Heterojunction	30
	1.4.5.1 Donor:Acceptor Mixing Ratio	30
	1.4.5.2 Effect of Solvents	30
	1.4.5.3 Annealing Effect	32
	1.4.5.4 Effect of Cosolvents	36
1.5	Aim	47
1.6	Plan of Work	48
	References	49

## 2. Characterization Techniques

2.1	Overview	56
2.2	Fabrication Techniques	57
	2.2.1 Laser Scribing	57
	2.2.2 Cleaning of Substrates	60
	2.2.3 Wet Processing of Active Layers	62
	2.2.3.1 Spin Coating	63
	2.2.4 Vacuum Systems	65
	2.2.5 Glove Box	70

2.3	Characterization Techniques	71
2.3.1	Contact Angle Measurement	71
2.3.2	Atomic Force Microscopy	73
2.3.3	Ultraviolet and Visible Light (UV-Vis) Spectroscopy	75
2.3.4	Grazing Incidence X-ray Diffraction (GIXRD) Measurement	78
2.3.5	Photoluminescence Spectroscopy	82
2.3.6	Current Density-Voltage Characterization	84
	<i>References</i>	88

### ***3. Effect of Different Cosolvents on the Photovoltaic Performance of an Inverted Organic Solar Cell***

---

3.1	Introduction	90
3.2	Experimental	92
	3.2.1 Materials	92
	3.2.2 Device Fabrication	92
3.3	Characterization	93
3.4	Results and Discussion	93
	3.4.1 Optical Characteristics	93
	3.4.2 Structural Characteristics	99
	3.4.3 Morphological Characteristics	102
	3.4.4 Photovoltaic Characteristics	103
3.5	Conclusion	105
	<i>References</i>	107

### ***4. Optimization of Processing Conditions of Cosolvent Addition in the Active Blend of Inverted Organic Solar Cell***

---

4.1	Introduction	109
4.2	Experimental	113
	4.2.1 Materials	113
	4.2.2 Device Preparation	113
4.3	Characterization	114
4.4	Results and Discussion	115
	4.4.1 Effect of Ageing of Precursor Solution	115
	4.4.2 Morphological Characterization	118
	4.4.3 UV-Visible Absorption Measurements	120

4.4.4	Grazing Incidence X-ray Diffraction (GIXRD) Measurements	121
4.4.5	Photovoltaic Characteristics	125
4.5	Conclusion	128
	<i>References</i>	129

## ***5. Investigation on Processing Pathway for Cosolvent Addition in Active Layer Preparation of Inverted Organic Solar Cell***

---

5.1	Introduction	131
5.2	Experimental	134
	5.2.1 Materials	134
	5.2.2 Device Preparation	135
5.3	Characterization	136
5.4	Results and Discussion	137
	5.4.1 UV-Visible Absorption Measurements	137
	5.4.2 Grazing Incidence X-ray Diffraction (GIXRD) Measurements	139
	5.4.3 Surface Characteristic	144
	5.4.3.1 Atomic Force Microscopy	144
	5.4.3.2 Contact Angle Measurements	146
	5.4.4 Photoluminescence Emission	147
	5.4.5 Photovoltaic Properties	150
5.5	Conclusion	154
	<i>References</i>	156

## ***6. Ternary Solvent Mixture Approach to Control the P3HT:PCBM Blend Morphology in Inverted Organic Solar Cells***

---

6.1	Introduction	158
6.2	Experimental	159
	6.2.1 Materials	159
	6.2.2 Device Fabrication	160
6.3	Characterization	161
6.4	Results and Discussion	162
	6.4.1 UV-Visible Measurements	162
	6.4.2 X-ray Diffraction Measurements	164
	6.4.3 Surface Morphological Study	166

6.4.4	Photoluminescence Emission	168
6.4.5	Photovoltaic Characteristics	170
6.5	Conclusion	172
	<i>References</i>	173

## **7. Conclusion and Future Scope**

7.1	Conclusion	174
7.2	Future Scope	176

### ***Curriculum Vitae***

## LIST OF TABLES

<i>Table No.</i>	<i>Caption</i>
<b>Table 3.1</b>	Hansen solubility parameters (HSP) of different solvents
<b>Table 3.2</b>	Interlayer spacing ( $d_{100}$ ) and P3HT crystallite sizes determined from the (100) diffraction peak in GIXRD pattern
<b>Table 3.3</b>	Photovoltaic device parameters under AM 1.5 G white light illumination for inverted polymer solar cell with active layer casted with different solvent mixtures
<b>Table 4.1</b>	Interlayer distances (d) and the size of P3HT crystallites of (100) diffraction peak at two grazing incidences $0.11^\circ$ and $0.3^\circ$ in the XRD pattern
<b>Table 4.2</b>	Photovoltaic device parameters for ITO/ZnO/P3HT:PCBM/MoO <sub>3</sub> /Ag polymer solar cell
<b>Table 5.1</b>	Summary of interlayer distances (d) and the size of P3HT domains
<b>Table 5.2</b>	Photovoltaic device parameters for ITO/ZnO/P3HT:PCBM/MoO <sub>3</sub> /Ag polymer solar cell
<b>Table 6.1</b>	Interlayer distances (d) and P3HT crystallite sizes using different solvent mixtures
<b>Table 6.2</b>	Photovoltaic parameters of inverted organic solar cell based on P3HT:PCBM active layer



## LIST OF FIGURES

<i>Figure No.</i>	<i>Caption</i>
<b>Figure 1.1</b>	a) Photoelectric effect and b) Photovoltaic effect
<b>Figure 1.2</b>	Organic molecules commonly applied in organic solar cells
<b>Figure 1.3</b>	Several solution processible conjugated polymers and a fullerene derivative used in organic solar cells (Upper row: the <i>p</i> -type hole conducting donor polymers; Lower row: the <i>n</i> -type electron conducting acceptor polymers)
<b>Figure 1.4</b>	Scheme of the double bond formation between two carbon atoms
<b>Figure 1.5</b>	Schematic representation of Frenkel, Wannier and CT excitons
<b>Figure 1.6</b>	Circuit diagram of a solar cell
<b>Figure 1.7</b>	Current-voltage characteristic of an ideal device in the light and under dark test conditions
<b>Figure 1.8</b>	Effect of (a) increasing series and (b) reducing parallel resistances (in each case the outer curve has $R_s = 0$ and $R_{sh} = \infty$ )
<b>Figure 1.9</b>	Charge carrier generation in OPVs
<b>Figure 1.10</b>	OPV architectures: a) a normal cell b) an inverted cell
<b>Figure 1.11</b>	Schematic of energy conversion in organic solar cells (a) bulk heterojunction cell (bottom) and corresponding energy levels (top) (b) bilayer cell (bottom) and corresponding energy levels (top)
<b>Figure 1.12</b>	Coupling regiochemistry of P3HT isomers
<b>Figure 1.13</b>	(a & b ) Structural changes of P3HT:PCBM films upon annealing (c) possible orientations of thiophene crystallites with respect to the substrate: From left to right a-axis, b-axis, c-axis orientations
<b>Figure 1.14</b>	AFM image of PCPDTBT/C <sub>71</sub> -PCBM BHJ film a) without and b) with 1,8-octanedithiol; AFM image of exposed polymer networks after removal of C <sub>71</sub> -PCBM c) without and d) with 1,8-octanedithiol; TEM image of exposed polymer networks e) without and f) with 1,8-octanedithiol
<b>Figure 1.15</b>	Proposed model of film evolution during the spin coating process Black wire: P3HT polymer chain; Large black dots: PCBM; blue dots: DCB molecules; and red dots: 1,8-octanedithiol molecules; a–c) correspond to three stages in the spin coating process when DCB is the sole solvent; d–f) when octanedithiol is added into DCB
<b>Figure 2.1</b>	Laser scribing machine (Electrox 600 Group, IR L6 1064 nm)
<b>Figure 2.2</b>	ITO pattern produced by IR laser processing system
<b>Figure 2.3</b>	UV-ozone cleaner (Jelight Company Inc., 144AX-220)
<b>Figure 2.4</b>	Schematic of the spin coating process

- Figure 2.5** Schematic arrangement of high vacuum system
- Figure 2.6** Schematic of diffusion pump
- Figure 2.7** Diagram of vacuum evaporator
- Figure 2.8** Model of the shadow mask for metal deposition
- Figure 2.9** Pictorial view of glove box from Jacomex
- Figure 2.10** Sessile drop fitted with fitted contour
- Figure 2.11** A block diagram of atomic force microscope
- Figure 2.12** Schematic illustration of the (a) sample assembly and (b) pictorial view of UV-Visible spectrophotometer
- Figure 2.13** Grazing incidence X-ray diffractometer (GIXRD, Rigaku Ultima IV)
- Figure 2.14** Schematic diagram of a grazing incidence X-ray diffraction
- Figure 2.15** Two diffractometers configurations in GIXRD
- Figure 2.16** A pictorial view of solar simulator (Model SS150AAA) alongwith computer controlled Keithley 2420 source measurement unit
- Figure 3.1** Absorption spectra of P3HT:PCBM films casted from different solvent mixtures
- Figure 3.2** Photoluminescence spectra of P3HT:PCBM films casted of different solvent mixtures
- Figure 3.3** GIXRD profile of P3HT:PCBM films casted from blend solution modified with different cosolvents
- Figure 3.4** AFM topographic image scans of P3HT:PCBM films casted of different cosolvents (a) anisole (b) benzaldehyde (c) cyclohexanone and (d) toluene
- Figure 3.5** Current density-voltage ( $J$ - $V$ ) characteristic of devices fabricated with active layer casted from different solvent mixtures
- Figure 4.1** Schematic representation of inverted and normal architecture of polymer based solar cell
- Figure 4.2** Absorption spectra of P3HT:PCBM films casted of precursor solutions aged for different time periods in *o*-DCB-cyclohexanone mixture
- Figure 4.3** GIXRD patterns for P3HT:PCBM films casted of precursor solutions aged for different time periods in *o*-DCB-cyclohexanone mixture

- Figure 4.4** Tapping mode AFM image scans of P3HT:PCBM films (a) without modification (b) with cyclohexanone modification
- Figure 4.5** Absorption spectra of P3HT:PCBM films with and without cosolvent
- Figure 4.6** a) Grazing incidence X-ray diffraction (GIXRD) profiles of P3HT:PCBM composite films at grazing incidence of  $0.11^\circ$  and (b)  $0.3^\circ$
- Figure 4.7** Current density-voltage ( $J$ - $V$ ) characteristic of devices fabricated with and without cosolvent modification
- Figure 5.1** UV-Visible absorption spectra of P3HT:PCBM composite films
- Figure 5.2** (a) Normalised grazing incidence X-ray diffraction (GIXRD) profiles of P3HT:PCBM composite films at grazing incidence of  $0.11^\circ$ , (b)  $0.13^\circ$ , and (c)  $0.3^\circ$
- Figure 5.3** AFM images of P3HT:PCBM composite films modified (a) individually mixed cyclohexanone and (b) blended cyclohexanone approaches and (c) & (d) are their height images, respectively
- Figure 5.4** Water contact angle images of P3HT:PCBM films (a) individually mixed cyclohexanone modified (b) conventional and (c) BLND addition
- Figure 5.5** Photoluminescence spectra of P3HT:PCBM composite films modified by individually mixed and blended cyclohexanone addition
- Figure 5.6** (a) Current density-voltage ( $J$ - $V$ ) characteristic of OSC devices under AM 1.5 G white light illumination (b) OSC devices tested in dark
- Figure 5.7** Pictorial view of inverted organic solar cell primed on  $5\text{ cm} \times 5\text{ cm}$  ITO/glass substrate comprising 4 cells each of  $0.09\text{ cm}^2$  area
- Figure 6.1** UV-Visible absorption spectra of P3HT:PCBM blend films
- Figure 6.2** GIXRD intensities of P3HT:PCBM films
- Figure 6.3** AFM topographic images of P3HT:PCBM films in tapping mode (a) ternary solvent mixture (b) single good solvent and (c) & (d) are 3D images of these films, respectively
- Figure 6.4** PL Emission spectra of P3HT:PCBM films
- Figure 6.5** Current density ( $J$ )-Voltage ( $V$ ) plot of P3HT:PCBM solar cells

## LIST OF ABBREVIATIONS

a.u.	Arbitrary Unit
Å	Angstrom
°C	Degree Celsius
$\theta$	Theta
nm	Nanometer
mL	Mililitre
g	Gram
mg	Milligram
h	Hours
eV	Electron Volt
V	Voltage
Amp	Ampere
I	Electric Current
$J_{sc}$	Short Circuit Current Density
$V_{oc}$	Open Circuit Voltage
$R_s$	Series Resistance
$R_{sh}$	Shunt Resistance
OSCs	Organic Solar cells
PV	Photovoltaic
Si	Silicon
OPV	Organic Photovoltaic
UV-Vis	Ultraviolet-Visible
RR	Regioregular
P3HT	Poly(3-hexylthiophene)
PCBM	[6,6]-phenyl-C <sub>61</sub> -butyric acid methyl ester
PCE	Power Conversion Efficiency
FF	Fill Factor
ITO	Indium Tin Oxide
BHJ	Bulk Heterojunction
AFM	Atomic Force Microscopy
GIXRD	Grazing Incidence X-ray Diffraction
PL	Photoluminescence

## PREFACE

---

**A**lthough significant progress has been made in organic solar cells based on conducting polymer-fullerene mixture as active layer, however the efficiency of current bulk heterojunction (BHJ) solar cells still does not warrant commercialization. A lack of understanding makes targeted improvement troublesome. The main theme of this thesis is to modify the morphology of active layer in inverted BHJ solar cells, relating the device performance to basic physics and material properties such as the preferential crystallization of donor polymer.

The first part of the dissertation focuses on introduction to the various aspects related to the **topic, literature perusal, basic principles of photovoltaic power conversion with semiconductors (both inorganic and organic)**. The working principle of organic bulk heterojunction solar cells and a critical review of the state of knowledge are also given in this chapter. In chapter 2, the details including **principles of the various analytical tools employed for the preparation and characterization of the organic solar cells** are summarized.

Chapter 3 describes the **effect of different cosolvents on the photovoltaic performance of an inverted organic solar cell**. The effect of varying polymer crystallinity, morphology, and optical property which is produced by addition of different cosolvents in to the poly(3-hexylthiophene) (P3HT):[6,6]-phenyl C<sub>61</sub>-butyric acid methyl ester (PCBM) solution, on the performance of an inverted polymeric solar device is considered in detail. Photovoltaic devices primed with cyclohexanone cosolvent showed the best performance with power conversion efficiency (PCE)

reaching a value of  $3.01\pm 0.05\%$ . This increase in efficiency of the inverted device is related to a combined effect of ordered P3HT crystallite growth, and precise size and phase separation of domains with the addition of cyclohexanone cosolvent.

Chapter 4 focuses on **optimization of processing conditions of cosolvent addition in the active blend of inverted organic solar cell**. In this work, the concept of solvent induced crystallization of donor poly(3-hexylthiophene) (P3HT) polymer was extended to the photoactive blend of inverted organic solar cells. An increase in power conversion efficiency of an OSC device from  $2.74\pm 0.05\%$  to  $3.01\pm 0.05\%$  was realized by addition of an optimized concentration of cyclohexanone cosolvent and ageing period of 2 h. This improvement of 10% in the efficiency of inverted device with cyclohexanone addition is related to the increase in the current density and fill factor of the device. Increase in the crystallinity of P3HT for efficient photoabsorption and commensurate vertical concentration gradient observed in P3HT fractions of the blend for efficient hole transport is possibly responsible for the betterment of the photovoltaic parameters in modified device.

In Chapter 5, **investigation on processing pathway for cosolvent addition in active layer preparation of inverted organic solar cell is reported**. The cosolvent addition pathway was changed from conventional blended mixture addition (one step addition) to two steps individually mixed addition. Such changes in the processing pathway led to an improvement of PCE from  $3.01\pm 0.05$  to  $3.39\pm 0.05\%$ . Our study indicated that improvement in the device efficacy is related to improved characteristic surface morphology as seen in AFM images, proven by improved crystallization of donor polymer supported by the UV-Visible spectroscopy, GIXRD and PL data. A fine coverage of homogeneously distributed well grown P3HT crystallites was evident

in the individually mixed cosolvent casted film promoting the enhanced photo absorption and charge transport properties which benefited the device in terms of increased short circuit current density ( $J_{sc}$ ) and power conversion efficiency. GIXRD results also support more favourable upright concentration gradient in the individually mixed film which eases the charge transport.

A new approach of morphology modification, i.e., **Ternary solvent mixture approach to control the P3HT:PCBM blend morphology in inverted organic solar cells** is been discussed in chapter 6. In this work, bulk heterojunction blend of poly(3-hexylthiophene):[6, 6]-phenyl C<sub>61</sub>-butyric acid methyl ester (P3HT:PCBM) which is prepared using a ternary solvent mixture is utilized as the active layer of an inverted organic solar cell. Ternary solvent mixture consisting of a good solvent *ortho*-dichlorobenzene and marginal solvents cyclohexanone and toluene offers limited solubility to the P3HT component of blended mixture. However, a decrease in power conversion efficiency from 2.74±0.05% in the unmodified OSC device to 2.64±0.07% in ternary solvent mixture modified device is observed. This decrease in the efficiency of mixed cosolvent modified active layer is due to less efficient photoabsorption by randomly crystallized P3HT domains.



# *Chapter 1*

## *Introduction*



- 1.1** *Importance of solar energy*
  - 1.2** *Different generations of solar cells*
  - 1.3** *Organic solar cells*
    - 1.3.1 Organic semiconductor materials*
    - 1.3.2 Solar cell characteristics*
  - 1.4** *Polymer solar cells*
    - 1.4.1 Principle of polymer solar cells*
    - 1.4.2 Device assembly*
    - 1.4.3 Concept of a heterojunction*
    - 1.4.4 Morphology of the polymer: fullerene photoactive layer*
    - 1.4.5 Approaches used to modify the polymer: fullerene bulk heterojunction*
      - 1.4.5.1 Donor:acceptor mixing ratio*
      - 1.4.5.2 Effect of solvents*
      - 1.4.5.3 Annealing effect*
      - 1.4.5.4 Effect of cosolvents*
  - 1.5** *Aim*
  - 1.6** *Plan of work*
- References**
- 

The research work presented in this thesis mainly focuses on the development and efficiency studies of organic solar cells (OSCs). The characteristic photoactive layer morphology, i.e., morphology evolution in donor/acceptor thin layers prepared through solvent based techniques can be controlled and manipulated with the aim to obtain highly efficient bulk heterojunction OSCs. The following sections of this chapter address an introduction to the basic principles of photovoltaic power conversion with semiconductors (both inorganic and organic) and the key factors determining the efficiency of photovoltaic devices, emphasizing particularly on the role of morphological organization of the photoactive layers. The conducting polymers properties with particular focus on optoelectronic

---

characteristics which are especially important for solar cells have also been discussed in detail.

### **1.1. Importance of Solar Energy**

With the recent exponential growth in technology and consequently, increase in the energy demands, utilization of fossil fuels (including coal, oil and gas) which is the main energy source at present is all together increasing. This advancement in our standard of living and gross domestic product is advantageous and destructive at the same time, as we have to compensate its cost in terms of major environmental and climatic deterioration. It is probable that these resources are set to decline in the years to come and that the carbon dioxide (CO<sub>2</sub>) emissions allied with the burning of these fuels adversely affect the climate [1]. The indication for global warming, primarily due to the combustion of fossil fuels, is overpowering. Hence, renewable energy sources will now have to take up the major responsibility of dealing these challenges. The sun being the main energy source on earth, and the straight conversion of its energy into heat or electricity seems to be an attractive way to satisfy the ever increasing energy needs of the modern world with modest influence on the natural balance [2]. The direct conversion of sunlight into electricity, i.e., photovoltaic power conversion, is possible at comparably low investment. Solar power will certainly be the dominant future global energy resource as only sun can provide more than enough energy to meet the global demand [3].

### **1.2. Different Generations of Solar Cells**

The photovoltaic (PV) effect was revealed by Alexandre-Edmond Becquerel in 1839 as he observed production of electric current in two plates of platinum or gold dipped in the solution of an acid or alkali and exposed to solar light [4]. In 1905,

Einstein described the phenomenon of photoelectric effect, which laid the basis of theoretical understanding of the concept of photovoltaic effect. When photons in the ultraviolet (UV) range light up the metal surface, free electrons break out of the surface due to transfer of the excitation energy from the incident light and thus these electrons are ejected into the atmosphere. When photons are absorbed in a material, they force the ground state electrons to the excited state, and the excited electrons then try to quickly relax back to the ground state. However, in photovoltaic devices, the excited electrons and the holes produced in the ground state have to be collected separately in order to generate power (Fig. 1.1).

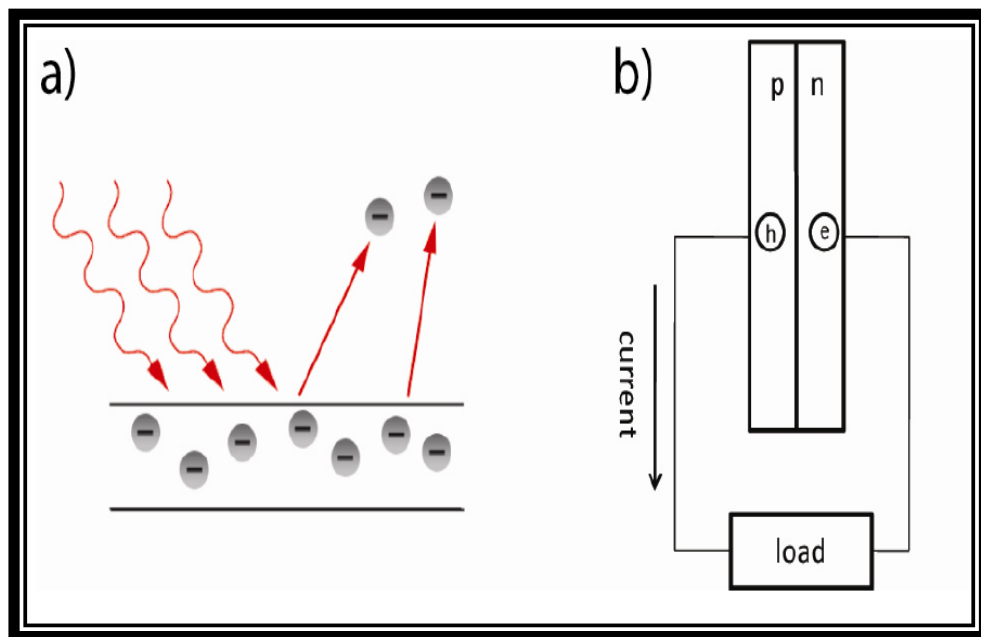


**Figure 1.1: a) Photoelectric effect and b) Photovoltaic effect**

The first PV device based on crystalline silicon (Si) (*p-n* junction) was developed at Bell Laboratories in 1954 by Chapin *et al.* with a conversion efficiency of 6% [5]. Recently, in crystalline Si solar cells, efficiency has reached to a record value of 24.7% under standard test conditions of global air mass 1.5 (AM 1.5) spectrum, light intensity of  $1000 \text{ W/m}^2$  [6]. Apart from monocrystalline silicon, their

cheaper alternatives, i.e., solar cells based on polycrystalline Si (Si wafers from multiple Si crystals) and amorphous Si (Si deposited as a thin layer on metals, glass etc.) were also developed in this generation of solar cells.

Non-silicon materials such as cadmium telluride (CdTe) and copper indium gallium diselenide (CIGS) based thin film solar cells dominated the second generation of solar cells [7]. This generation attempted at reducing the material consumption, to reduce the production cost of the solar cell compared to the *p-n* junction based first generation solar cells. However, their efficiency is still less than that of the crystalline Si based solar cells. Third generation of solar cells so called organic solar cells are based on organic materials such as small molecules or polymers for energy harvesting. With the advantage of flexibility of organic molecules and its easy fabrication process, organic solar cells are potentially cost effective for photovoltaic applications.

### 1.3. Organic Solar Cells

Organic solar cell is a type of solar cell that uses organic semiconductors such as conducting polymers or small molecules for solar light absorption and its subsequent conversion to electricity by the photovoltaic effect. Organic semiconductors are a less expensive substitute to inorganic semiconductors like Si. They also have particularly high optical absorption coefficients which present them with the possibility of very thin film production (of the order of 100-200 nm) for the development of thin film solar cells [8]. Additional features of organic PVs include their probability of flexible device fabrication using low temperature techniques and large scale production practices such as printing techniques in a roll-to-roll process. Besides the cost benefits stated above for organic materials, the band gaps and other

optical properties of these materials can be easily tuned through suitable modifications of their molecular structure.

### 1.3.1 Organic Semiconductor Materials

Materials having a delocalized  $\pi$ -electron system are capable of sunlight absorption, creating photoinduced charge carriers, and responsible for the transport of these generated charge carriers. Plants utilize the natural phenomena of photosynthesis for obtaining chemical energy from sunlight via absorption of light by the chlorophyll molecule. Chlorophyll pigments are functional as photoactive layer in a single layer solar cell [9]. In addition to the absorption of sunlight and successive generation of photoinduced charge carriers, these materials should also have the ability to transport these charge carriers as well. Both of these properties are commonly found in materials that have an extended delocalized  $\pi$ -electron system.

#### ❖ Organic Small Molecules

Small molecules are predominantly insoluble in common organic solvents and therefore these materials in general deposited using vacuum sublimation technique. Such a method usually results in amorphous or polycrystalline films with different extent of disorders. Vacuum based thermal deposition technique involves evaporation of depositing molecules from a hot source and the molecules are then carried onto the substrate via vacuum created in the depositing chamber. Condensation of these molecules then produces thin film on the substrate surface.

Such a device concept is based on the thermal evaporation of at least two conducting materials, i.e.,  $n$  and  $p$  type materials. Phthalocyanine belongs to a group of  $p$ -type, hole-conducting material functioning as electron donor. The perylene and its derivatives show  $n$ -type conduction, and act as electron acceptor material. Both of

these molecules are more frequently included in the evaporated solar cells [10]. Excitons are generated due to the absorption of light in the respective organic materials. These excitons have to reach to an interface between *n*- and *p*- type conducting layer (*p-n* junction) where splitting into free electrons and holes takes place owing to the prevailing energetic conditions. Finally, the individual charge carriers are transported towards their respective electrodes for collection.

As the band-gap in most of the organic materials is of the order of 2 eV so, a decrease in the number of intrinsic charge carriers generated as a result of thermal excitation is obvious as compared to smaller band gap inorganic semiconductors. Again, the disorder and limited interaction among the electronic wave functions (van der Waals interactions), also leads to relatively lesser charge carrier mobilities in organic materials and hence these small molecules are considered mostly as insulators. However, practices of molecular or electrochemical doping can increase the charge carrier concentration in these materials. Donor type materials show a doping effect when exposed to oxygen or other strong oxidizing agents such as iodine.

And, for *n*-type doping, perylene was doped on exposure to hydrogen [11]. Due to these doping effects, once the insulating materials possess free charge carriers and their bilayer devices can be effective like classical *p-n* junctions. However, as doping with gases becomes uncontrollable so, a more controlled approach of doping is achieved by the co-evaporation of matrix material and dopant. The buckminster fullerene C<sub>60</sub> (and derivatives) molecule can also function as a strong electron acceptor. When blended with hole conducting materials, it does not only enhance the charge transport in the dark, but also brings about a large increase in photoconductivity under illumination owing to a photoinduced charge transfer, and

hence this phenomenon can be identified as “photodoping” [12]. The chemical structures of some semiconductor molecular materials are depicted in Fig. 1.2 [ZnPc (zinc-phthalocyanine), MePtcdi (N, N'-dimethyl-perylene-3,4,9,10-tetracarboximide), and C<sub>60</sub> fullerene].

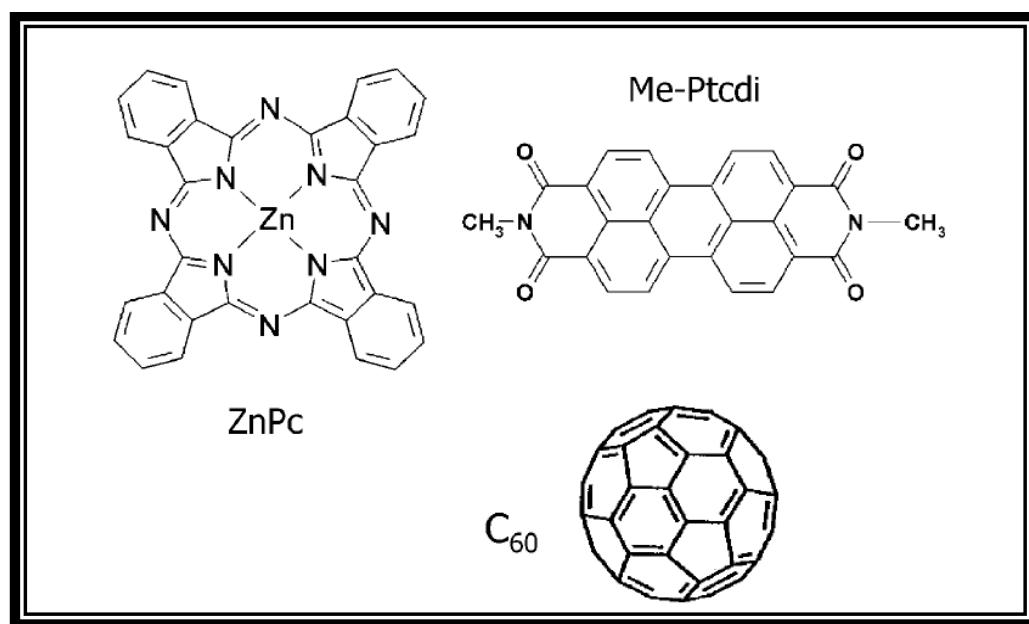


**Figure 1.2: Organic molecules commonly applied in organic solar cells**

❖ Conducting Polymers

Conducting polymers correspond to a novel class of materials with superior properties and potential applications. This special class of polymers referred as “**Synthetic Metals**” possess the unique electronic, electrical, magnetic and optical properties of a metal along with known advantages of conventional polymers like light weight, easy solution processibility and low cost etc.

Conducting polymers were first discovered in 1976. In 1970s, the first conducting polymer polyacetylene, was prepared as a result of a serendipitous experiment conducted in Shirakawa’s group [13]. The succeeding innovation by Alan J. Heeger and Alan G. MacDiarmid that led to an increase of 12 orders of magnitude

in the conductivity value by oxidative doping of the polymer echoed in and around the polymer and electrochemistry communities followed by a more intensive search for other conducting polymers by several other researchers [14]. The importance of conducting polymers is demonstrated by the honour of *Nobel Prize in Chemistry* (2000) to MacDiarmid, Shirakawa and Heeger for the discovery of conducting polymers.

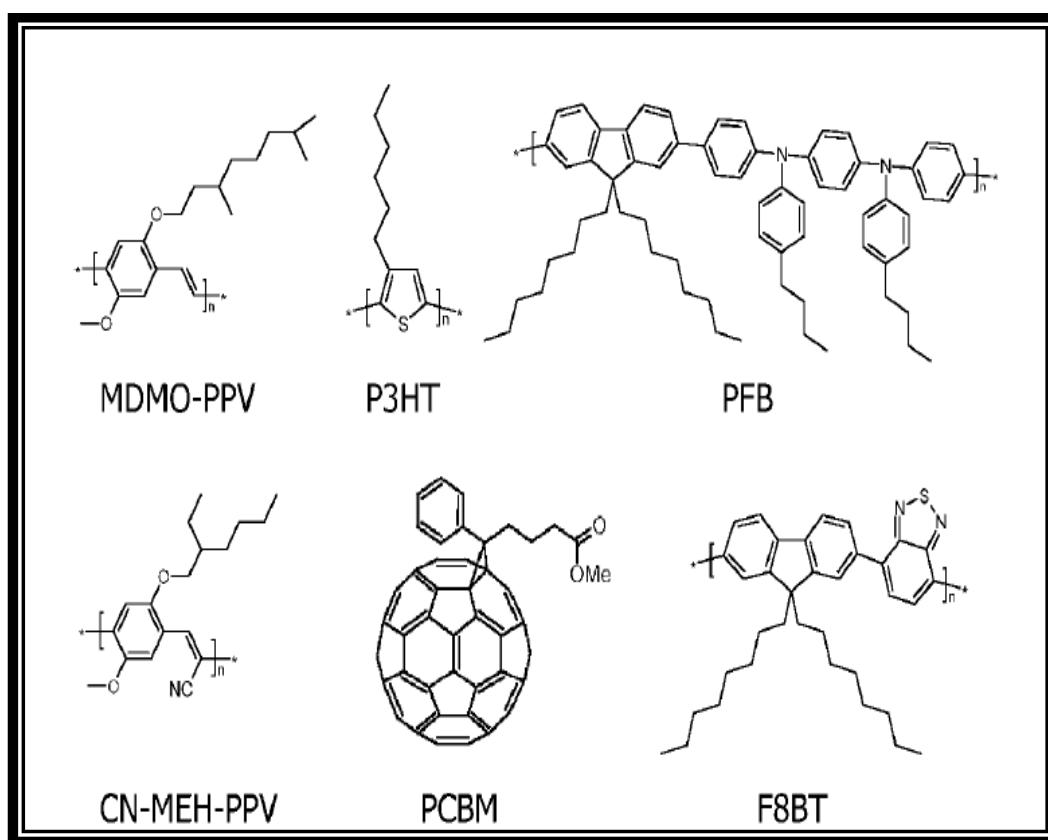


**Figure 1.3: Several solution processible conjugated polymers and a fullerene derivative used in organic solar cells (Upper row: the *p*-type hole conducting donor polymers; Lower row: the *n*-type electron conducting acceptor polymers)**

Three main hole-conducting donor type polymers MDMO-PPV (poly[2-methoxy-5-(3,7-dimethyloctyloxy)-1,4-phenylenevinylene], P3HT (poly(3-hexylthiophene-2,5-diyl) and PFB (poly(9,9'-dioctylfluorene-co-bis-*N,N'*-(4-butylphenyl)-bis-*N,N'*-phenyl-1,4-phenylenediamine) together with representative



electron-conducting acceptor polymers like CNMEH-PPV (poly-[2-methoxy-5-(2'-ethylhexyloxy)-1,4-(1-cyanovinylene)-phenylene] and F8TB (poly(9,9'-dioctylfluorene-co-benzothiadiazole) and a soluble derivative of C<sub>60</sub>, namely PCBM ([6,6] phenyl C<sub>61</sub> butyric acid methyl ester) are shown in Fig. 1.3. All of these materials are solution processible due to the presence of side-chain, and the polymers show photo- and electroluminescence [15].

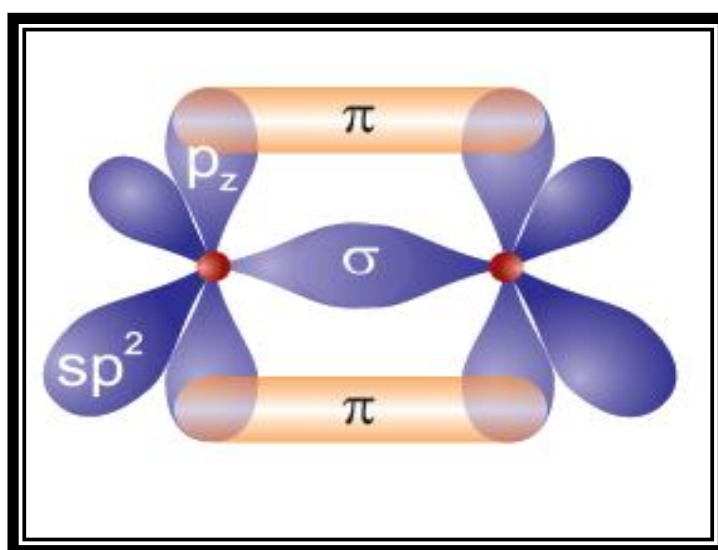


**Figure 1.4: Scheme of the double bond formation between two carbon atoms**

A feature common with both the small molecules and polymers used in organic photovoltaics is their enormous conjugated systems. A conjugated system is the one where carbon atoms can bond covalently with alternating single and double bonds; or can be identified as chemical reactions of hydrocarbons. The electron orbitals of the carbon atoms in the conjugated double bonds are hybridized which means that one atom has three planar sp<sup>2</sup> orbitals and one vertical p<sub>z</sub> orbital. Due to the overlap of the sp<sup>2</sup> orbitals strongly localized σ bonds are formed which are responsible for the binding of the atoms. These hydrocarbon electrons residual p<sub>z</sub> orbitals overlap and form a delocalized π bonding orbital and an antibonding

$\pi^*$  orbital. It is strongly delocalized, so that energy bands are formed over long polymer chains [16].

The delocalized  $\pi$  orbital is the highest occupied molecular orbital (HOMO), and  $\pi^*$  orbital is the lowest unoccupied molecular orbital (LUMO). The difference between HOMO and LUMO orbital confers the band gap of organic electronic materials. A schematic illustration of the double bond between two carbon atoms is displayed in Fig. 1.4. Normally, the band gap of organic semiconductors falls in the range of 1–4 eV. The optical and electrical properties of organic semiconductor material are related to this band gap [17].

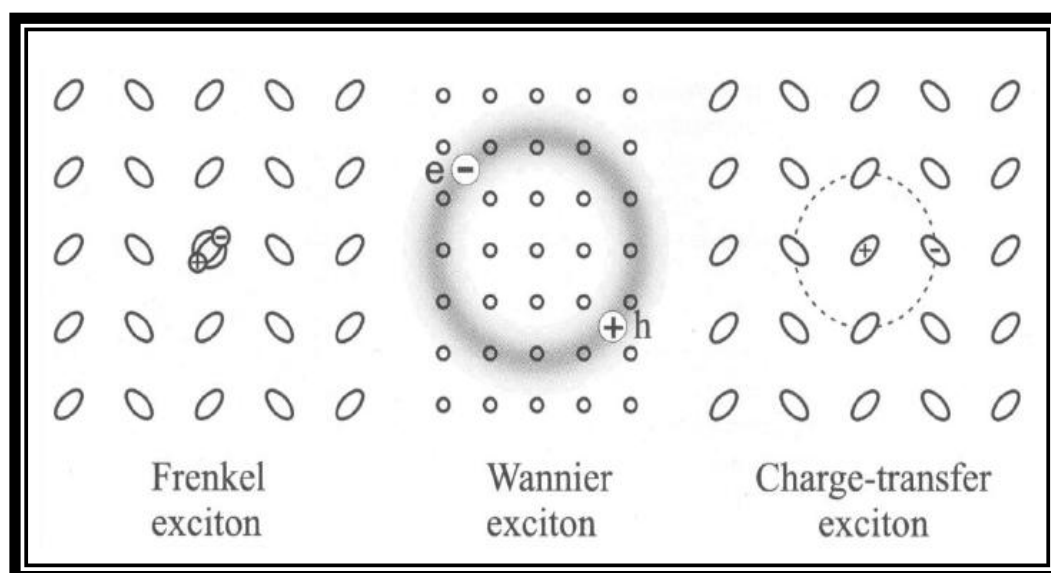


**Figure 1.5: Schematic representation of Frenkel, Wannier and CT excitons. (Adapted from Reference [18])**

When these materials absorb a flux of photon, an excited state is produced which is restricted to a molecule or a region on the polymer backbone. The excited state thus created can be characterized as an electron-hole pair coupled together by electrostatic interactions, i.e., excitons. Different types of excitons can be produced as a result of photon absorption. The subtypes of excitons produced in the field of

inorganic semiconductors include the Mott-Wannier and Frenkel excitons shown in Fig. 1.5 [18]. Frenkel excitons are localized on one molecule while Wannier and charge transfer (CT) excitons are extended over several molecules.

The Mott-Wannier excitons confirm very weak coulombic attraction caused by screening effects, concurrent with extensive diffusion in all directions, resulting in a significantly improved charge separation in silicon based photovoltaics. Frenkel excitons demonstrate stronger coulombic attraction, decreasing the length of diffusion [19]. While classifying conductive polymers, the excitations generate the so called “charge transfer (CT)” excitons, which exhibit very strong coulombic attraction restricting the exciton diffusion within the polymer backbone. The possibility of such diffusion is more if the polymer chain is straight and devoid of any defects or twists. This depiction will support the straightforward electronic contact among the neighbouring chains [20]. This perspective is important while considering the conduction process in conjugated polymer and will be discussed in greater detail in the subsequent sections. Though both organic small molecule based and conjugated polymers based organic solar photovoltaic have their own advantages and disadvantages but, conjugated polymer based photovoltaic device or polymer solar cell will be considered further throughout in this thesis.

### **1.3.2 Solar cell Characteristics**

A solar cell can be expressed in terms of several parameters described in detail in the following sections. An ideal solar cell works like a diode in parallel with a current source (Fig. 1.6). Evaluating solar cell's current as a function of varying voltage and formulating  $I$ - $V$  curves (see Fig. 1.7) can present the majority of the particulars, fundamental to characterize a solar cell. These characteristics are

generally measured in the dark as well as under monochromatic and solar spectrum illuminations. In the dark, the cell presents a standard diode-like characteristic with its  $I$ - $V$  curve passing through the origin (Fig. 1.7). Under illumination, the current measured on a solar cell is called the photocurrent. The measurement of photocurrent depends on various parameters other than just the quality of the device. For instance, dissimilar photocurrents are obtained depending on the wavelength or intensity of the incident light or the area of the device under illumination. Hence, the photovoltaic response should be accounted in terms of quantities that are universally acknowledged. The absorption of light generates a current, and generated power is given by equation 1.1,

$$P = I \times V \quad (1.1)$$

Where,  $I$  is the current and  $V$  is voltage.

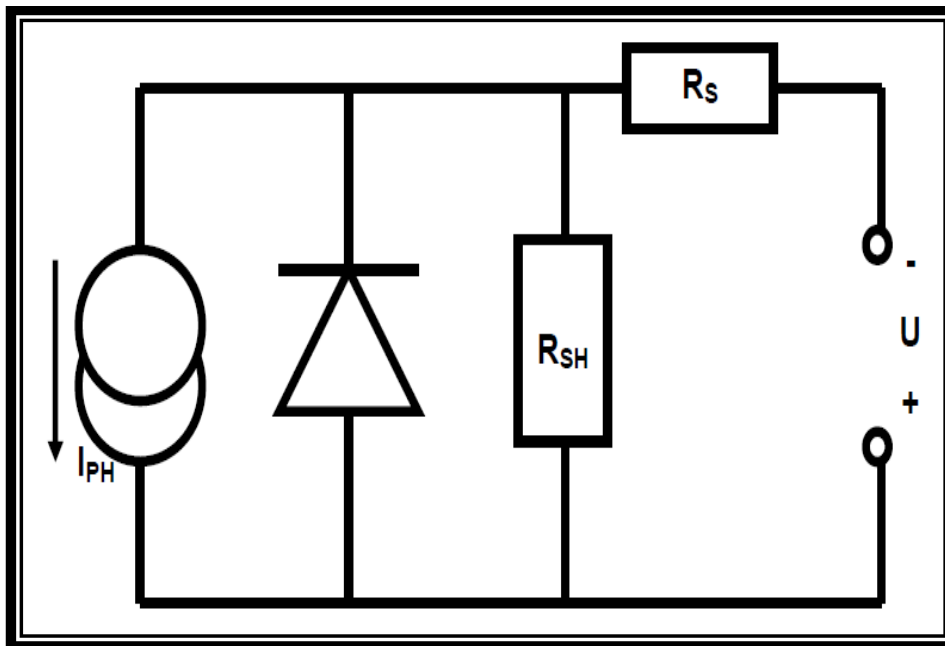


**Figure 1.6: Circuit diagram of a solar cell**

So, the conversion of solar light to electricity is expressed in terms of photovoltaic power conversion efficiency (PCE) which is the overall efficiency of a

solar cell under illumination, given by equation 1.2. This term counts the effectiveness of electrical power extraction for a particular optical power supplied to the device. It is a unitless quantity and also, wavelength dependent and in general, is quoted in percentages.

$$\text{Efficiency} = P_{out}/P_{in} \quad (1.2)$$

Where  $P_{in}$  is the incident light power which is generally standardized to AM 1.5 spectrum.  $P_{out}$  is the electric power generated by the cell at the maximum power point (mpp or  $P_{max}$ ), and the solar cell's maximum power can be derived from the  $I$ - $V$  curve. Maximum power point (mpp or  $P_{max}$ ) is identified as the point where the product of the current and the voltage attains a maximum value. The device has to be operated at this point.  $V_{max}$  and  $I_{max}$  are the characteristic voltage and current at this point.

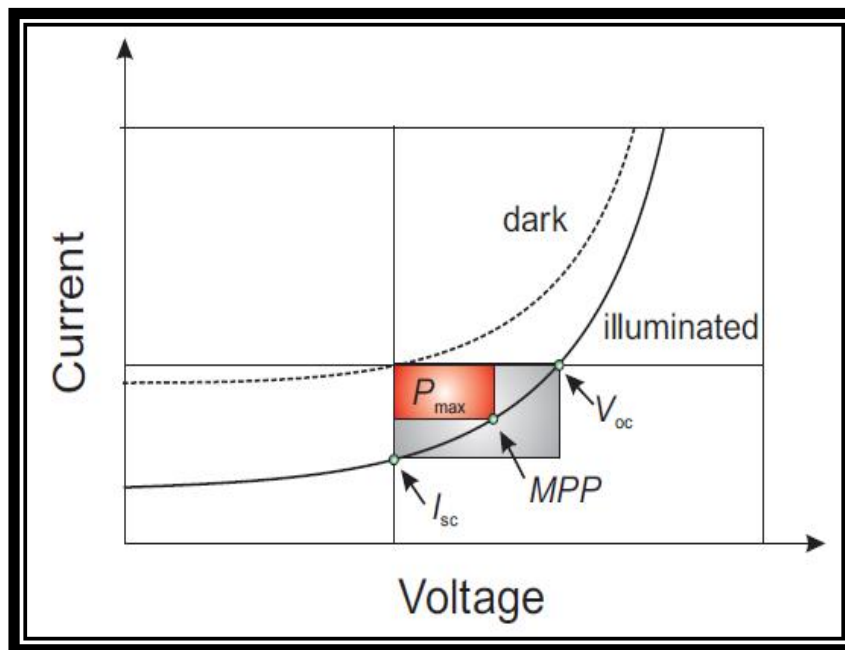


**Figure 1.7: Current-voltage characteristic of an ideal device in the light and under dark test conditions**

It should be noted that the fill factor (FF) specifies the effectiveness of the device fabrication practice given that it compares the power obtained experimentally

to the power that could have been possibly attained had the same device performed ideally. Fill factor is a ratio of maximum measured power to maximum theoretical power. The FF describes the diode behaviour of the solar cell and can be given by equation 1.3.

$$FF = \frac{I_{max} V_{max}}{I_{sc} V_{oc}} \quad (1.3)$$

The photovoltage build up when the terminals of the cell are separated is called the open circuit voltage ( $V_{oc}$ ).  $V_{oc}$  is the maximum possible voltage developed by a solar cell and the current is zero at this particular voltage. For heterojunctions, the difference in energy between HOMO of the donor and LUMO of the acceptor is supposed to be the limiting value for the  $V_{oc}$  [21]. The photocurrent drawn when the terminals are coupled is the short-circuit current ( $I_{sc}$ ).  $I_{sc}$  is the current flowing through the circuit when no external field is applied, and charges are just drifting owing to the internal build up of field. Internal build up of field is considered to be dependent on the work functions of the two electrode materials. The cell in short circuit conditions aligns the fermi-level of the two electrodes. So,  $I_{sc}$  carries information about transport characteristic of the materials and charge separation and the operating regime of a solar cell is the range of bias from 0 to  $V_{oc}$  wherein the cell delivers power.

Under solar light illumination, a non-zero photocurrent identified for zero applied voltage is the short circuit current ( $I_{sc}$ ). Photogenerated electrons descend the band, from p-type to n-type semiconductor side, in the reverse direction of the forward bias. This negative photocurrent appears in the fourth quadrant of the  $I$ - $V$  curve (Fig. 1.7) [22]. As the forward bias is raised, this reverse photocurrent reduces, i.e., the applied voltage reduces the energy offset, and hence, the degree of band

bending. This decreases the driving potential for the photogenerated charges, reducing the reverse photocurrent. This external bias at which the photocurrent is zero is the open circuit voltage ( $V_{oc}$ ) and when the biasing crosses this value, majority carriers dominates and an exponential increase of current in the forward bias direction is observed.

These four quantities  $I_{sc}$ ,  $V_{oc}$ ,  $FF$  and efficiency ( $\eta$ ) are the key performance characteristic parameters of a solar cell. All these photovoltaic parameters should be defined for particular illumination conditions. The standard test conditions (STC) include a constant temperature of the PV cells ( $25^{\circ}\text{C}$ ), the intensity of radiation ( $1000\text{ W/m}^2$ ), and the spectral distribution of the light (air mass 1.5 or AM 1.5 global, which is the spectrum of sunlight that has been filtered by passing through 1.5 thickness of the earth atmosphere).

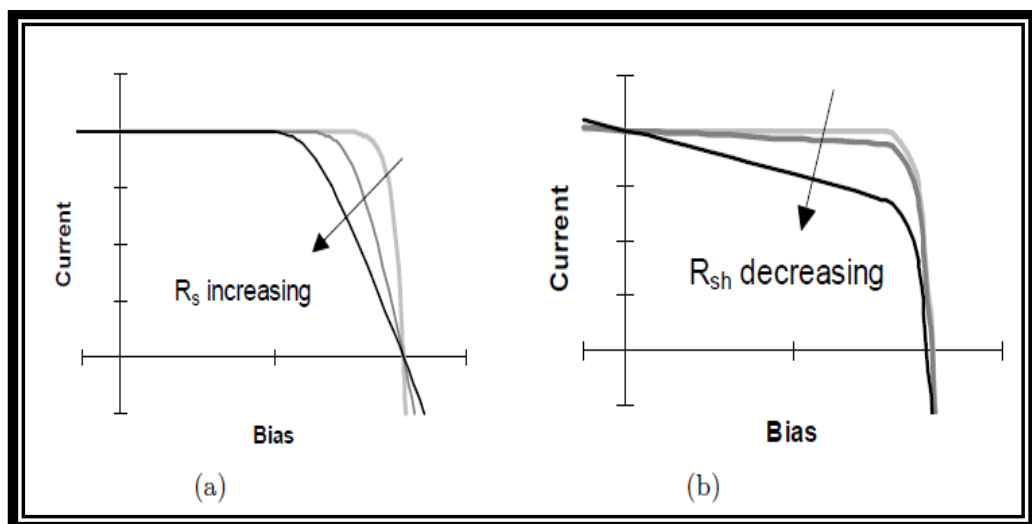


**Figure 1.8: Effect of (a) increasing series and (b) reducing parallel resistances (in each case the outer curve has  $R_s = 0$  and  $R_{sh} = \infty$ )**

The correlation between the photocurrent density and the incident spectrum is defined as the cell's external quantum efficiency (EQE). The EQE is defined as the ratio of the photocurrent and incident photon flux at a particular wavelength. EQE of

a cell is a function of the absorption coefficient of the solar cell material, the efficiency of charge separation process and the charge collection in the device. The EQE is independent of the incident spectrum, and consequently a key factor describing solar cell performance under different conditions.

Through the photo conversion process, the efficiency of solar cells decreases by the dissipation of power across internal resistances. These parasitic resistances can be represented as parallel shunt resistance ( $R_{sh}$ ) and series resistance ( $R_s$ ). For an ideal cell,  $R_{sh}$  would be infinite so that no alternative pathway for current flow (zero leakage current) exist, while  $R_s$ , the series resistance resulting from the resistance of the cell material to current flow, predominantly through the front surface to the contacts, and from resistive contacts would be zero, ensuing in no voltage drop ahead of the load [23]. Decreasing  $R_{sh}$  and increasing  $R_s$  will decrease the fill factor ( $FF$ ) and  $P_{max}$  as shown in Fig. 1.8. If  $R_{sh}$  is decreased too much,  $V_{oc}$  will go down, while increasing  $R_s$  can lead to drop in  $I_{sc}$

#### 1.4. Polymer Solar Cells

Polymeric material based photovoltaic devices for sustainable energy have been the focus of most researchers worldwide in recent years and considerable advancement in numerous aspects has been reported in this field. Organic materials, particularly conjugated polymers, have emerged as a means to drastically reduce the costs of photovoltaic devices, as they can be dissolved in solutions to be deposited onto substrates by simple and scalable techniques such as spin coating, drop-casting, spraying, and ink-jet printing. The prospect of roll-to-roll mass production onto flexible substrates is feasible in such a material system. In the relatively short period,



the conjugated polymers have been explored in solar cell applications, and much has been accomplished already.

#### 1.4.1 Principle of Polymer Solar Cell

Organic materials are responsible for generating free charge carriers by utilizing sun's radiation in solar cells. The operational mechanism of organic photovoltaics (OPVs) is illustrated in Fig. 1.9 and can be summarized as follows

##### ❖ Photoexcitation, Excitons Generation and Separation, and Charge Transfer

Firstly, on absorption of a photon with energy larger than the band gap of the organic material, an electron in the highest occupied molecular orbital (HOMO) of an organic material is excited into the lowest unoccupied molecular orbital (LUMO), creating an exciton (bound electron hole pair). A key point of differentiation between solar cells based on inorganic or organic semiconductors is that in inorganic semiconductors based solar cells, photons are directly transformed into free charge carriers. These charge carriers can then be collected at their respective electrodes. This cannot be the case with organic photovoltaic devices, where photoexcitation of a molecule generates electron-hole pairs, called 'excitons' [24]. These excitons are the coulombically bound charge carriers, with binding energies in the range of 0.05 to >1 eV [25]. They can diffuse over a length of approximately 5-15 nm and afterwards decompose either radiatively or nonradiatively.

Secondly, for photovoltaic applications, excitons have first to be dissociated into free charges. In photovoltaic cells, excitons are split apart into free electrons and holes by effective fields. The effective fields are laid down by means of building up a heterojunction between two dissimilar materials. One technique adopted to bring about such a separation is to use an acceptor molecule. Effective fields split up the

excitons and the electron falls from the conduction band of the absorber to the conduction band of the acceptor molecule. An essential requirement for such a process is that the conduction band edge of acceptor material be lower than that of the absorber material [26]. So, if the exciton produced can diffuse to a different material whose LUMO is lying lower than the absorber, the electron is transferred to the accepting unit. The exciton diffuses to the interface between two materials (electron donor and electron acceptor) and is dissociated or separated at the interface [27]. And, finally the newly split free charge carriers diffuse through an external load to the electrodes at opposite ends of the cell, and collected into the external circuit, in a way converting the sun's magnificent light energy into electricity.

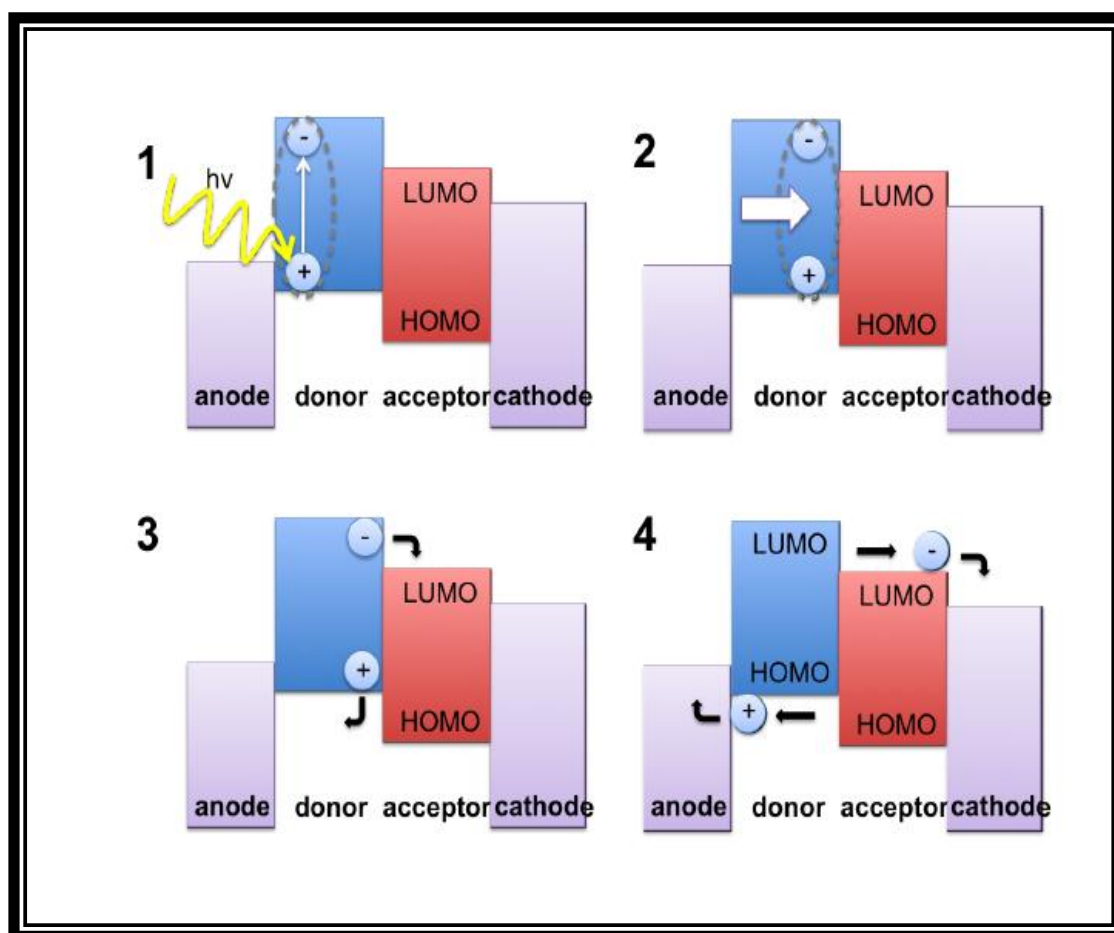


Figure 1.9: Charge carrier generation in OPVs (Adapted from Reference [24])

### 1.4.2 Device Assembly

All organic photovoltaic cells include a planar layered structure, consisting of the organic active layer(s) is (are) packed in between two electrodes with different work functions. One of the electrodes must be transparent enough to permit the incoming photons to strike the photoactive layer. A transparent conductive oxide (TCO) is employed; and usually indium tin oxide (ITO) is the TCO as it provides good results. The other electrode is very often aluminium (Al) electrode, although calcium (Ca) has a better work function, but the Al is much more stable in air than Ca. From the above consideration, it is assumed that different device architectures can be developed. Two universally accepted architectures employed for solar device fabrication are discussed in the following sections (Fig. 1.10).

#### ❖ Normal Cell

For thin film device fabrication, an individual has to begin with a carrier on top of which the different layers can be applied. In photovoltaics, this carrier can be called a superstrate, if the thin film solar cell is light up through the carrier and is called a substrate, if the lighting is from the opposite end. For OSCs, most frequently the first layer is the hole contact formed by the transparent conductive oxide, i.e., indium tin oxide (ITO) and a thin layer of poly(styrenesulfonate) doped poly(3,4-ethylenedioxythiophene) (PEDOT:PSS), since it has shown to enhance the contact property. Thereafter, the absorber blend (photoactive blend) consisting of donor and acceptor molecule is applied and ultimately the electron contact is made, usually by evaporating a low work function metal like Al or Ca [28]. This ITO superstrate arrangement is termed as standard setup as it is the most commonly used device structure.

However, metals with low work function are sensitive to oxygen and moisture of air and so, these are not very stable as the top electrode [29]. To facilitate the protection of top electrode and to improve the performance of OSCs and organic light-emitting diodes (OLEDs), bi-layered metal combination such as Ca/Al or magnesium (Mg)/Al has been employed for use as composite cathode. Furthermore, the application of PEDOT:PSS at ITO contact has also shown to degrade the performance of OSCs owing to the strong acidic nature of PSS on the ITO surface [30].

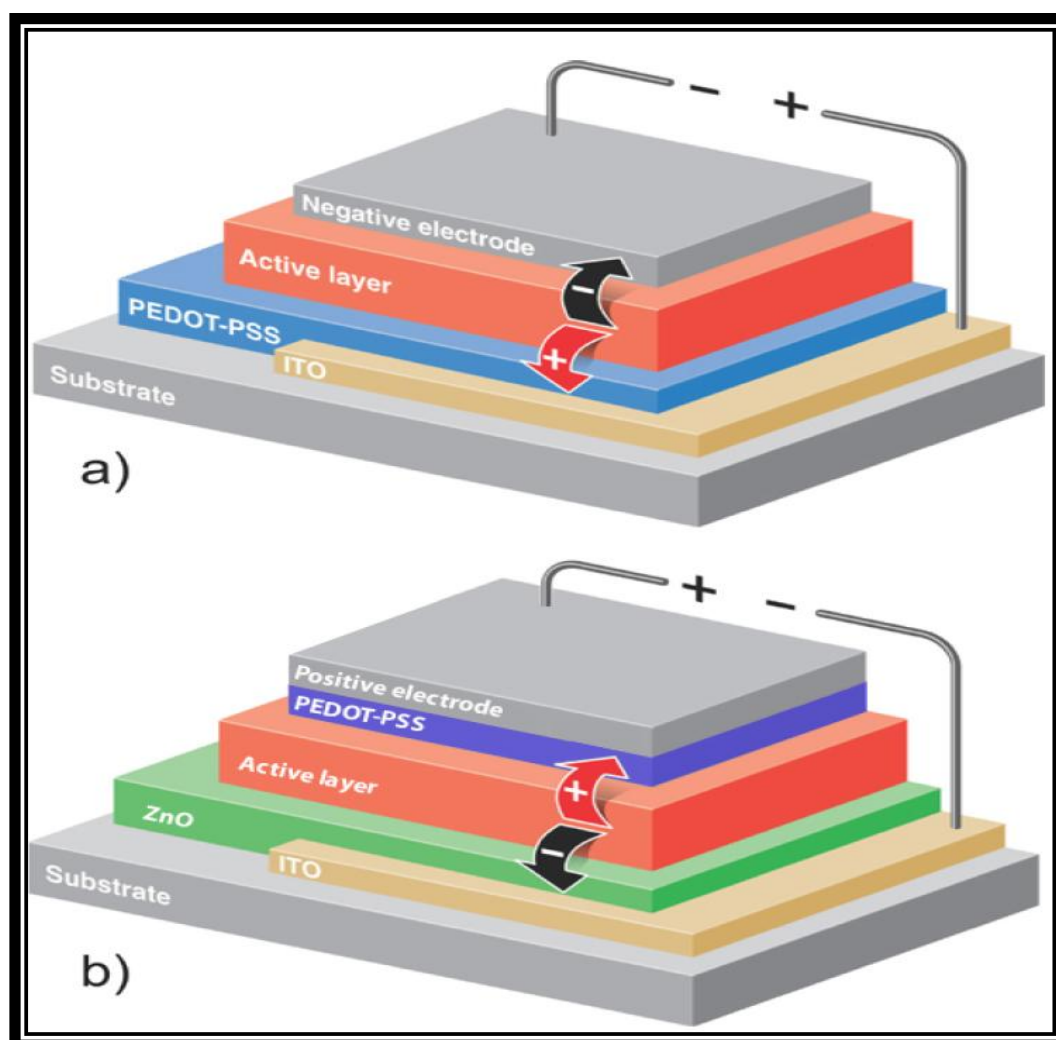


**Figure 1.10: OPV architectures: a) a normal cell b) an inverted cell (Adapted from Reference [28])**

**❖ Inverted Cell**

As ITO's work function ( $\approx 4.5$  to  $4.7$  eV) falls in between the HOMO and LUMO values of some common organic photovoltaic materials, it is competent enough of collecting either holes or electrons. The polarization of the ITO electrode is a function of the contact properties. For extraction of hole, ITO can be deposited with a high-work-function material, such as PEDOT:PSS, which has been known to form an ohmic contact with p-type polymer donor material [31]. Alternatively, ITO was shown to function as cathode for electron collection by lowering its work function via spin coating an ultrathin caesium carbonate ( $\text{Cs}_2\text{CO}_3$ ) layer [32]. Such a regulation of the ITO-electrode work function ascertains the basis of a different configuration for polymer solar cells, i.e., an inverted structure. In such an inverted configuration, ITO serves as the cathode for electron collection, while the anode is built up on the opposite side with a high-work-function electrode.

Few publications in literature explored superstrate configuration of organic solar cells with the ITO electrode transformed into an electron contact by depositing another layer of metal oxide (such as zinc oxide, ZnO or titanium oxide,  $\text{TiO}_2$ ), such that the layer sequence is inverted, i.e., starting with the electron contact and eventually ending with the hole contact [33]. The inverted cell structure investigated in this thesis is a substrate configuration, as the electron contact is formed by transparent metal onto which the absorber blend is applied. The hole contact can be formed either by using PEDOT:PSS or hole transporting metal oxide layer such as molybdenum oxide ( $\text{MoO}_3$ ) as in the standard setup, however with a variation that this layer is applied on top of the absorber blend as the last layer in the sequence of layers and used to transport the current laterally.

Inverted device configuration of OSCs with ITO as the transparent cathode altered with a low work function metal and a high work function metal like (silver, Ag or gold, Au) functioning as anode at air interface could avoid the device degradation brought out by moisture of the atmosphere and by contamination of metal cathodes. The inverted configuration of OSCs also avoids the use of PEDOT:PSS at ITO interface, which is identified as detrimental for device performance due to the strong acidic nature of PSS [34].

The inverted configuration of OSC is also known to seize the advantage of the P3HT:PCBM vertical phase separation which is otherwise detrimental to the normal configuration [35]. The vertical phase separation is characteristic of the surface energy difference between the blended components and their interactions with the substrates. This heterogeneous distribution of the donor and acceptor components in the photoactive layer affects the performance of normal configuration OSCs considerably, gathering inverted configuration OSCs as a potential alternative.

### **1.4.3 Concept of a Heterojunction**

As discussed above, the idea following the conception of a heterojunction is to use two materials with different electron affinities and ionisation potentials. This concept of heterojunction favours the exciton dissociation with electron being accepted by the organic material having larger electron affinity and the hole by the one with the lower ionisation potential. Such a heterojunction is required as excitons in most organic semiconductors do not dissociate readily.

The idea of heterojunction was brought in by Tang in 1986 which established as an immense measure towards advancement of organic photovoltaics. Tang raised a bi-layer device engaging copper phthalocyanine (CuPc) as the donor and a perylene

tetracarboxylic derivative (PC) as the acceptor. The device showed a power conversion efficiency of about 1%, which was an order of magnitude in excess of single-material organic photovoltaics build up then. Moreover, his experimentation highlighted the key role of donor-acceptor interface in determining the photovoltaic properties of the cell than that of the electrode contacts. Tang described the behaviour of his bilayer cell by proposing the mechanism of excitons diffusion to the interface region between the CuPc and PC, where they dissociated to free holes and electrons, and thereafter CuPc carried the holes to the ITO electrode while PC carried electrons to the Ag electrode [10].

Again, one of the most used acceptors in heterojunction cells is the fullerene molecule  $C_{60}$  [36]. Besides having a high electron affinity,  $C_{60}$  is comparatively transparent and also has reasonable share of electron conductance ( $10^{-4} \text{ Scm}^{-1}$ ). This makes fullerenes a good component in PV cells. A conducting polymer/ $C_{60}$  cell was first accounted in 1993 by Sariciftci *et al.* [37]. In one of the experiments, ITO-coated glass spin coated with poly[2-methoxy-5-(2'-ethyl-hexyloxy)-1,4-phenylenevinylene] (MEH-PPV) layer was vacuum deposited with fullerene layer and Au was used as the electron-collecting electrode. The cell had a comparatively high FF of 0.48 and a PCE of 0.04% under monochromatic illumination. An increase of more than 20 folds in the photocurrent value, with the introduction of  $C_{60}$  molecule emphasized the role of fullerene molecule in charge separation.

It is evident that the active layer donor-acceptor composite manages all aspects of the photo conversion mechanism as discussed above, apart from charge collection, which is based on the electronic interaction of the active layer composite and the respective electrodes. Therefore, it was accepted that to improve the

performances in heterojunction devices, the quality of the interface can be a significant feature which can be effectively structured. To meet out the basic requirements of competent photon to charge conversion, different device architectures have been build up. Fig. 1.11 shows device designs of solar cells consisting of two components, an electron donor (D) and an electron acceptor material (A). Charge separation takes place at the interface of these two materials. Ideally, the D- material should make contact with the higher work function electrode (typically ITO) and the A-material should be in touch with the lower work function electrode (typically Al). In the subsequent section, we present a concise outline of the two different architectures of the photoactive layer known today, together with their strengths and weak points:

#### ❖ **Bilayer Architecture**

The concept of bilayer architecture supported realization of higher efficiencies in OSCs. The practice of bilayer material design in the photoactive layer of OSC significantly reduced the charge carrier recombination as such a design reduces the distance that the excitons have to travel before it undergoes dissociation. This proposal of new planar heterojunction seemed to be an important step forward in OSC engineering. It consists of the combination of an electron donor (*D*) and an electron acceptor (*A*) material layer over one another. These two layers are packed between two metal electrodes, e.g., Au/*D-A*/Al. The two electrodes are selected such that their work function strictly matches the highest occupied molecular orbital (HOMO) of donor and lowest unoccupied molecular orbital (LUMO) of acceptor [38].

This bilayer structural design can offer several benefits over the single material device. One such advantage is the efficient exciton dissociation by means of



the well developed donor/acceptor material structure. Photon absorption is also expected to improve, if the two organic materials overlap complementary domains of the solar spectrum. The possibility of recombination among the carriers also decreases by the use of bi-layers as it promotes separate charge transport layers. However, the problem of smaller active domain, i.e., the donor/acceptor interface still continues and small number of excitons near the depletion layer can only reach the interface for getting dissociated [39].

As the semiconductors used in organic photovoltaics are intrinsic, organic solar cells are majority carrier devices; where the density of photogenerated charge carriers is large in contrast to the small number of intrinsic carriers, so that the band structure of the device is known to change significantly with the illumination intensity. In a bilayer organic solar cell, photogenerated charges are mostly generated in the vicinity of the planar interface between the donor and acceptor materials, and these charge carriers are driven to their respective extracting electrode with the effect of electric field applied [40]. However, the carriers also undergo a drift in the opposite direction due to their electrostatic attraction to the partner charges. With the increase in the illumination intensity, the generation rate of carrier increases and the electric field is also reduced at the interface due to the accumulation of space charges. At suitably high intensity of illumination, field produced from the space charge build up of large number of generated charges wholly cancels the effect of applied field. Photocurrent possibly will increase with illumination because of diffusion, but the electric field at the heterojunction may point in the wrong direction given sufficiently large generation rates. So, an improvement to this basic device structure is presented below.

### ❖ Bulk Heterojunction Architecture

Bulk heterojunction (BHJ) is the most universal and well-organized arrangement of the donor-acceptor material in the active layer of an OSC. So far, highest PCEs reported for single or tandem OSC devices have been using this active layer architecture [41]. This is often identified as a blended structure, without including a planar interface between the donor (hole conducting) and the acceptor (electron conducting) materials.

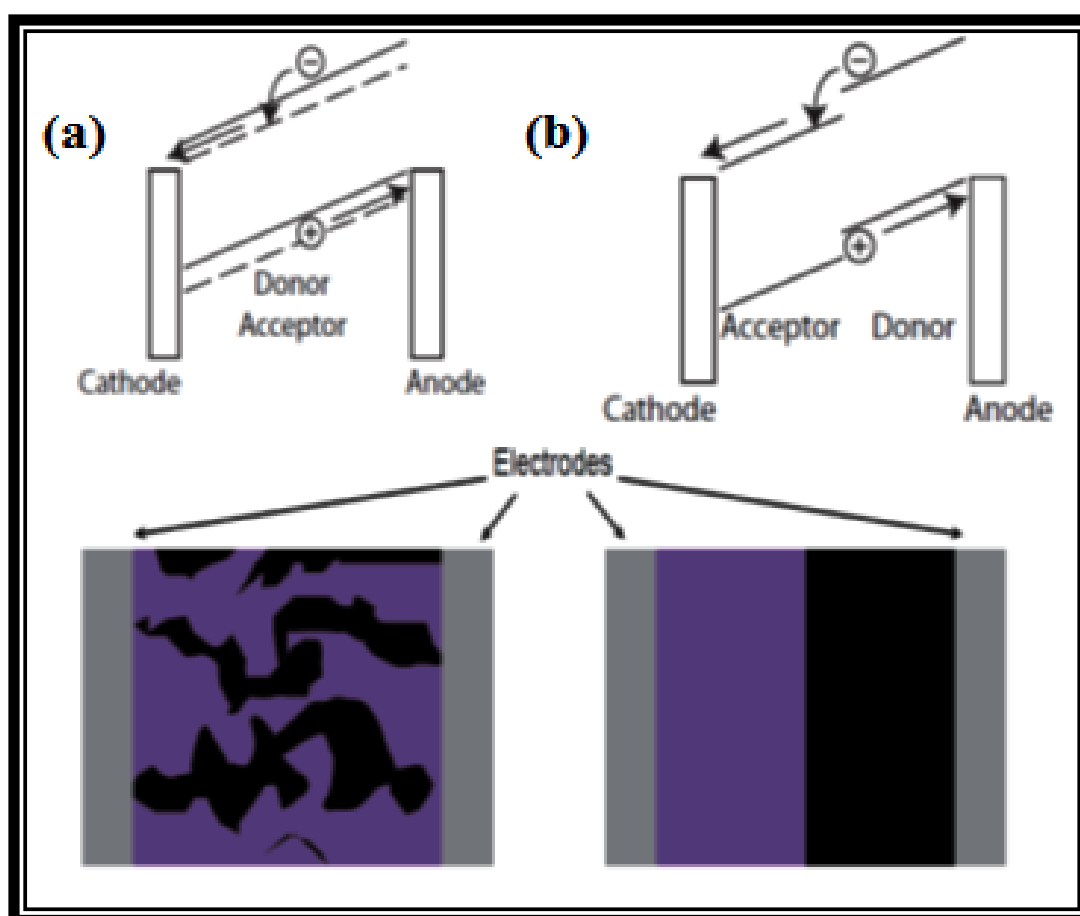


**Figure 1.11:** Schematic of energy conversion in organic solar cells (a) bulk heterojunction cell (bottom) and corresponding energy levels (top) (b) bilayer cell (bottom) and corresponding energy levels (top)

It is well known that to facilitate absorption of most of light, the thickness of the photoactive layer should be at least of the order of 100 nm however, limitation

related with the small diffusion lengths of exciton in organic semiconductors (typical in the range of 10 nm), limits the efficiency of cells. The bulk heterojunction architecture resolves the trouble of small diffusion length of excitons by blending the donor and acceptor into a single interpenetrating network of phases. BHJ introduces the idea of large interface area in to the active layer of solar cells so that the majority of the excitons reach the D/A interface [42]. Upon illumination on the active layer, excitons produced diffuse to an interface, splitting into electrons and holes. Electrons are still confined to the acceptor and holes to the donor; but as the respective donor-acceptor phases are dispersed all through the film so, there is no particular charge carrier build up in a particular place. As a whole, the field due to the photogenerated charges cancels, and the net field is that enforced by the electrodes.

Such dispersed heterojunction however suffers from the problem of solid state miscibility of the materials as organic conjugated systems are not very miscible and again, the stability of such systems are still a subject of debate. Therefore, the blend should be prepared out of equilibrium. Spin coating and co-evaporation methods can prove to be good option for fabrication of intermixed and fully dispersed heterojunction designs.

#### **1.4.4 Morphology of the Polymer: Fullerene Photoactive Layer**

Although there may be a preminent electronic relationship among the donor and acceptor, still the physical contacts of the donor and acceptor components manifested in by the composite film's morphology decide the performance of solar cells. The model of bulk heterojunction solar cell is definite in provisions of bicontinuous donor and acceptor domains with a large interfacial area for exciton dissociation and mean domain size of the components proportionate with the exciton

diffusion length (5–10 nm). In other words, the active layer in BHJ OSC is an intricate diffusive interface between the two materials in the form of a ‘bicontinuous interpenetrating network’ to get the most out of the existing interface area (Fig. 1.11). BHJ structure consists of nanoscale domains of donor and acceptor network with phase separation in a length scale of 10–20 nm, so that each interface is within a distance lesser than the exciton diffusion length from the photon absorbing sites [43, 44]. The motivating part is that one can successfully maximize the exciton dissociation by utilising a BHJ active layer structure.

Maximum ordering within each phase and demixing of the two components in the blend leading to phase-segregation of a suitable length scale allows effective charge transport in continuous pathways to the electrodes and minimal recombination of free charges. The composite formed out of blended solution should self-assemble into the most favourable morphology with minimal application of external treatments, and should have lasting stability. Such requirements necessitate a proper control over the mixing and demixing of the two components.

The morphology of the active layer is interplay of several intrinsic and extrinsic parameters. The intrinsic properties are inherent to the polymer and the fullerene molecule, together with the essential contact parameters between the two components. These parameters take an account of the crystalline properties of the two materials and their relative miscibility. The extrinsic factors take an account of all the exterior stipulations associated with device fabrication, such as the choice of solvent, concentration of the blend components, deposition technique employed (spin coating, ink-jet printing, roller casting, etc.), evaporation rate of solvent, as well as thermal and/or solvent annealing techniques [45]. Thus, there are number of factors that affect

the morphology of the active layer and these factors are also particular of the polymer–fullerene duo. These factors are considered with the perspective of the two particular components MDMO-PPV:PCBM and P3HT:PCBM which are the two classical examples of BHJ solar cells.

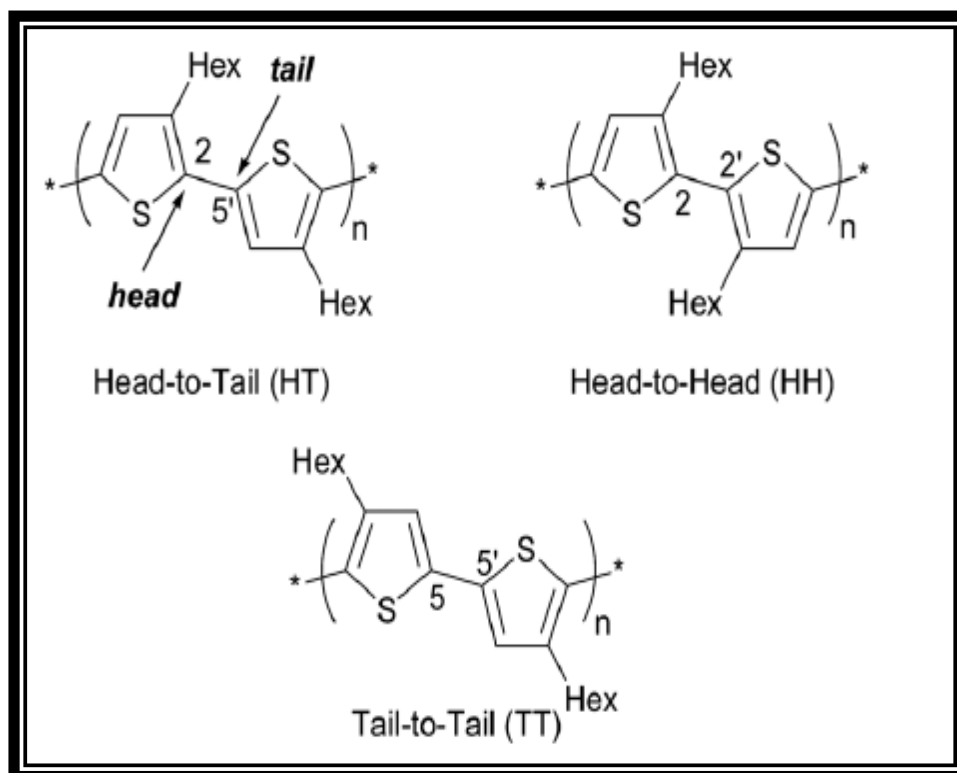


**Figure 1.12: Coupling regiochemistry of P3HT isomers**

P3HT being the most studied donor semiconductor for organic photovoltaic, is used as the donor polymer throughout our study. P3HT consists of an aromatic ring with one sulphur atom (thiophene) alongwith an attached hexyl chain of carbon atoms. This extra alkyl chain accounts for the solubility of P3HT in non-polar solvents. Charge transport is facilitated along the four  $\pi$ -electrons of the two double bonds and the two electrons of the sulphur  $p_z$  orbital. The coupling of the 3-hexylthiophene monomers can occur in different ways and depending on the production process, three different coupling along the polymer chain, i.e., 2, 5'-(head-

to-tail, HT), 2, 2'-(head-to-head, HH) and 5, 5'-(tail-to-tail, TT) may take place (Fig. 1.12). The most favourable configuration is the head-to-tail coupling [46]. The percentage of these couplings is called regioregularity (RR). The greater the RR, the more is the optical absorption and the field-effect mobility. RR-HT-P3HT architecture is prestructured for three dimensional (3-D) self-assembly, resulting in efficient two-dimensional (2-D) hole transport with high mobilities and current density. Self organization in P3HT results from interchain stacking of 2-D conjugated sheets in to lamellar structure.

#### **1.4.5 Approaches Used to Modify the Polymer:Fullerene Bulk Heterojunction**

##### **1.4.5.1 Donor:Acceptor Mixing Ratio**

A straightforward means to persuade the nano-morphology is by altering the mixing ratio of donor (D) and acceptor (A) material. The ideal D:A mixing ratio varies from 1:0.6 to 1:4 in case of general polymer: fullerene system. Though, the fullerene absorbs only a small part of the incident light and a small amount of about 5% is enough for complete exciton diffusion however, a blend ratio of 1:4 may be needed to form percolating pathways to the collecting electrodes [47].

##### **1.4.5.2 Effect of Solvents**

Solution processing technique offers several benefits over other film fabrication technologies, which are generally costly and time consuming procedures involving complex instruments as well. Consequently, solution processing technique emerged as the most preferred methodology for producing organic optoelectronic devices. Solution processing also provides the choice of organizing the phase separation and molecular self-organization through the solvent evaporation step and/or the film treatment step. The solvent stimulates the environment for the growth

of ordered film, and accordingly affects the final morphology of the blend film. Selection of solvents is a critical parameter influencing the morphology in polymer blend films, and is well-documented in the literature [48, 49]. Spin coating from single-solvent solution results in thin films, which possess optoelectronic properties determined by the solution parameters and the spin coating process, for example concentration, blending ratio, spin speed and time, etc. Meanwhile, solvent properties, such as boiling point, vapour pressure, solubility, and polarity, also have considerable impact on the final film morphology.

In 2001, Shaheen et al. demonstrated the effect of solvent and morphology on device performance for the poly[2-(3,7-dimethyloctyloxy)-5-methyloxy]-paraphenylene-vinylene (MDMO-PPV):[6,6]-phenyl-C<sub>61</sub>-butyric acid methyl ester (PCBM) blend system [50]. By replacing toluene with chlorobenzene (CB), the PCE of the device dramatically improved to 2.5%. A more intimate mixing and stronger interchain interaction accounted for this improvement. The solubility of the polymer blend is much better in chlorobenzene (CB) than in toluene; thus, a much more uniform mixing of the donor and acceptor is expected. This improved intermixing is evidenced by the roughness of the polymer-blend film, where the chlorobenzene-based sample has a much smoother film surface. Ma et al. also observed that P3HT:PCBM polymer films were smoother and more uniform when chloroform was replaced with CB [51]. The high efficiency is the result of improved morphology, crystallinity, and cathode contact due to the better choice of solvent as well as post-annealing treatment. Because of the better solubility of fullerenes in CB, its use instead of toluene resulted in a finer phase separation, while thermal annealing in both cases led to coarsening of the phases [52].

### 1.4.5.3 Annealing Effect

Optoelectronic properties of the polymer-blend films can be modified by adopting a variety of post-treatment methods. Post-treatment practicing of thermal or solvent annealing is usually employed to improve molecular order and charge carrier mobility. Annealing processes can broadly be arranged into two separate classes: thermal annealing [51, 53, 54] and solvent annealing [48, 55–57]. These two processes aim at improving the nanoscale lateral phase separation of the crystalline P3HT aggregates and PCBM domains.

#### ❖ Thermal Annealing

Thermal annealing can be done both on the final device (post-annealing) as well as on the polymer blend film (pre-annealing), and the change in the annealing sequence can have different affects on the final performance of the device. The time and temperature of annealing process are the two factors that are critical to the performance of the fabricated device. Moreover, the processing solvent used and evaporated metal electrodes could also influence the ultimate device performance.

During the realization study of electroluminescence property in polythiophene derivatives by Berggren *et al.*, thermal annealing has shown to improve the crystallinity of the polymer domains [58]. Again, the efficiency of P3HT:fulleropyrrolidine solar cells was reported to increase from 0.1 to 0.6% by thermal annealing at a temperature as low as 55<sup>0</sup>C [59]. Dittmer *et al.* observed an improvement by a factor of 1.6 with an EQE of 11% in a system comprising of P3HT and a small-molecule dye N,N'-bis(1-ethylpropyl)-3,4:9,10-perylene bis(tetracarboxyl diimide) (EP-PTC) with thermal annealing at 80<sup>0</sup> C for 1 h when compared to an unannealed device [60]. Further, Padinger's work in 2003 marked the



importance of both post-annealing treatment and annealing with an external bias in the field of polymer solar cells (PSCs) with efficiency as high as 3.5% achieved by annealing the RR-P3HT:PCBM blend [61]. With more comprehensive studies on the subject, PCE values of up to 5% were accounted *via* thermal annealing [51].

Other variations of the thermal annealing also materialized, one such approach is of the microwave annealing reported by Chen *et al.* [62]. The performance of the polythiophene/fullerene blend solar cell is decided by the corresponding optical and electrical properties of the blended components and also by the self-organization property of polymer which in turn is dependent on the processing condition.

In P3HT:PCBM composites, PCBM is thought to suppress the formation of P3HT crystallites. PCBM is likely to be dispersed on molecular basis between P3HT chains, restricting aggregation or crystallization of P3HT chains. With the annealing at higher temperature, a reorganization of PCBM takes place and isolated molecules of PCBM then diffuse to form larger aggregates (Fig. 1.13). In the PCBM free regions, P3HT aggregates rearrange to P3HT crystallites. It has been shown that the crystallinity of P3HT is increased by thermal annealing, forming crystallites with the conjugated chain parallel to the substrate (*a*-axis orientation, i.e., main chain parallel and side chains perpendicular to the substrate) (Fig. 1.13c) [63]. An improvement in crystallinity enhances the near-infrared (NIR)-region absorption, hole mobility, and decreases the rate of recombination among the separated charges due to the presence of improved percolation channels in the blended mixture resulting in better device performances. Kim *et al.* have also accounted the role of P3HTs regioregularity in its self-organization, and also reported increase in crystallinity with thermal annealing [64].

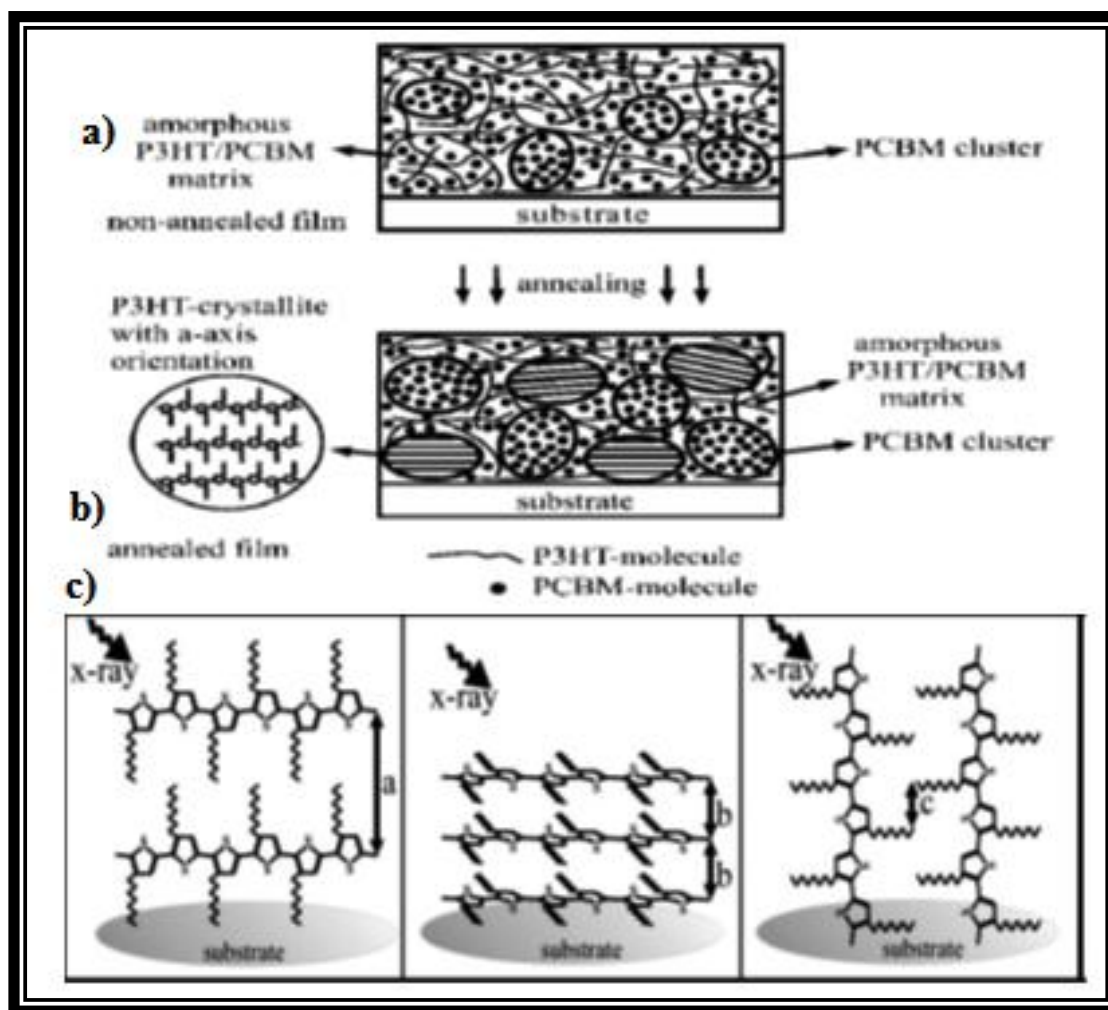


**Figure 1.13: (a & b ) Structural changes of P3HT/PCBM films upon annealing (c) Possible orientations of thiophene crystallites with respect to the substrate: From left to right a-axis, b-axis, c-axis orientations (Adapted from Reference [63])**

#### ❖ Solvent Vapour Annealing

As supposed, solvent annealing process is not an annealing technique in the right sense, as it does not involve heating of the sample. For a solvent annealing treatment, the time period of spin coating is held short, with the intention that the resulting layer remains wet. Then, the sample is gradually dried up under a Petri dish in solvent vapour atmosphere. In this saturated solvent atmosphere, the polymers are able to reorganise and crystallise [65]. So, the solvent-annealing approach is the type

of post treatment that takes care of the polymer nanomorphology via manipulating the speed of solvent removal. In the literature, Zhao *et al.* explained a solvent-vapour-annealing approach based on a similar principle [66].

On the way to achieving a highly efficient PV device, the sufficient absorption of solar radiation in conjunction with a more competent transport of separated charges to the respective collecting electrodes are prerequisite. In the RR-P3HT based systems, the improvement in the crystallinity of the polymer is known to augment both the photo absorption in the long wavelength range and the hole mobility. However, thermal annealing is recognized to bring about only a partial recovery of the RR-P3HTs crystallinity and hence a small improvement in the photo absorption by the blend film, suggesting that this approach alone cannot serve the purpose and is not sufficient to wholly exploit the potential of the RR-P3HT:PCBM system. Further supporting fact is that a thicker photoactive film cannot be employed for increasing the absorption and hence, the efficiency of the device as there existed the bottleneck of carrier transport.

These constraints can be overcome by adopting another technique called “solvent annealing” (or slow growth). This approach preserves the ordering within the polymer domains during the film formation stage as opposed to improving the crystallinity (ordering) of RR-P3HT aggregates which was lost during the fast solvent removal (fast spin coating) process. By reducing the rate of solvent removal during the growth of active polymer layer from solution to the solid state, the self-organization in polymer chains can be controlled. The inherent polymer self organization potential (i.e., well oriented structure) can provide higher absorption,

higher carrier mobility, and balanced carrier transport increasing the efficiency of as formed devices.

#### 1.4.5.4 Effect of Cosolvents

Post-treatment methods cannot be easily put into the practice in real processes. As, flexible substrates with a low glass transition temperature are incompatible with the use of thermal annealing, and solvent vapour annealing approach is unsuitable for existing roll-to-roll processes owing to the risks associated with the solvent vapour. As a result, there was a need to develop new processing activities that produce highly ordered structures and morphologies without post treatment for the advancement of high performance OSCs. Additions of solvent additives in to the active layer spin coating solution or the use of solvent mixtures for active layer preparation can prove to be effective in tuning the morphology of photoactive layer. This newer approach of solvent additives or solvent mixtures can affect the performance of OSCs in several ways. Some of the effects of this method on the photovoltaic parameters are discussed in the following sections.

#### ❖ Improvement in Optical Absorption and Photocurrent Generation

Numerous research groups have attempted at enhancing the molecular ordering of semiconducting polymer films and their electrical properties [67–72] by adding a small amount of processing additive in to the host solvent. One such approach was successfully demonstrated by Kiriya *et al.* [73] as they produced polythiophene nanowires in dilute solutions by adding a poor solvent, hexane, to the blend solutions. Moule´ and Meerholz [48] and Li *et al.* [74] recently produced ordered P3HT aggregates in solution by using a similar method, which was found to enhance photovoltaic device performance when employed in the active layer of OSC.

It has also been reported that solvent mixtures have a significant effect on film morphology and device performance, namely on  $J_{sc}$ ,  $V_{oc}$ , and FF. Previous efforts on the solvent-mixture approach focussed on two miscible solvents, which offer considerable solubility to both the polymers and fullerenes. Recently, solvent mixture approaches take advantage of the cooperative effect of solvents offering distinct solubility to the blend components [75]. The incorporation of additives into a host solvent signifies a revolutionary method and an important step towards controlling the BHJ morphology. It offers a unique presentation approach to examine the film-formation dynamics in the spin coating process.

However, it is very important to indicate that such solvent mixtures raises a more complicated situation in both the solution and film evolutions, as the solutions now develop into multicomponent (phase) systems. Therefore, to maintain simplicity, two solvents are generally engaged in the solution system when studying on the elementary principles for improving the performance. However, solvent-mixture method should not be limited to only two solvents; ternary- or even quaternary-solvent systems are also rational approaches.

The solvent mixture systems have been intensely investigated by several groups, presenting a clear realization of the solvent selection rules for desirable morphology [76]. Again, a perfluorinated compound, 4-amino-2-(trifluoromethyl) benzonitrile (ATMB), was included as an additive to the P3HT [poly(3-hexylthiophene)]:PCBM [[6, 6]-phenyl-C<sub>61</sub>-butyric acid methyl ester] blend films. The incorporation of 6 wt% ATMB to a P3HT:PCBM layer increased the power conversion efficiency to 5.03% attributable to the better short circuit current and fill factor compared to a conventional cell without additive. In contrast, the devices with

4-aminobenzonitrile as an additive (not containing fluorine atoms in the molecule) showed lower PCEs than that of the conventional cell. The ultraviolet–visible (UV-Vis) absorption measurements, X-ray measurements and carrier mobility studies demonstrated that ATMB supported ordering of the P3HT chains, ensuing higher absorbance, formation of larger P3HT crystallites and better hole mobility [77].

Alkane dithiols have been the best acknowledged class of “processing additive”, effectual in modifying the morphology in reasonably large number of polymer classifications including classical P3HT donor polymer as well some low band gap polymers. Addition of alkyl thiols, which are bad solvents for P3HT, to P3HT/PCBM blend solution in toluene can increase the photoconductivity and carrier lifetime, owing to the enhanced structural order [78]. More recently, Peet *et al.* accounted twofold increase in efficiency from 2.8 to 5.5%, with  $J_{sc}$  reaching value as high as  $16.2 \text{ mA cm}^{-2}$  by incorporating a few volume percent of alkane dithiols into the poly[2,6-(4,4-bis(2-ethylhexyl)-4*H*-cyclopenta[2,1-*b*;3,4-*b'*]-dithiophene)-*alt*-4,7-(2,1,3 benzothiadiazole)] PCPDTBT:C<sub>71</sub>-PCBM polymer blend solution [79]. Such a great improvement in efficiency was credited to the improved interactions among the polymer chains and/or between the polymer and fullerene phases upon alkane dithiol addition, confirmed from the absorption spectra.

#### ❖ Improvement in Crystallinity and Charge Carrier Mobility

Earlier, the formation of fullerene nanocrystallites by addition of “bad” solvent was reported by Alargova *et al.* [80]. It was thought that fullerene molecules have a propensity for crystallization upon contact with a “bad” solvent in order to decrease the overall energy. The size of these closely dispersed aggregates is thought to be related to the concentration of fullerene and selections of solvent, regardless of

the volume of the “bad” solvent added. However, further detailed studies brought out that it is the well ordered crystallization of donor polymer that is responsible for improved performance of the devices rather than the crystallization of fullerene component upon addition of the bad solvent. A comprehensive account of alkane dithiol incorporation was done by Lee *et al.* to elucidate the mechanism of structural organization, with the alkane dithiols participating as “processing additive”, without reacting with any of the polymer or fullerene components [81].

The alkanedithiol selectively solubilised the fullerene phase, while the PCPDTBT remained comparatively insoluble. As a result of the higher boiling points of the alkanedithiols (b.p. >160 °C), the fullerene phase remained in the solution, and polymer gets more freedom to self-align and crystallize first. Consequently, the phase-separation morphology can be controlled by various alkanedithiols and by tailoring their relative ratios.

Additionally, the polymer domains are retained even after removal of the fullerene phase, allowing the study of the rendered polymer network. Fig. 1.14 shows the atomic force microscopy (AFM) and transmission electron microscopy (TEM) images of the PCPDTBT:C<sub>71</sub>-PCBM films with and without 1, 8-octanedithiol (OT), as well as the exposed PCPDTBT network after selective dissolution of the C<sub>71</sub>-PCBM. These figures noticeably illustrate larger PCPDTBT and C<sub>71</sub>-PCBM domains due to OT addition, representing better percolating pathways for both carriers from these larger interconnected domains thereby improving the performance of device [81]. Carrier transport studies also identified enhanced network by the improved electron mobility [82].



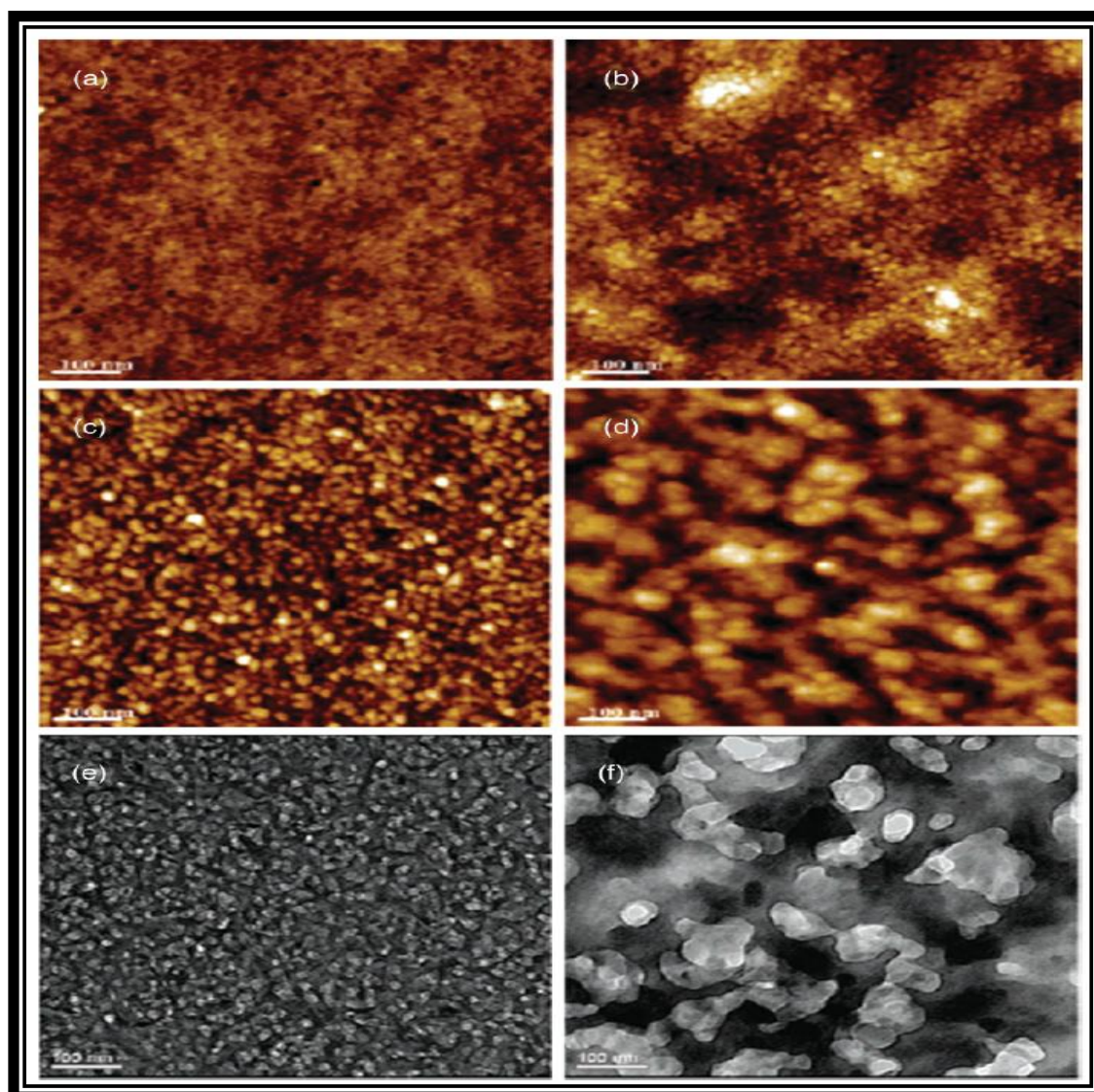


**Figure 1.14:** AFM image of PCPDTBT/C<sub>71</sub>-PCBM BHJ film a) without and b) with 1,8-octanedithiol; AFM image of exposed polymer networks after removal of C<sub>71</sub>-PCBM c) without and d) with 1,8-octanedithiol; TEM image of exposed polymer networks e) without and f) with 1,8-octanedithiol (Adapted from Reference [81])

The mechanism for introduction of n-dodecylthiol to P3HT:PCBM solution to improve the P3HT crystallinity and to enhance the P3HT:PCBM phase separation has been detailed by Liu *et al.* It was elucidated that n-dodecylthiol played a significant role in the solution and during the film-forming process. In solution, n-dodecylthiol decreased the P3HT chains entanglement facilitating coil-to-rod transformation of



P3HT chains and enhanced the P3HT crystallinity. During the film-forming process, introduction of n-dodecylthiol reduced the amount of PCBM which dissolved in the amorphous regions of P3HT, promoting the aggregation of PCBM and hence, supported uninterrupted crystallization of P3HT contributing to the controlled nanoscale phase segregation between the domains. Thus, an increased P3HT crystallinity and a commensurate scale of phase separation balancing for excitons dissociation and charge transport and/or collection led to nearly threefold increase in the device efficiency when the volume fraction of additive is 2.0%. An important conclusion from their study was that the addition of additive promotes the dispersion of P3HT in solution rather than the aggregation of P3HT, resulting in an increase of the solution's shelf lifetime that can promote the relevance of mass production manufacturing [83].

In view of that, two provisions were recommended for incorporating alkanedithiols to control the blend film morphology: i) selective solubility of the fullerene component and ii) a higher boiling point (lower vapour pressure) than the host solvent. This study paved insight into the mechanism of morphology evolution in blend film considering addition of a "bad" solvent, and specified a rule for selection of different solvent additives.

Even though chloroform and chlorobenzene offer good solubility for conjugated polymers, but they are somewhat poor solvents for asymmetric C<sub>70</sub>-fullerene derivatives such as PC<sub>71</sub>BM necessitating the involvement of a solvent additive that can cut down the miscibility gap between the conjugated polymer and PC<sub>71</sub> BM in order to form more-homogeneous films. Particularly, 1, 8-di(*R*) octanes, with different functional groups *R* (such as iodo, thiols), can improve the miscibility

of PC<sub>71</sub>BM with the polymer [84]. Moreover, the chain length of the alkyl group in the additive can also considerably affect the morphology of the active layer and hence, influence the performances of photovoltaic device.

The use of processing additive was further investigated for the polymer poly{bi(dodecyl)thiophene-thieno[3,4-*c*]pyrrole-4,6-dione} (PBTPD) in the PBTPD:PC<sub>71</sub>BM system by Su *et al.* and found that PCE of a device with PBTPD:PC<sub>71</sub>BM (1:1.5, w/w) as the active layer can be improved from 5 to 7.3% (approximately 45% increase) following the addition of 1, 6-diiodohexane (DIH) additive having appropriate alkyl chain length during active layer preparation. DIH provided finest dispersion of PC<sub>71</sub>BM due to a balance between the solubility of PCBM and interaction among the additive and polymer component. They also revealed precise morphology of active layer with the use of techniques such as simultaneous synchrotron grazing-incidence small/wide-angle X-ray scattering (GISAXS/GIWAXS) and transmission electron microscopy (TEM) and ascertained that apart from inducing higher polymer crystallinity (2.4 and 3.6 times in the out-of-plane and in-plane directions, respectively) the additive DIH also reduced the average size of the aggregated fractal-like PC<sub>71</sub>BM clusters from 150 to 30 nm by eliminating the grain boundaries compared to other similar types of solvent additives like 1,4-diiodobutane (DIB), and 1,8-diiodooctane (DIO) [85].

In addition to solvent additives mentioned above, nitrobenzene solvent was also known to have the capability of controlling the polymer blend film morphology [86]. It has been identified that P3HT exists as crystalline aggregates and as amorphous structures in the polymer blend film, giving rise to a multicomponent (amorphous P3HT rich and poor in PCBM, and aggregated P3HT rich and poor in

PCBM) phase separated system. The amorphous-to-aggregated P3HT ratio can be quantified in both the liquid and solid phases by means of solvatochromatic shift in its absorption spectra. PCE of this device without any post-treatment reached a value as high as 4% by addition of 4.25% nitrobenzene in the solution resulting in a completely aggregated P3HT in the composite film.

With an analogous method of addition of a bad solvent for P3HT, i.e., hexane into a well-dissolved solution of P3HT Li *et al.* established the structuring of ordered P3HT aggregates via interchain  $\pi$ - $\pi$  stacking [87]. The preformed ordered P3HT gradually aggregated in the solution and brought about the alignment and crystallization of the P3HT chains improving the conductivity [88]. Also, addition of high-boiling-point solvent, 1-chloronaphthalene (Cl-naph), into the common solvent di-chlorobenzene (DCB) led to better self organization of the P3HT chains by reducing the rate of solvent evaporation [89]. The improved crystallinity decreased the series resistance and improved the device efficiency.

Park *et al.* also detailed the growth of P3HT nanostructures as a function of the aging time of a precursor solution in a marginal solvent, methylene chloride. Dilute solutions produced near spherical particles at short aging times, and with further aging P3HT developed into one-dimensional rod-like structures with lengths of up to several microns. Dense nanowires were progressively formed at higher P3HT concentrations and longer P3HT solution aging times, improving the electronic properties of the films. This improvement was attributed to the change in P3HT organization in the precursor solution from a random-coil conformation to an ordered aggregate on account of aging in a marginal solvent, methylene chloride [90].

An effective approach to manage self-assembly of the all-conjugated diblock copolymer poly(3-butylthiophene)-*b*-poly(3-hexylthiophene) (P3BHT) into nanostructured morphologies by means of mixed solvent approach were looked at in detail for the first time. The effects of solvent and temperature on the self-assembly process of P3BHT through cooling and successive crystallization route were also explored. It was understood that the ratio of poor/good solvent (*i.e.*, anisole/chloroform) controls the different kinetic pathways adopted by P3BHT chains, yielding nanowires at a low anisole/chloroform ratio ( $\leq 2:1$ ), while nanorings in conjunction with some nanowires were observed at a high anisole/chloroform ratio ( $\geq 6:1$ ). The nanowires were considered to be a direct outcome of strong interchain stacking, whereas the formation of nanorings is a reflection of solvophobic interactions between conjugated blocks and the poor solvent anisole diminishing the unfavourable interactions between the poly(3-butylthiophene) (P3BT) block (50 °C) and later P3HT (below 35 °C) block and anisole [91].

#### ❖ Vertical Phase Segregation

Polymer blends can probably demix (phase separation) when spin coated from their blend solutions owing to their low entropy of mixing [92]. The fast quenching of the solvent leads to nonequilibrium morphology; and accordingly such a film evolution to a certain extent is a complicated process, wherein both thermodynamic and kinetic factors have significant role to play. Vertical stratification results from the different solubilities and surface energies of the blend components and from the kinetics of the spin coating process. A volatile solvent is expected to produce a homogeneous film, while vertical phase separation becomes apparent in a viscous solvent casted film. Upon vertical phase separation, the component with low surface

energy is likely to be segregated at the surface or interface in order to decrease the overall energy of the system. An optimal morphology with lateral and vertical phase segregation can be obtained by controlling the drying rate of film *via* adjusting the solvent viscosity and spin coating condition, as well as with certain surface treatment. Some “bad” solvents can act as “processing additives” to form PCBM aggregates, which aid the self-organization of both components, and encourage vertical phase separation. If the vertical segregation in the active layer can be controlled to the level of optimal structural morphology, with a donor-enriched anode and acceptor-enriched cathode, efficient charge dissociation and charge transport are likely to take place *via* interpenetrating network and interconnected pathways, respectively to improve the performance of photovoltaic device.

Efforts were also concentrated on exploring the insight of vertical stratification in P3HT:PCBM blend on OT addition. Incorporation of OT was determined to maintain the crystallinity of P3HT even at heavier loadings of PCBM on the basis of reorganization among the P3HT and PCBM phases in the blend film. AFM images revealed more rough surface for the composite films upon OT addition, with fibrillar crystalline P3HT domains. As ion bombardment methods are known to introduce artefacts in the film that alter its properties so, top and bottom surface compositions of the film were analyzed by X-ray photoelectron spectroscopy (XPS) *via* separating its top and bottom fractions with unique “float-off” method, without disturbing the film composition [93, 94]. XPS analysis confirmed a heterogeneous distribution (vertical phase separation) of the blend components upon OT addition with the interface of PEDOT:PSS/active blend being populated with PCBM fraction. Such PCBM-enriched anode is unsuitable for hole collection in the regular device structure, but can

prove to be beneficial for the inverted configuration, as in such a configuration the ITO side behaves as the cathode.

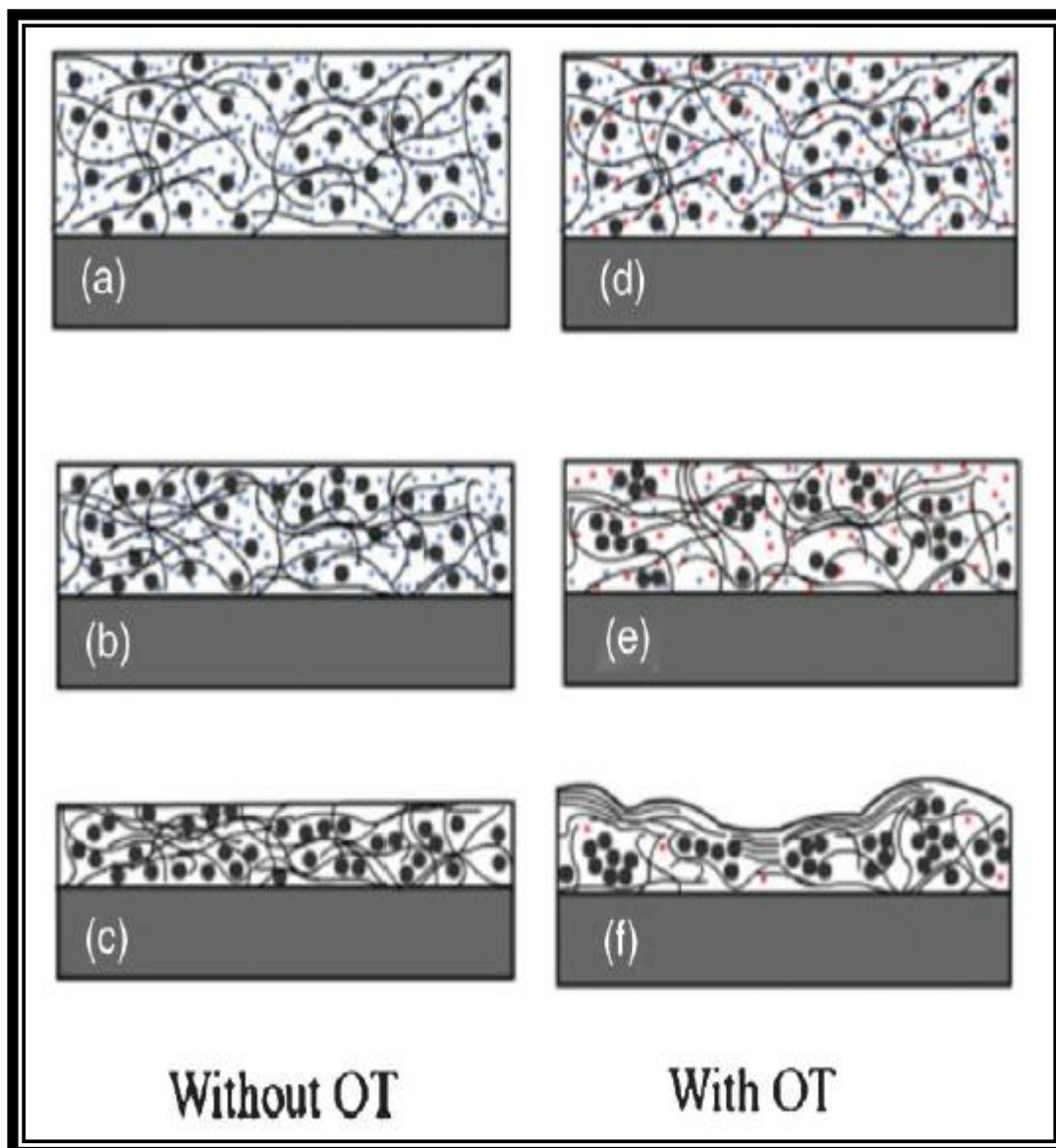


**Figure 1.15: Proposed model of film evolution during the spin coating process. Black wire: P3HT polymer chain; Large black dots: PCBM; blue dots: DCB molecules; and red dots: 1,8-octanedithiol molecules; a–c) correspond to three stages in the spincoating process when DCB is the sole solvent; d–f) when octanedithiol is added into DCB (Adapted from Reference [95])**

Fig. 1.15 demonstrates the effect of OT incorporation during the spin coating process. The host solvent DCB has a lower boiling point (198 °C) than OT (270 °C), but offers higher solubility for PCBM. Accordingly, the concentration of OT

increased progressively during the process of spin coating, with PCBM forming clusters and aggregates in the OT phase simultaneously. P3HT has a higher surface energy than PCBM. Thus, in order to reduce the overall energy, P3HT tends to accumulate at the top (air) surface, while PCBM correspondingly segregates at the PEDOT:PSS interface. Accordingly, the preformed PCBM aggregated, and resulting P3HT crystallites formed percolation pathways for both carriers with a favourable vertical phase-separated morphology in the inverted structure [95].

In accordance with the solvent-mixture criteria proposed by Lee, two more additives, di(ethylene glycol)-diethyl ether (DEGDE) and N-methyl-2-pyrrolidone (NMP) with similar benefits were also identified. Their work demonstrated a unique method to investigate the buried interface without altering the film properties, and revealed the vertical phase separation of the P3HT:PCBM blend upon “bad” solvent addition. It was pointed out that the inverted configuration might offer a promising alternative to the regular structure by taking advantage of the vertical phase separation. Furthermore, recent studies also inferred the occurrence of vertical phase separation even without additive incorporation [96].

### **1.5. Aim**

Polymer solar cells (PSCs) are still in the research and development phase. To bring them closer to the stage of commercial efficient devices, several issues should be addressed, including further improvements of their efficiency and stability. These, in turn, are determined to a large extent by the morphological organization of the photoactive layer, i.e., the layer where light is absorbed and converted into electrical charges.

The scope of the present work is to look into the ways to control and manipulate the morphology of ultra-thin (100-200 nm) donor/acceptor photoactive layers prepared *via* solvent-based techniques, and to establish the relationship between the (three dimensional) morphological organization of photoactive layers and the PSC performance in an inverted organic solar cell.

### 1.6. Plan of Work

This work mainly consists of controlling the morphology of ultra-thin (100-200 nm) donor/acceptor photoactive layers prepared *via* solvents based technique and the same is accomplished through the following steps:

- a) An unmodified (without cosolvent addition) inverted solar cell with a layer structure of glass/ITO/ZnO/P3HT:PCBM/MoO<sub>3</sub>/Ag was prepared and a detailed study of its efficiency.
- b) The concept of solvent induced crystallization of donor poly(3-hexylthiophene) (P3HT) polymer was extended to the photoactive blend of inverted organic solar cells
- c) Different cosolvents (with different solubility index) were evaluated for active layer preparation.
- d) A comparison study of conventional (blended addition) method of cosolvent addition to the active layer spin coating solution with the new two step individually mixed cosolvent addition.
- e) Ternary solvent mixture approach for active layer preparation was applied to the inverted OSC.



**References**

1. (a) J. A. Turner, *Science*, 1999, 285, 687 (b) M. I. Hoffert, K. Caldeira, G. Benford, D. R. Criswell, C. Green, H. Herzog, A. K. Jain, H. S. Kheshgi, K. S. Lackner, J. S. Lewis, H. D. Lightfoot, W. Manheimer, J. C. Mankins, M. E. Mauel, L. J. Perkins, M. E. Schlesinger, T. Volk and T. M. L. Wigley, *Science*, 2002, 298, 981.
2. [http://www.sc.doe.gov/bes/reports/files/SEU\\_rpt.pdf](http://www.sc.doe.gov/bes/reports/files/SEU_rpt.pdf), Report of the Basic Energy Sciences Workshop on Solar Energy Utilization'', US-DOE, April 18–21, 2005.
3. Energy Information Administration, U.S. Department of Energy, Overview, Annual Energy Outlook 2003.
4. E. Becquerel, Memoire sur les effets electriques produits sous l'influence des rayons solaires, *C. R. Acad. Sci.*, 1839, 9, 561.
5. D. M. Chapin, C. S. Fuller and G. L. Pearson, *J. Appl. Phys.*, 1954, 25, 676.
6. M. A. Green, K. Emery, D. L. King, S. Igari, and W. Warta, *Progress in Photovoltaics*, 2005, 13, 49.
7. L. L. Kazmerski, *Renew. Sustain. Energy Rev.*, 1997, 1, 71.
8. J. M. C. R. Nunzi, *Physique*, 2002, 3, 523.
9. C. W. Tang and A. C. Albrecht, *J. Chem. Phys.*, 1975, 62, 2139.
10. C. W. Tang, *Appl. Phys. Lett.*, 1986, 48, 183.
11. M. Hiramoto, Y. Kishigami, and M. Yokoyama, *Chem. Lett.*, 1990, 19, 119.
12. N. S. Sariciftci and A. J. Heeger, *Handbook of Organic Conductive Molecules and Polymers*; Vol. 1, (Ed: H.S. Nalwa), John Wiley & Sons Ltd., Chichester, U.K., 1997, 413.
13. A. J. Heeger, *Angew. Chem. Int. Ed.*, 1976, 40, 2591.
14. A. J. Heeger, *Synth. Met.*, 2002, 125, 23.

15. J. H. Burroughes, D. D. C. Bradley, A. R. Brown, R. N. Marks, K. Mackay, R. H. Friend, P. L. Burns and A. B. Holmes, *Nature*, 1990, 347, 539.
16. M. S. Freund and B. A. Deore, *Self-Doped Conducting Polymers*, John Wiley & Sons Ltd., Chichester, 2007.
17. P. Y. Bruice, *Organic Chemistry, Fourth Edition*, Pearson Prentice Hall, Upper Saddle River, New Jersey, 2004.
18. M. Schwoerer and H. C. Wolf, *Organic Molecular Solids*, Wiley-VCH, Weinheim, Germany, 2007.
19. G. D. Scholes and G. Rumbles, *Nat. Mater.*, 2006, 5, 683.
20. A. J. Heeger, *Primary Photoexcitations in Conjugated Polymers: Molecular Exciton Versus Semiconductor Band Model*, (Ed: N. S. Sariciftci), World Scientific Publishers, Singapore, 1997, 20.
21. P. Würfel, *Physics of Solar Cells: From Principles to New Concepts*, Wiley-VCH, Berlin, Germany, 2004.
22. H. Hoppe and N. S. Sariciftci, *J. Mater. Chem.*, 2004, 19, 1924.
23. L. J. A. Koster, V. D. Mihailetschi and P. W. M. Blom, *Appl. Phys. Lett.*, 2006, 88, 09351.
24. F. C. Krebs, *Polymeric Solar Cells: Materials, Design, Manufacture*, DEStech Publications, Inc., Lancaster, Pennsylvania, 2010.
25. B. A. Gregg, *J. Phys. Chem. B*, 2003, 107, 4688.
26. N. S. Sariciftci, L. Smilowitz, A. J. Heeger and F. Wudl, *Synth. Met.*, 1993, 59, 333.
27. N. S. Sariciftci, L. Smilowitz, A. J. Heeger and F. Wudl, *Science*, 1992, 258, 1474.

- 
28. S. E. Shaheen, N. Kopidakis, D. S. Ginley, M. S. White and D. C. Olson, *Inverted Bulk-Heterojunction Plastic Solar Cells*. SPIE Newsroom, 2007.
29. M. Jorgensen, K. Norrman and F. C. Krebs, *Sol. Energy Mater. Sol. Cells*, 2008, 92, 686.
30. K. W. Wong, H. L. Yip, Y. Luo, K. Y. Wong, W. M. Lau, K. H. Low, H. F. Chow, Z. Q. Gao, W. L. Yeung and C. C. Chang, *Appl. Phys. Lett.*, 2002, 80, 2788.
31. M. M. de Kok, M. Buechel, S. I. E. Vulto, P. van de Weijer, E. A. Meulenkaamp, S. H. P. M. de Winter, A. J. G. Mank, H. J. M. Vorstenbosch, C. H. L. Weijtens and Vv. Elsber, *Physics of Organic Semiconductors* (Ed: W. Brutting), Wiley-VCH, Weinheim, Germany 2005.
32. G. Li, C. -W. Chu, V. Shrotriya, J. Huang and Y. Yang, *Appl. Phys. Lett.*, 2006, 88, 253503.
33. A. K. K. Kyaw, X. W. Sun, C. Y. Jiang, G. Q. Lo, D. W. Zhao and D. L. Kwong, *Appl. Phys. Lett.*, 2008, 93, 221107.
34. M. P. de Jong, L. J. van Ijzendoorn and M. J. A. de Voigt, *Appl. Phys. Lett.*, 2000, 77, 2255.
35. Z. Xu, L. M. Chen, G. W. Yang, C. H. Huang, J. H. Hou, Y. Wu, G. Li, C. S. Hsu and Y. Yang, *Adv. Funct. Mater.*, 2009, 19, 1227.
36. (a) Md. K. H. Bhuiyan and T. Mieno, *Thin Solid Films*, 2003, 441, 187.  
(b) M. T. Rispens and J. C. Hummelen, *Dev. Fullerene Sci.*, 2002, 4, 387.  
(c) N. Martin, L. S!anchez, B. Illescas and I. P!erez, *Chem. Rev.*, 1998, 98, 2527.
37. (a) N. S. Sariciftci, L. Smilowitz, A. J. Heeger and F. Wudl, *Synth. Met.*, 1993, 59, 333.
-

- (b) N. S. Sariciftci, D. Braun, C. Zhang, V. I. Srdanov, A. J. Heeger, G. Stucky and F. Wudl, *Appl. Phys. Lett.*, 1993, 62, 585.
38. H. Spanggaard and F. C. Krebs, *Sol. Energy Mater. Sol. Cells*, 2004, 83, 125.
39. K. -S. Liao, S. D. Yambem, A. Haldar, N. J. Alley and S. A. Curran, *Energies*, 2010, 3, 1212.
40. J. Rostalski and D. Meissner, *Sol. Energy Mater. Sol. Cells*, 2000, 63, 37.
41. G. Dennler, M. C. Scharber and C. J. Brabec, *Adv. Mater.*, 2009, 21, 1323.
42. B. Kippelen and J. -L. Bredas, *Energy Environ. Sci.*, 2009, 2, 251.
43. S. Gunes, H. Neugebauer and N. S. Sariciftci, *Chem. Rev.*, 2007, 107, 1324.
44. M. Helgesen, R. Sondergaard and F. C. Krebs, *J. Mater. Chem.*, 2010, 20, 36.
45. L. -M. Chen, Z. Hong, G. Li, and Y. Yang, *Adv. Mater.*, 2009, 21, 1434.
46. A. Marrocchi, D. Lanari, A. Facchetti, and L. Vaccaro, *Energy Environ. Sci.*, 2012, 5, 8457.
47. S. Cataldo and B. Pignataro, *Materials*, 2013, 6, 1159.
48. G. Li, V. Shrotriya, Y. Yao, J. Huang and Y. Yang, *J. Mater. Chem.*, 2007, 17, 3126.
49. H. Hoppe and N. S. Sariciftci, *J. Mater. Chem.*, 2006, 16, 45.
50. S. E. Shaheen, C. J. Brabec, N. S. Sariciftci, F. Padinger, T. Fromherz and J. Hummelen, *Appl. Phys. Lett.*, 2001, 78, 841.
51. W. Ma, C. Yang and A. J. Heeger, *Adv. Funct. Mater.*, 2005, 15, 1617.
52. H. Hoppe, M. Niggemann, C. Winder, J. Kraut, R. Hiesgen, A. Hinsch, D. Meissner and N. S. Sariciftci, *Adv. Funct. Mater.*, 2004, 14, 1005.
53. G. Li, V. Shrotriya, Y. Yao, J. Huang and Y. Yang, *J. Appl. Phys.*, 2005, 98, 043704.

54. V. D. Mihailetschi, H. X. Xie, B. de Boer, L. J. A. Koster and P. W. M. Blom, *Adv. Funct. Mater.*, 2006, 16, 699.
55. G. Li, Y. Yao, H. Yang, V. Shrotriya, G. Yang and Y. Yang, *Adv. Funct. Mater.*, 2007, 17, 1636.
56. V. Shrotriya, Y. Yao, G. Li and Y. Yang, *Appl. Phys. Lett.*, 2006, 89, 063505.
57. G. Li, V. Shrotriya, J. Huang, Y. Yao, T. Moriarty, K. Emery and Y. Yang, *Nat. Mater.*, 2005, 4, 864.
58. M. Berggren, G. Gustafsson, O. Inganäs, M. R. Andersson, O. Wennerström and T. Herberg, *Appl. Phys. Lett.*, 1994, 65, 1489.
59. N. Camaioni, G. Ridolfi, G. Casalbore-Miceli, G. Possamai and M. Maggini, *Adv. Mater.*, 2002, 14, 1735.
60. J. J. Dittmer, E. A. Marseglia and R. H. Friend, *Adv. Mater.*, 2000, 12, 1270.
61. F. Padinger, R. S. Rittberger and N. S. Sariciftci, *Adv. Funct. Mater.*, 2003, 13, 85.
62. C. -J. Ko, Y. -K. Lin and F. -C. Chen, *Adv. Mater.*, 2007, 19, 3520.
63. T. Erb, U. Zhokhavets, G. Gobsch, S. Raleva, B. Stühn, P. Schilinsky, C. Waldauf and C. J. Brabec, *Adv. Funct. Mater.*, 2005, 15, 1193.
64. Y. Kim, S. Cook, S. M. Tuladhar, S. A. Choulis, J. Nelson, J. R. Durrant, D. D. C. Bradley, M. Giles, I. McCulloch, C. -S. Ha and M. Ree, *Nat. Mater.*, 2006, 5, 197.
65. A. J. Pearson, T. Wang and D. G. Lidzey, *Reports on Progress in Physics*, 2013, 76, 022501.
66. Y. Zhao, Z. Xie, Y. Qu, Y. H. Geng and L. X. Wang, *Appl. Phys. Lett.*, 2007, 90, 043504.
67. H. Shimotani, G. Diguët and Y. Iwasa, *Appl. Phys. Lett.*, 2005, 86, 022104.
-

- 
68. M. J. Panzer and C. D. Frisbie, *J. Am. Chem. Soc.*, 2005, 127, 6960.
69. C. K. Chiang, C. R. Fincher, Jr, Y. W. Park, A. J. Heeger, H. Shirakawa, E. J. Louis, S. C. Gau and A. G. MacDiarmid, *Phys. Rev. Lett.*, 1977, 39, 1098.
70. K. Lee, E. K. Miller, A. N. Aleshin, R. Menon, A. J. Heeger, J. H. Kim, C. O. Yoon and H. Lee, *Adv. Mater.*, 1998, 10, 456.
71. I. N. Hulea, H. B. Brom, A. J. Houtepen, D. Vanmaekelbergh, J. J. Kelly and E. A. Meulenkaamp, *Phys. Rev. Lett.*, 2004, 93, 166601.
72. Y. Chen, I. Shih and S. Xiao, *J. Appl. Phys.*, 2004, 96, 454.
73. N. Kiriy, E. Ja'hne, H. -J. Adler, M. Schneider, A. Kiriy, G. Gorodyska, S. Minko, D. Jehnichen, P. Simon, A. A. Fokin and M. Stamm, *Nano Lett.*, 2003, 3, 707.
74. A. J. Moule'and K. Meerholz, *Adv. Mater.*, 2008, 20, 240.
75. L. Li, G. Lu and X. Yang, *J. Mater. Chem.*, 2008, 18, 1984.
76. J. Peet, J. Y. Kim, N. E. Coates, W. L. Ma, D. Moses, A. J. Heeger and G. C. Bazan, *Nat. Mater.*, 2007, 6, 497.
77. A. Pivrikas, H. Neugebauer, and N. S. Sariciftci, *Solar Energy*, 2011, 85, 1226.
78. S. Jeong, S. -H. Woo, H. -K. Lyu and Y. S. Han, *Sol. Energy Mater. Sol. Cells*, 2011, 95, 1908.
79. J. Peet, C. Soci, R. C. Coffin, T. Q. Nguyen, A. Mikhailovsky, D. Moses and G. C. Bazan, *Appl. Phys. Lett.*, 2006, 89, 252105.
80. J. K. Lee, W. L. Ma, C. J. Brabec, J. Yuen, J. S. Moon, J. Y. Kim, K. Lee, G. C. Bazan and A. J. Heeger, *J. Am. Chem. Soc.*, 2008, 130, 3619.
81. R. G. Alargova, S. Deguchi and K. Tsujii, *J. Am. Chem. Soc.*, 2001, 123, 10460.
82. I. -W. Hwang, S. Cho, J. Y. Kim, K. Lee, N. E. Coates, D. Moses and A. J. Heeger, *J. Appl. Phys.*, 2008, 104, 033706.
-

- 
83. J. Liu, S. Shao, H. Wang, K. Zhao, L. Xue, X. Gao, Z. Xie and Y. Han, *Org. Electron.*, 2010, 11, 775.
84. M. S. Su, H. C. Su, C. Y. Kuo, Y. R. Zhou and K. H. Wei, *J. Mater. Chem.*, 2011, 21, 6217.
85. M. -S. Su, C. -Y. Kuo, M. -C. Yuan, U-S. Jeng, C. -J. Su, and K. -H. Wei, *Adv. Mater.*, 2011, 23, 3315.
86. J. K. J. van Duren, X. N. Yang, J. Loos, C. W. T. Bulle-Lieuwma, A. B. Sieval, J. C. Hummelen and R. A. J. Janssen, *Adv. Funct. Mater.*, 2004, 14, 425.
87. L. G. Li, G. H. Lu and X. N. Yang, *J. Mater. Chem.*, 2008, 18, 1984.
88. S. D. D. V. Rughooputh, S. Hotta, A. J. Heeger and F. Wudl, *J. Polym. Sci. Part B*, 1987, 25, 1071.
89. F. -C. Chen, H. -C. Tseng and C. -J. Ko, *Appl. Phys. Lett.*, 2008, 92, 103316.
90. Y. D. Park, S. G. Lee, H. S. Lee, D. Kwak, D. H. Lee and K. Cho, *J. Mater. Chem.*, 2011, 21, 2338.
91. M. He, L. Zhao, J. Wang, W. Han, Y. Yang, F. Qiu, and Z. Lin, *ACS Nano*, 2010, 4, 3241.
92. M. Geoghegan and G. Krausch, *Prog. Polym. Sci.*, 2003, 28, 261.
93. A. Turak, D. Grozea, X. D. Feng, Z. H. Lu, H. Aziz and A. M. Hor, *Appl. Phys. Lett.*, 2002, 81, 766.
94. S. G. MacKay, M. Bakir, I. H. Musselman, T. J. Meyer and R. W. Linton, *Anal. Chem.* 1991, 63, 60.
95. Y. Yao, J. H. Hou, Z. Xu, G. Li and Y. Yang, *Adv. Funct. Mater.*, 2008, 18, 1783.
96. Z. Xu, L. -M. Chen, G. Yang, C. -H. Huang, J. Hou, Y. Wu, G. Li, C. -S. Hsu and Y. Yang, *Adv. Funct. Mater.*, in press.
-



*Chapter 2*

*Characterization  
Techniques*



## CHARACTERIZATION TECHNIQUES

---

- 2.1 Overview**
- 2.2 Fabrication Techniques**
  - 2.2.1 *Laser scribing*
  - 2.2.2 *Cleaning of substrates*
  - 2.2.3 *Wet processing of active layers*
    - 2.2.3.1 *Spin coating*
  - 2.2.4 *Vacuum systems*
  - 2.2.5 *Glove box*
- 2.3 Characterization Techniques**
  - 2.3.1 *Contact angle measurement*
  - 2.3.2 *Atomic force microscopy (AFM)*
  - 2.3.3 *Ultraviolet and visible light (UV-Vis) spectroscopy*
  - 2.3.4 *Grazing incidence X-ray diffraction (GIXRD)*
  - 2.3.5 *Photoluminescence*
  - 2.3.6 *Current density-voltage characterization*

### **References**

---

#### **2.1 Overview**

This chapter throws light on the materials and techniques employed in the fabrication process of organic bulk heterojunction solar cells. All stages of solar cell fabrication starting with the methods for cleaning glass substrates to the techniques used to deposit the different layers have been discussed in detail.

Fabrication being just the initial step towards realization of the properties and characteristics of OPV devices, further extensive variety of techniques are available that can be utilized to characterize OPV devices. The techniques used in this work are illustrated systematically. The typical measurement methods used comprises of electrical measurements, such as photoluminescence and solar cell characterization by

means of solar cell test circuit and current-voltage ( $I$ - $V$ ) measurements. Different spectroscopic techniques such as; ultraviolet and visible (UV-Vis) and grazing incidence X-ray diffraction (GIXRD) have been used to evaluate the optical performance of the materials. Eventually, microscopic techniques such as atomic force microscopy (AFM), contact angle measurement have been employed to envisage the surface characteristic and morphological attributes of the deposited films. All the phases in solar cell fabrication and characterization are discussed in this chapter.

## **2.2 Fabrication Techniques**

### **2.2.1 Laser Scribing**

The ITO or transparent conducting layer in thin film solar cell modules has a considerable effect on its power conversion efficiency [1, 2]. To facilitate reduction in the resistive losses and active area losses of solar cells, ordered patterning of ITO thin films is essential in the structuring of interconnect lines and assembly of thin film solar cells [3]. A variety of techniques have materialized for patterning ITO electrodes with sharp edges and electrically insulated channels between the conductor contours for thin film solar cells. Thin film patterning techniques include the most popular photolithographic technique with wet etching in acidic solutions [4]. However, such a method involves several process steps and the requirement of costly equipment as well as lethal chemicals. Also, such methods give rise to grooves with disseminated edges owing to lesser or excessive etching. Consequently, it became elemental to produce a nonlithographic or direct patterning approach to put together well defined structures with fine edges on ITO electrodes.

Laser ablation is the method of removing materials from a substrate by direct absorption of laser energy, thus creating the required arrangement of narrow and clean patterning on account of their assistance in localized heating and material removal [5–7]. Laser scribing (laser thin film removal) is thought to be an ideal tool as it allows fast, non-contact, narrow and clear-cut removal of the thin films. For electrical isolation of the individual segments of electrically conducting substrates from short circuiting, an insulating layer is required in between these conducting segments of solar cells. Such a practice includes the irradiation of a glass pane with a strongly focused laser beam, resulting in the removal of one or more layers of thin film from either thin film material, or from the glass pane itself.



**Figure 2.1: Laser scribing machine (Electrox 600 Group, IR L6 1064 nm)**

Maskless patterning of ITO films using a diode-pumped Q-switch neodymium-doped yttrium aluminium garnet ( $\text{Nd:Y}_3\text{Al}_5\text{O}_{12}$ , Nd:YAG) laser at its

fundamental wavelength ( $\lambda=1047\text{nm}$ ) in the infrared (IR) region had been established to give in clear-cut line in the present work. Experimental setup consists of a Nd:YAG IR laser, the optical system, the XY table and the computer-based controller (Fig.2.1). The experimental sample (size 50 mm  $\times$  50 mm) fixes on the vacuum chuck positioned on the XY table which is controlled by a linear motor. The IR laser beam is directed by the optical system and focused on the test specimen by means of the focusing lens. Consequently, the focusing laser beam removes the ITO film on the glass and the ITO circuit patterns would be generated. In the laser patterning processing, depending on the material to be removed and the depth of scribing, the process parameters such as the laser repetition rate, the laser power and the feeding speed of XY table can be altered.

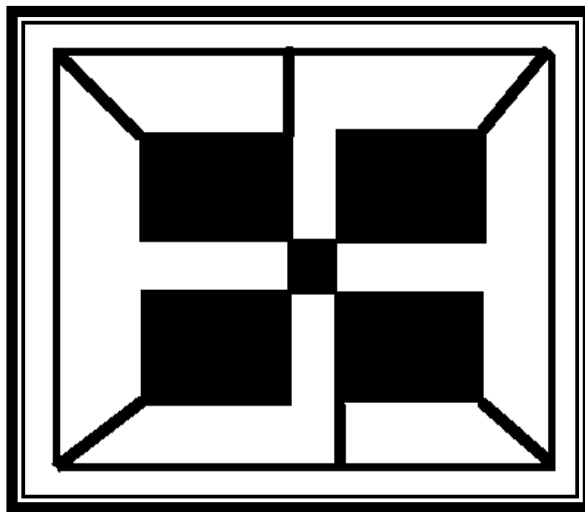


**Figure 2.2: ITO pattern produced by IR laser processing system**

ITO films on the glass substrate absorbs about 20% of incoming IR laser light making the exposed regions of the glass substrate completely transparent. Fig. 2.2 shows the ITO patterns which is formed by the IR laser processing system (darker portion is free of ITO), for which the processing parameters are set as follows: laser power is 1.0 W, the feed speed is 10 mm/s and the line-width is 20  $\mu\text{m}$ .

### 2.2.2 Cleaning of Substrates

There are two essential techniques used in the cleaning of glass substrates such as chemical cleaning and UV-ozone cleaning processes. The substrate used throughout this work is ITO coated glass slide (Moserbaer India Ltd., India). Typically, glass slides were cut into 50 mm squares and laser patterned prior to cleaning. UV-ozone and chemical cleaning approaches were applied for cleaning of ITO coated glass.

#### ❖ Chemical Cleaning

The process steps for cleaning glass substrate are as follows; the entire procedure was carried out in a clean room excluding the drying process that was accomplished in a laminar flow bench to make certain of a dirt free surrounding and to avoid the break out of vapours of the solvents.

The glass slides were arranged tidily in a slide holder or zig and placed in a beaker with a 5% solution of Triton-X detergent in de-ionised water; this was then placed in an ultrasonic bath and sonicated for 15 min at 50°C. After this process, the samples were repeatedly washed with deionised water to completely get rid of the detergent solution and thereafter, rinsed in fresh deionised water for 15 min in the ultrasonic bath. The samples were then placed in a fresh beaker filled with acetone and covered; the beaker was then placed in the ultrasonic bath for 15 min. The samples were put back to another fresh beaker filled with isopropyl alcohol and ultrasonicated for 15 min. The slides were then placed onto a clean drying rack and blow dried using the nitrogen gun. The slide holder was then positioned in an oven at 100°C for 1 h to finally dry the slides. The slides were then cooled, and once cooled then they were set aside in a clean slide box and stocked up until needed.

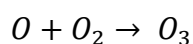
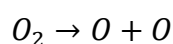
### ❖ UV-ozone Cleaning

UV-ozone ( $O_3$ ) cleaning efficiently removes organic compounds, but it is not helpful in getting rid of dust and inorganic salts. Further, if a thick film is build up by the organic compounds of contaminants, ultraviolet irradiation may decompose most of the polymers on the surface. Conversely, the polymers contained within and having no oxygen crosslink with each other, do not undergo photolysis. For this reason, effective UV- $O_3$  cleaning requires first round of chemical cleaning of the surface. The initial cleaning is done mainly to eliminate the contaminants such as dust and salts that may not be transformed into volatile products by the deed of oxidising UV- $O_3$  cleaning, and also to get rid of a thick covering of the contaminants, the most of which is expected to be converted into a UV-resistant coating by the crosslinking action of ultraviolet rays radiating from the surface. Fig. 2.3 shows the picture of UV-ozone cleaner used in this work.



Figure 2.3: UV-ozone cleaner (Jelight Company Inc., 144AX-220)

The principle of UV-O<sub>3</sub> cleaning is based on the fact that the organic compounds are converted into volatile substances (e.g., water, carbon dioxide, nitrogen) by a combined action of decomposition *via* ultraviolet rays and thereafter strong oxidisation with atomic oxygen (O) produced during the formation and decomposition of O<sub>3</sub>. The volatile compounds thus produced are removed from the contaminated surface. The major wavelengths of the ultraviolet rays radiated from a well-known low pressure mercury vapour lamp are 184.9 and 253.7 nm. When atmospheric oxygen (O<sub>2</sub>) is irradiated with ultraviolet rays of 184.9 nm wavelength, the oxygen absorbs the ultraviolet rays to form O<sub>3</sub> by the following reaction:



Ozone (O<sub>3</sub>) so formed when irradiated with ultraviolet rays with a wavelength of 253.7 nm, it decomposes. At some point in the process of formation or decomposition of O<sub>3</sub>, atomic oxygen is produced which have strong oxidising ability. Then, contaminant organic compounds are irradiated with ultraviolet rays, and absorb the ultraviolet rays to cause photolysis and generate the following substances:

Organic compounds irradiated with ultraviolet rays	{	Ions, Free radicals Excited molecules, Neutral molecules
---	---	---

These excited contaminants, or the free radicals formed by the photolysis, react with atomic oxygen to form simple molecules such as CO<sub>2</sub>, H<sub>2</sub>O, N<sub>2</sub> and O<sub>2</sub>, that are then removed from the surface.

### 2.2.3 Wet Processing of active layers

Several methods are available for depositing thin films of polymers or other materials onto substrates from its well dissolved solution for example; spin coating,

drop casting, painting and printing. The fundamental idea following all of these “wet” processes is to find a suitable solvent for the material(s), i.e., one that will suitably dissolve the materials to be deposited without spoiling either of the substrate or disturbing other layers that may already be there as in the case of multi layer devices [8-10]. During this work, wet processing technique employed for depositing various layers is spin coating; however, other techniques such as drop casting and printing are preferred for large scale preparation of films when the eventual blend mixture has been realized.

### 2.2.3.1 Spin Coating

Spin coating is the main technique used to deposit the polymeric layers on the substrate in the present research work. Spin coating is a process wherein, a small amount of solution is laid onto the substrate which is then spun at high speeds (up to 10,000 rpm) evaporating bulk of the solvent and setting up a thin film of uniform thickness. In general, the substrate is clenched to a rotating chuck through a vacuum pump and spun at high speeds, and air or a neutral gas such as nitrogen is flushed in to the chamber to assist drying the solvent (Fig.2.4). The spin speed goes up to the desired rate, continues at that speed for a particular span of time and then falls back to a nil pace, upon which the substrate can be taken out from the spin coater.

Description of the spin coating process is intricate, as different factors such as: solution viscosity, rate of evaporation, spin speed and air or nitrogen flow rate are to be taken in to the account. However, a general expression indicating the relationship between film thickness ( $d$ ) and the other process parameters can be stated in as:

$$d=k\omega\alpha \quad (2.1)$$



Where,  $\omega$  is the angular velocity,  $k$  and  $\alpha$  are empirical constants associated with the type of solution. The value of  $\alpha$  is typically around -0.5 and the value of  $k$  can depend upon the initial viscosity of the solution [11].

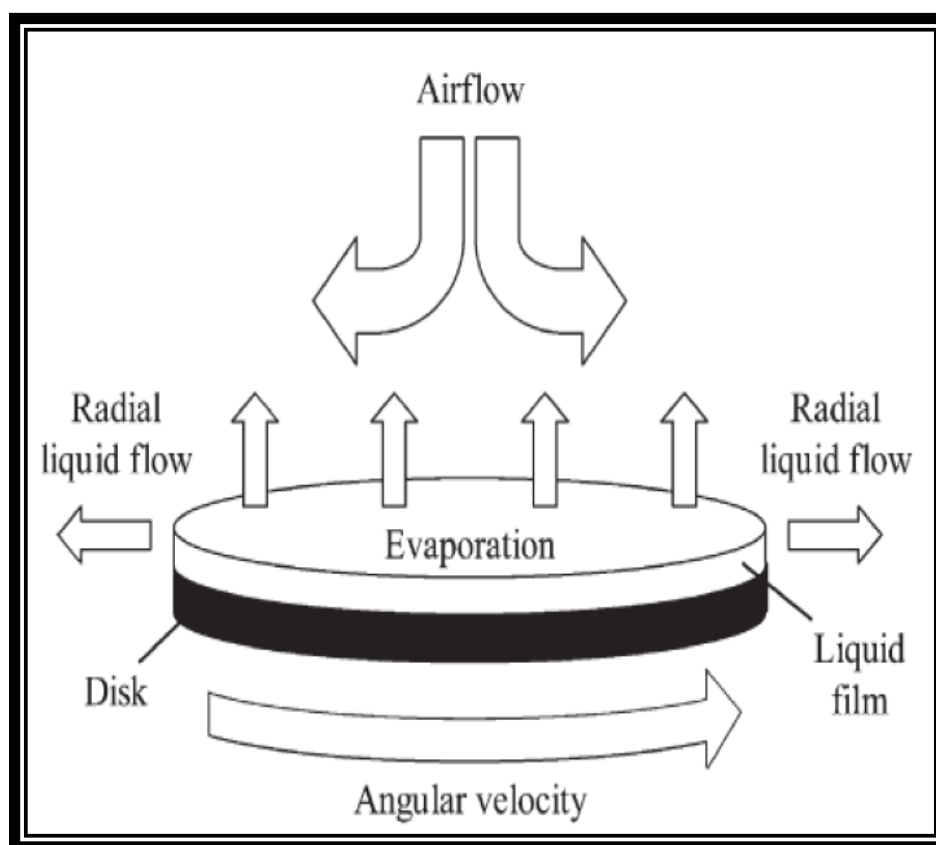


**Figure 2.4: Schematic of the spin coating process (Adapted from Reference [12])**

Considering the above mentioned factors, it becomes essential to optimize the spin coating process by coating an array of samples with the desired viscosity at various spin speeds to settle on the best possible speed and viscosity for the required film thickness. Generally, the film thickness is known to decrease with an increase in angular velocity for a particular concentration of solution. Spin coating is recognized to be an excellent technique for depositing thin films of organic materials, but reproducibility of the process to a great extent is reliant on the ability of the operator to produce films of high quality.

At a given spin speed, more concentrated or viscous solutions will produce thicker layers. This affects the fabrication of solar cells as, in most of the cases, pure polymer is not the sole component in the solution and other materials such as fullerenes and/or other nanomaterials are added which affects the viscosity and hence, the thickness of film [12].

There are two types of spin coating processes such as static or dynamic spin coating process. In static spin coating, the solution is dropped on the substrate before starting the spinning while, in dynamic spin coating, the solution is dropped onto the already spinning substrate. These two types of spin coating (static or dynamic) processes can bring about variations in film quality and thickness. One of the main shortcomings of the spin coating technique is that the bulk of the material goes wasted in this process. While, some share of this loss is due to the evaporation of solvent however, wastage in terms of polymer and nanoparticles is still a very high percentage of the original solution.

#### **2.2.4 Vacuum Systems**

Several methods followed in the solar cells fabrication use different vacuum systems. To avoid explaining the concept of vacuum systems repetitively we shall start by describing the basic principles of the types of vacuum systems used by us and the following section will describe the vacuum based dry deposition processes. There are a few important reasons for depositing materials in vacuum given as below:

1. The probability of contamination or oxidation is decreased, as air and other gas pollutants or dust particles are removed from the chamber before deposition.
2. Superior film quality, as in air the mean free path (MFP) of a molecule is  $\sim 10 \times 10^{-6}$  cm, i.e., a molecule can move about that distance prior to colliding with other

molecule. The MFP being inversely related to the pressure in the chamber, so that reducing the pressure, we can increase the MFP and subsequently decrease the scattering for getting better quality film. For a vacuum of the order  $10^{-6}$  mbar, the MFP is increased to around 5 cm. Typically, a molecule can be involved in up to 10 collisions ahead of any evident divergence as of its original pathway, so fine film quality will be sustained if the substrate is held within 10 MFP distance from the material [13].

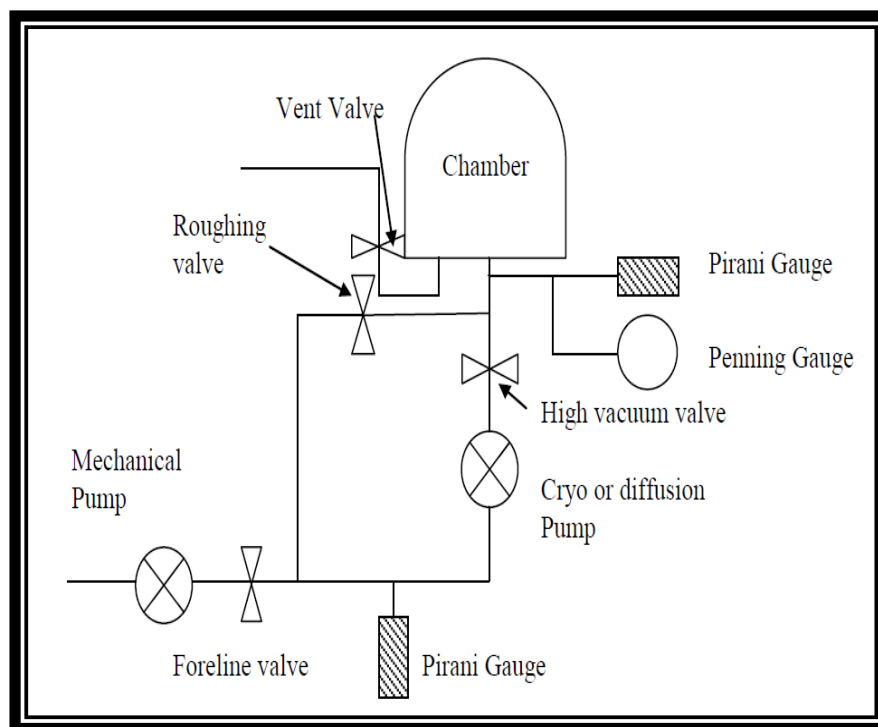


**Figure 2.5: Schematic arrangement of high vacuum system**

The typical arrangement of a vacuum system is shown in Fig. 2.5. Two pumps are exploited in all the systems. A mechanical (usually rotary) pump is used to take the system down to a pressure where the high vacuum pumps can function ( $\sim 10^{-2}$  mbar). The Hind High Vacuum (HHV) system has two types of high vacuum pumps, the thermal evaporators use diffusion pumps as shown in Fig.2.6 and the RF Magnetron sputterer uses a cryopump.

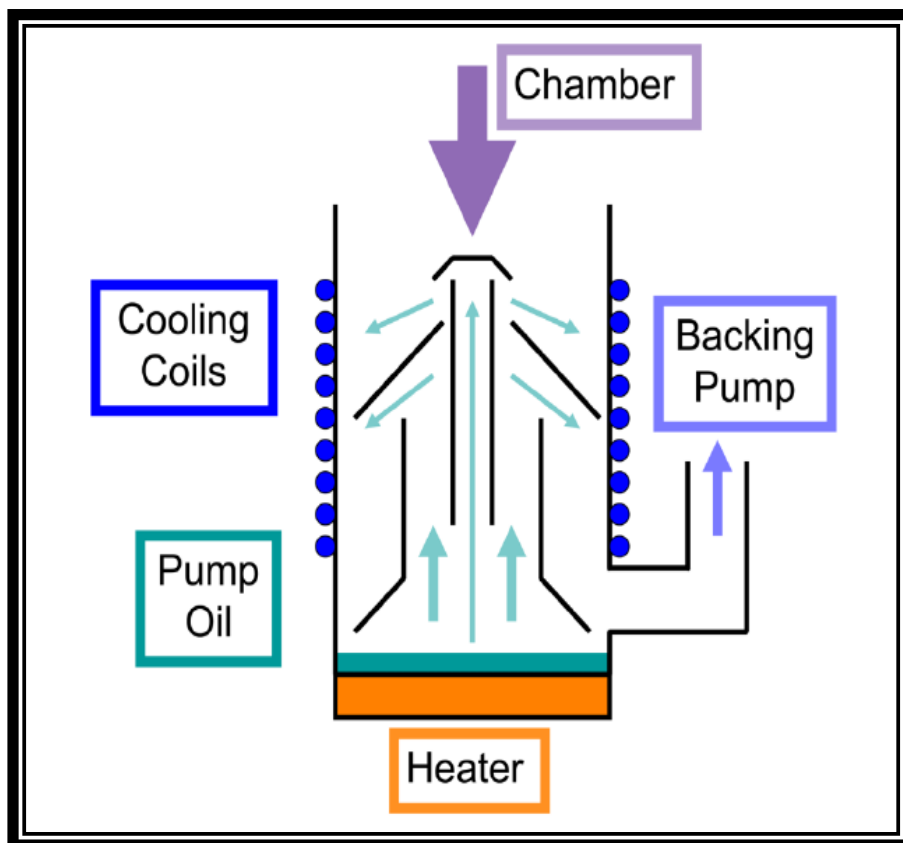


**Figure 2.6: Schematic of diffusion pump (Adapted from Reference [15])**

The working of diffusion pump can be summarized as heating of the oil which evaporates all the way through a chain of concentric tubes [14]. To cool the oil, water is forced around the exterior of the pump, which drops back on condensation. The convection effect of this action pulls down the gas from the chamber which is carried out by the backing pump. The oil stays behind in the pump until rendered to pressures in excess of  $10^{-2}$  mbar while hot, in such a case the oil can then vent into the chamber causing contamination. Superior diffusion pump efficiency can be achieved by including a “cold trap” at the top of the pump into which liquid nitrogen can be placed. This cools the pump further and avoids “backstreaming”, where oil vapours leave into the chamber. The oil has to be replaced at regular intervals as it becomes spoiled following repetitive usage [14].

Cryopumps operate by freezing gas or vapour from the chamber onto very cold surfaces; which is cooled to ~15K using liquid helium from a compressor unit, which is regularly passed throughout the system in the course of operation. The drained out gases remain frozen in the pump, apart from very light elements which cannot be frozen out entirely and are frequently isolated with attached carbon traps. As the gases remain frozen in the pumps so, it becomes essential to “regenerate” the pump, i.e., warm it to escape the trapped gasses, at regular intervals. Failure of cryopump regeneration decreases its efficiency [15]. To deposit metal layer, vacuum based dry deposition technique such as thermal evaporator is used.

❖ *Thermal Evaporator/ Vacuum Evaporator*

Thermal evaporation is a process to deposit thin film of metal or small molecule organic semiconductors in the vacuum. The metal evaporation can be controlled using the process parameters such as vacuum chamber pressure, source material purity, and evaporation power, which is related with the evaporation rate. In order to realize high-quality film deposition, the pressure of the vacuum chamber should be kept around  $6.67 \times 10^{-7}$  mbar. When the deposition is carried out at higher pressure than  $1.33 \times 10^{-6}$  mbar, hot vaporized metal particles react with left over oxygen molecules and form metal oxide. Deposited layers in such a circumstance lack metallic reflection and electrical properties. Fig. 2.7 shows the set up of a vacuum evaporator. Material purity is also an essential parameter for high quality thin film deposition. Purity of material should be over 99.99%. High purity of source material reduces the possibility of side reactions or impurity formation during evaporation. The evaporation rate ranges from 1 to 3 Å/sec. Low evaporation rate of source materials ensures protection of the sub-layer, which may otherwise be damaged by hot vapours.

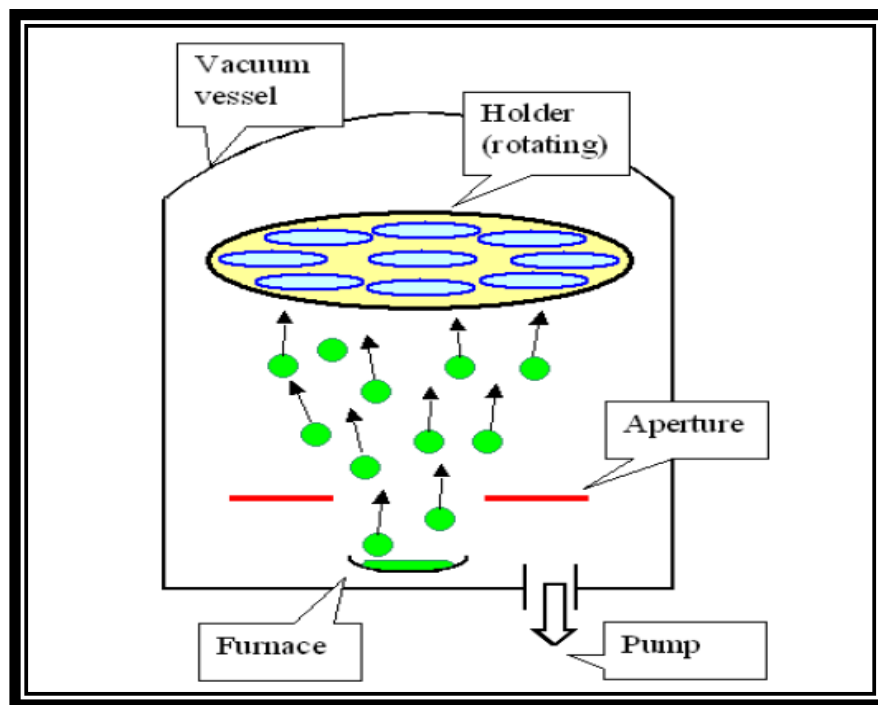


**Figure 2.7: Diagram of vacuum evaporator**

Fig. 2.8 shows the design of the shadow mask used to deposit various metallic layers in the devices. The design of the shadow mask depicts four cells each of area  $0.09 \text{ cm}^2$ .

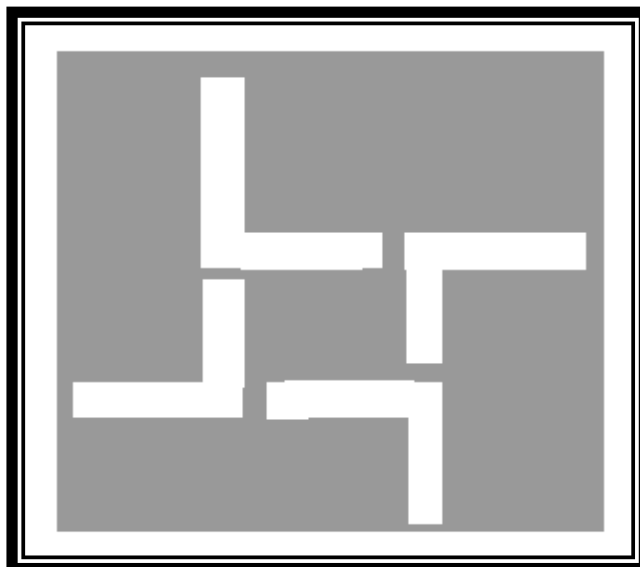


**Figure 2.8: Model of the shadow mask for metal deposition**

### 2.2.5 Glove Box

A glove box is a fastened box that is proposed where a separate work atmosphere is considered necessary. The sides of the glove box are fitted with gloves set up in such a way that the researcher can put their hands into the gloves and carry out their chores inside the box without violating containment. A part or the entire box is made transparent for user's convenience so that they can observe what is being carried out inside (Fig. 2.9). There are two types of glove boxes: one allows an individual to work with hazardous substances, such as radioactive materials; the other allows managing of materials that must be contained in a very clean inert atmosphere, such as argon or nitrogen. It is also likely to exploit a glove box for keeping the articles in a vacuum chamber.



**Figure 2.9:** Pictorial view of glove box from Jacomex

The gas in a glove box is driven *via* a series of action mechanisms removing solvents, water and oxygen from the chamber. Heated copper metal (or some other finely divided metal) is commonly used to get rid of oxygen. This oxygen removing column is by and large regenerated by passing a hydrogen/nitrogen mixture through it while heated: the water formed is exhausted of the box with the excess of hydrogen and nitrogen. Molecular sieves are commonly used to eliminate water by adsorbing it in their pores. Such a glove box is more commonly used by organometallic chemists to move dry solids from one storage place to another. Inert atmosphere glove boxes are normally held at a higher pressure than the surrounding air, so that any microscopic escapes are predominantly pouring out inert gas in preference to allowing air into the box.

## **2.3 Characterization Techniques**

### **2.3.1 Contact Angle Measurement**

When an interface is present between a liquid and solid, the angle between the surface of the liquid and outline of the contact surface is expressed as the contact angle  $\theta$  (theta). The contact angle (wetting angle) is a measure of the wettability of a solid by a liquid. In case of complete wetting (spreading), the contact angle is  $0^\circ$ . When the angle is lying between  $0$  and  $90^\circ$ , the solid is wettable and above  $90^\circ$ , it is not wettable. For ultrahydrophobic materials with the so-called lotus effect, the contact angle comes up to the theoretical limit of  $180^\circ$ . The contact angle is significant in processes where the extent of the phase contact between liquid and solid substances is required to be considered such as coating, painting, cleaning, printing, hydrophobic or hydrophilic coating, bonding, dispersing etc.



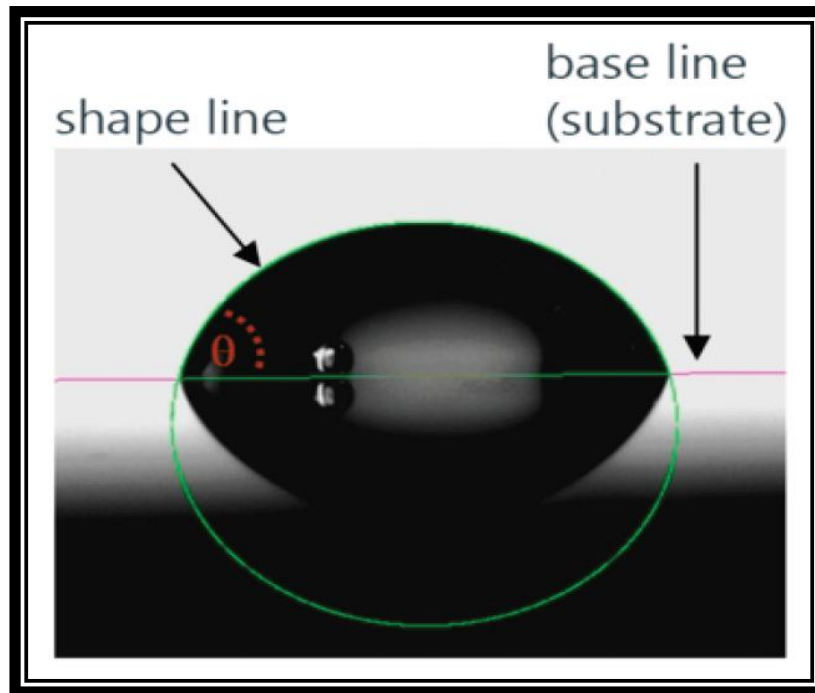


**Figure 2.10: Sessile drop fitted with fitted contour**

Contact angle measurements were attempted on Drop Shape Analysis (DSA) system; Model DSA10MK2 from Kruss GmbH, Germany. DSA is an image analysis method in order to find out the contact angle from the shadow representation of a sessile drop and the surface tension or interfacial tension from the shadow image of a hanging drop. A drop is placed onto a solid sample (sessile drop) or is positioned at the tip of a needle (pendant or hanging drop). A picture of the drop is taken with a camera and reassigned to the drop shape analysis software. A contour recognition is initially carried out based on the grey-scale analysis of the image. In the second step, a geometrical model relating the drop shape is fitted to the contour. The contact angle is given by the angle between the calculated drop shape function and the sample surface, the projection of which in the drop image is referred to as the baseline as shown in Fig. 2.10.

### 2.3.2 Atomic Force Microscopy (AFM)

Scanning Probe Microscopy (SPM) is a technique wherein a sharp probe is moved backward and forward across a sample surface to acquire a 2D or 3D image in a manner analogous to the creation of image on a television screen [16]. Atomic Force Microscopy (AFM) was used in this work to take surface images of the polymeric layers. AFM is a sort of SPM that was initially used in 1986 to look at the surface of insulators [16]. Fig. 2.11 shows a schematic representation of the operation of AFM. In this set up, the test sample is positioned on top of a table and instead of moving the probe tip; the table is moved right through the scanning operation. The tip consists of a cantilever with a sharp tip towards the end. The material composition of the tip depends upon the desired scan type, but silicon or silicon oxide is most commonly used. The tip can be layered with gold or other conducting metal, if a conductive tip is required for electrical measurements.

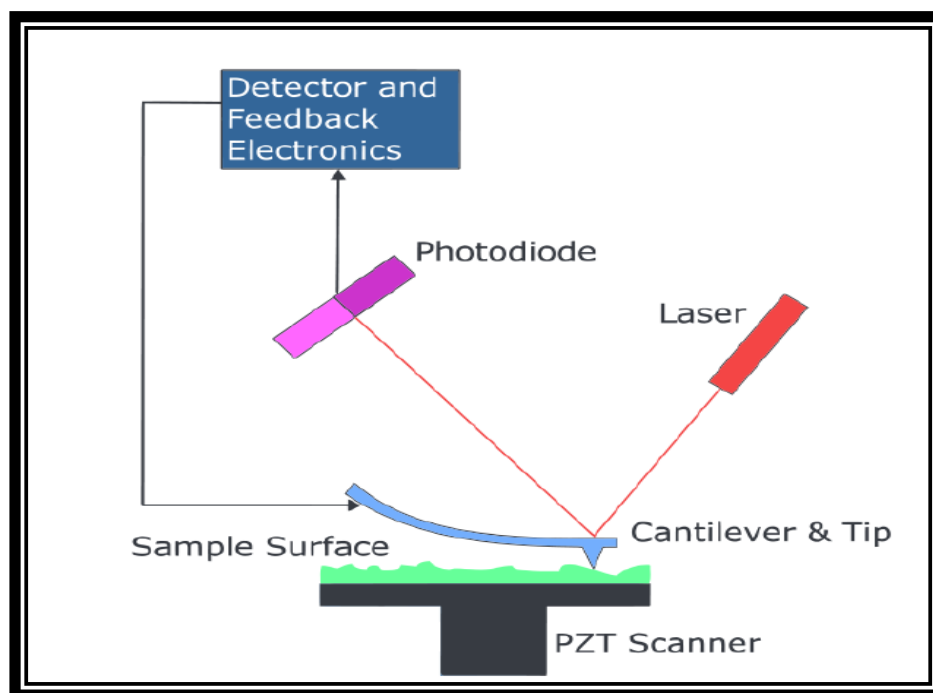


**Figure 2.11: A block diagram of atomic force microscope (Adapted from Reference [17])**

Further, the tip is irradiated with a monochromatic laser and the reflected light is then identified using a four segment photodiode. The location of the reflected beam on the photodiode is to be worked out by the detector and response electronics facilitate the x, y and z arrangement of the cantilever corresponding to the surface of the sample. In certain modes, such as non contact mode, the tip can also be forced to vibrate at its resonant frequency by a piezoelectric transducer; the van der Waals force at the surface enables the tip to be held at an identified distance over the sample as the resonant frequency is reduced [16].

Depending upon the type of sample to be tested and the measurements required, an AFM can be operated in three different modes: contact mode, tapping mode and non-contact mode. In contact mode, the tip is pulled through the test surface, presenting an accurate topographical idea of the surface, but such an operation mode can lead to damage of both the sample and the tip on account of developed forces between the surface and the tip. In tapping mode, the tip has a short contact with the surface prior to being raised; this process is continued over rest of the selected surface of the sample. Such a mode is helpful for scanning the surface of soft or fragile samples. Non contact mode assesses the van der Waals force existing between the surface and the tip to acquire images of the surface. The van der Waals force accumulated upon non-contact mode is much weaker than those in either of the contact or tapping modes and is complemented by additional oscillation of the tip and application of an AC voltage. As numerous trials have been conducted on polymers in this work so, the tapping mode AFM was chosen as the most consistent means to acquire images without spoiling the polymer surface [17].

### 2.3.3 Ultraviolet and Visible light (UV-Vis) Spectroscopy

UV-Vis spectroscopy was employed to consider the absorption and transmission characteristics of the different materials used in the device fabrication. The absorption characteristics of the materials were used to determine the regions with maximum light absorption. UV-Vis spectroscopy evaluates the attenuation of light while the light transmits through a transparent material or when it reflects from a surface [18]. A light beam in the UV-Visible range (200-800 nm) was transmitted through the sample and the absorption is measured. The calculated loss of beam light can be explained in terms of scattering, absorption, reflection or interference. The absorbed light results in electronic transitions and creation of either excitons or free charge carriers thus affecting the electrical properties of the material. Such electronic phenomenon builds up interest in this technique concerning the absorption characteristics of solar cells.

The transmittance ( $T$ ) at each wavelength can be determined from the ratio of the initial radiant power ( $P_0$ ) and the final radiant power ( $P$ ) using following equation 2.2 which is expressed in terms of percentage. It can also be stated in terms of initial and final intensity of the light  $I_0$  and  $I$ , respectively [18].

$$T = \left( \frac{P}{P_0} = \frac{I}{I_0} \right) \times 100 \quad (2.2)$$

The absorbance ( $A$ ) of light in the sample is considered to be linear within certain limits and obeys the Beer-Lambert's law as stated in equation 2.3 [18]:

$$A = a \times b \times c \quad (2.3)$$

Where,  $a$  is the wavelength dependent absorption coefficient,  $b$  is the path length and  $c$  is the analyte concentration. In this work, only thin films have been used on plain

glass or ITO coated glass slides and so, we can ignore the last term as it is insignificant when materials are not in solution form. The absorbance is related to the transmission by equation 2.4 as:

$$A = -\log T = -\log \frac{P}{P_0} \quad (2.4)$$

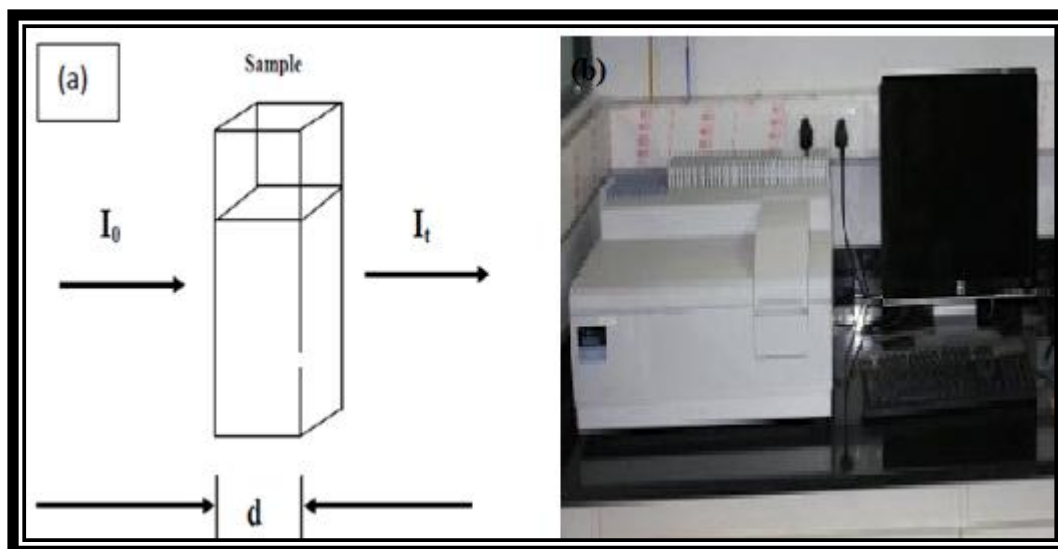


**Figure 2.12: Schematic illustration of the (a) sample assembly and (b) pictorial view of UV-Visible spectrophotometer**

Both  $T$  and  $A$  are unitless quantity and are expressed in arbitrary units, usually as a coefficient between 0 and 1. Perkin Elmer 35 Lambda UV-Vis spectrometer has been used to characterize the samples (Fig. 2.12). This instrument is a dual beam spectrometer that uses a beam splitting device to obtain a background scan of clean substrate prior to testing the thin films on the same substrate and uses a clean reference substrate in the scanning process. This allows the substrate to be corrected automatically during the scanning process and generates a spectrum meant for the film only and not for the substrate [19].

The spectrometer comprises of a light source with monochromator, a chamber in which the sample and reference cells are positioned, and a detector. The working

system includes a double-beam arrangement, such that the source radiation is split into two beams of identical intensity that pass through the two light pathways of one and the same length; one through the reference compartment and other through the sample compartment. Evaluating the intensity of the light which has gone through the reference and sample cell allows for absorption corrections of the empty cells and solvent to be applied to the final sample absorption, and also to include the corrections due to the variations in power of the radiation source.

An ideal light source is the one which has consistent intensity over the whole range of wavelengths. The Perkin Elmer 35 lambda spectrometer uses a tungsten-halogen lamp with a useable wavelength range of 400-1100 nm, and a deuterium gas discharge lamp with a working wavelength range of 190-400 nm. A single grating monochromator is used to sweep through the wavelength ranges. The monochromator is a holographic concave grating with 1053 lines/mm in the center. A single grating monochromator uses broad band light which is diffracted by a slit placed at the effective focus of a curved mirror. The light reflected from this mirror is efficiently collimated (parallel light rays). The collimated light is then diffracted by a grating and reflected off another curved mirror. This second curved mirror refocusses the dispersed light back through an exit slit onto the end object. Rotary motion of the diffraction grating causes the dispersed light to move relative to the exit slit, allowing only certain wavelengths to reach to the sample and reference. UV-Visible spectrometer used in this thesis work has a low stray light optics, a spectral bandwidth as small as 0.5 nm, and high bandpass resolution of 0.5 nm sufficient to fully resolve the absorbance peaks characteristic of all the environmental test procedures, including the narrow bandwidth chlorophylls.

This Perkin Elmer spectrophotometer includes a dual silicon photodiode detector and a peltier-cooled lead sulphide (PbS) photocell. The photomultiplier consists of an evacuated tube containing a cathode which an incoming photon strikes leading to the release of an electron. This electron will strike a dynode which is set at a positive voltage corresponding to the cathode. The dynode releases more electrons, which then strike a succession of dynodes releasing a pour of electrons which eventually strikes on to an anode providing a large quantifiable signal for every received photon. Sample and reference cuvettes are made of quartz, so that absorption is almost nil at the significant wavelengths, and cuvettes remain chemically nonreactive to organic solvents. Since, double-beam optics is used in the spectrometer so, to minimize the error percentage and to have equal or nearly equal absorption of the two cells, comparable cells were employed.

#### **2.3.4 Grazing Incidence X-ray Diffraction (GIXRD) Measurement**

Grazing incidence X-ray diffraction (GIXRD) is a systematic method used for phase identification of a crystalline material and this technique also supplies useful informations on unit cell dimensions and other associated aspects of the crystalline sample. The GIXRD patterns of the samples were recorded on Rigaku Ultima-IV grazing incidence diffractometer (Fig. 2.13) employing  $\text{CuK}_{\alpha 1}$  radiation at a scan rate of  $1^\circ/\text{min}$  and step size 0.02 as of  $2\theta$  ranging  $3\text{-}25^\circ$ . X-ray diffraction measurements of "thin" (1-1000 nm) films using conventional  $\theta/2\theta$  scanning methods by and large generates a weak signal from the film and a strong signal from the substrate. One of the approaches to avoid such a situation and to get stronger signal from the film itself is to carry out a  $2\theta$  scan with a fixed grazing angle of incidence, commonly recognized as GIXRD. This fixed grazing is usually kept at low angle and is carefully

selected so that it remains greater than the critical angle for total reflection of the film material. Compatible with thin films, this technique employs an X-ray beam fixed at a low angle, typically greater than the angle for total external reflection. So, most of the signals will be generated from thin film, whereas negligible penetration into the substrate takes place, ensuring in small, if any signal being produced by the substrate.

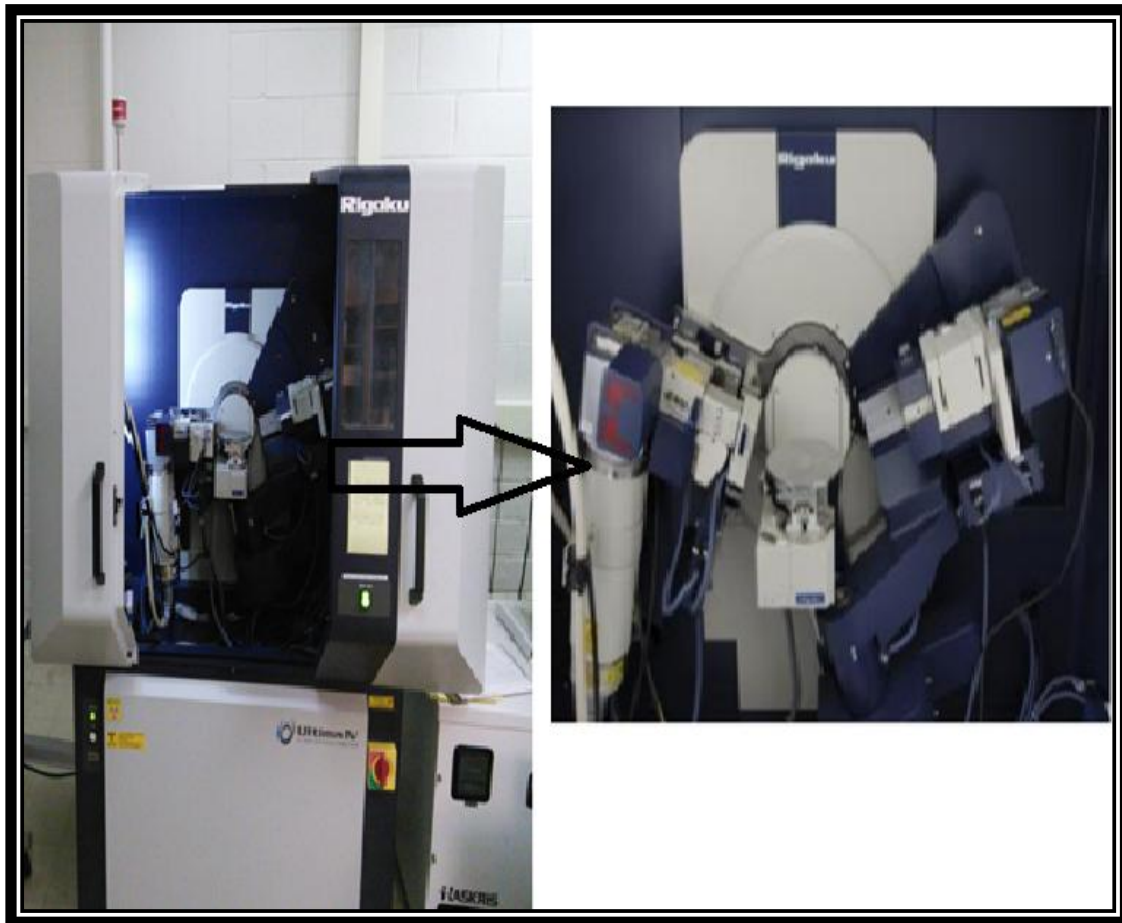


**Figure 2.13: Grazing incidence X-ray diffractometer (GIXRD, Rigaku Ultima IV)**

Grazing incidence diffraction is a scattering geometry, wherein the condition of Bragg is merged with the circumstances for X-ray total external reflection from crystal surfaces. So, such an advanced feature of GIXRD when compared to the other diffraction systems support three orders reduction in the penetration depth (typically



from 1-10 mm to 1-10 nm (10-100Å) of X-rays inside the slab favouring the study of thin film surface. As we know that at high energies of X-ray beam, the refractive index of the majority of materials is slightly *less than* 1 and therefore, total *external* reflection occurs from a surface, if the incident angle is sufficiently small (typically 1–25 milliradians or 0.05–1.5°, depending on the substrate electron density and the X ray energy). At this instant, the substrate is not completely concealed to X-rays, but only short-lived wave transverses into and scatters from it. The intensity of X-ray becomes highest at the surface, as required. Surface selectivity can be further increased by reducing the incident angle and accordingly making the evanescent wave to emerge faster. So, grazing incidence geometry is thought to be surface selective, i.e., largely avoids scattering from the substrate, and does not require a transparent substrate.

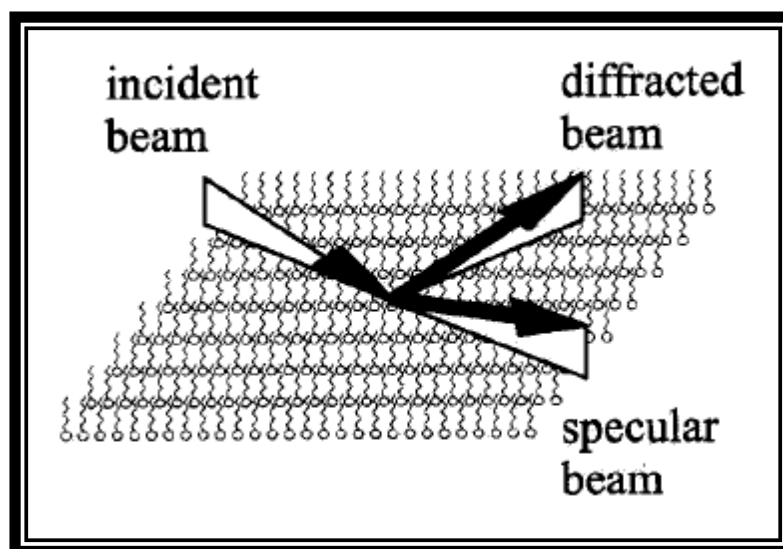


**Figure 2.14: Schematic diagram of a grazing incidence X-ray diffraction**

Fig. 2.14 shows a specular beam; if the incident beam is coming in at angle less than the critical angle for total reflection, the specular beam does not carry useful information. However, lateral order at the surface (or in a monolayer at the surface)

can generate diffraction peaks. The diffracted beam need not to be observed only at grazing exit angles, but may be detected at any angle, resulting in a  $K$  that has both horizontal and vertical components [20].

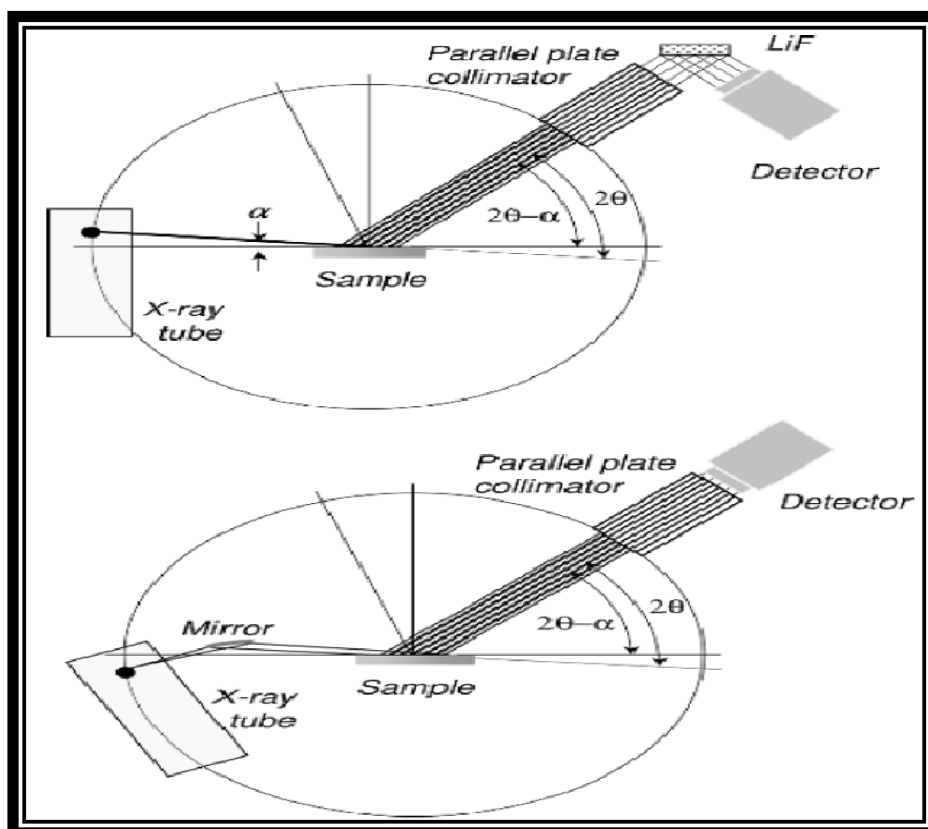


**Figure 2.15: Two diffractometers configurations in GIXRD.**

Three basic components of an X-ray diffractometer are: an X-ray tube, a sample holder and an X-ray detector (scintillation counter). X-rays are produced in a cathode ray tube by heating a filament to produce electrons, which are then accelerated towards the target for bombardment by means of voltage application. When the electrons have gained enough energy to knock out electrons from the inner shell of the target material, distinctive X-ray spectra is formed. These spectra include many constituents,  $K_\alpha$  and  $K_\beta$  being the most standard one among them.  $K_\alpha$  consists of two parts, i.e.,  $K_{\alpha 1}$  and  $K_{\alpha 2}$ .  $K_{\alpha 1}$  is of somewhat shorter wavelength and twofold

intensity as  $K_{\alpha 2}$ . The specific wavelengths are characteristic of the target material (copper Cu, Iron Fe, Molybdenum Mo, Chromium Cr). Monochromatic X-rays essential for diffraction measurements are normally produced by crystal monochromators.  $K_{\alpha 1}$  and  $K_{\alpha 2}$  radiation beams are suitably close in wavelength so that it can be represented by weighted average of the two. Copper with  $CuK_{\alpha}$  radiation wavelength of 1.5418 Å is the most common target material for X-ray generation. These X-ray beams are rendered parallel and focussed onto the sample. In parallel beam method for thin films, X-ray tube remains fixed and only detector moves unlike the Bragg-Bentanno configuration where both the X-ray tube and detector moves. When the detector is being rotated, the intensity of the diffracted X-rays is recorded.

When the geometry of the incident X-rays falling on the sample satisfies the Bragg's equation, constructive interference occurs and a peak in intensity occurs. A detector records and processes this X-ray signal and converts the signal to a count rate which is connected to an output device such as a computer. Fig. 2.15 shows the diffractometer configuration adopted in GIXRD measurements. The geometry of an X-ray diffractometer is designed in such a way that the sample rotates in the path of the collimated X-ray beam at an angle  $\theta$ , while the X-ray detector rotating at an angle  $2\theta$  is mounted on an arm to collect the diffracted X-rays.

### 2.3.5 Photoluminescence Spectroscopy

Photoluminescence (PL) uses light in the near infra-red to the ultra-violet range to excite the molecules of a sample and record its resultant luminescence. Excited state electrons return back to ground state energy levels with the emission of photons or luminescence which is then assessed. Photoluminescence can be categorised into two types namely, fluorescence and phosphorescence. Fluorescence

takes place when an electron in the singlet excited state jumps to the ground state with the emission of photon; this transition is normally a fast process and the lifetime of excited state electron is typically of the order of  $10^{-8}$ - $10^{-9}$  s (i.e., ns time scale). Phosphorescence is known to take place when the photon emission is from an electron in the triplet state to the ground state. And, since the ground state electron has the same spin orientation as the triplet excited state electron, therefore, such an electron relaxation process is said to be forbidden. Excited state lifetimes in such cases are much longer, on an average of milliseconds to seconds.

To probe the energy levels using PL, light energy is used to excite the electrons from the ground state to excited states, as thermal energy alone would not be sufficient to populate the excited states on account of the large energy gap between these states. Photon absorption promotes a ground state electron to one of the vibrational levels in a higher electronic excited state. And, as the electrons are not very stable in the higher excited states, so they relax back to the lowest vibrational level in the first electronic excited state through an internal conversion process within  $10^{-12}$  s of their excitation, which is much more faster than their decay to the electronic ground state. Electron then decays to one of the vibrational levels of the electronic ground state with the emission of a photon. It is this transition from the lowest vibrational level of first electronic excited state to one of the vibrational states of the electronic ground state that is measured and builds up the vibrational structure in emission spectra [21].

Electrons in an excited singlet state can also undertake transition to the triplet state via intersystem crossing with the reversal of its electron spin and thus, excited electron is no longer spin paired with the ground state electron. Intersystem crossing

from a triplet state to the singlet state is forbidden, and so is the decay from the excited triplet state to the ground state, and hence lifetimes are much longer; this is known as Phosphorescence. The vibrational levels seen in the luminescence spectra are similar to those seen in the UV-Vis spectra as the vibrational levels are much the same for the ground and excited electronic states. Two modes of the operation for photoluminescence are excitation and emission spectroscopy.

**Excitation spectroscopy:** In excitation spectroscopy, the wavelength of the incident light is scanned while one wavelength is examined.

**Emission spectroscopy:** In emission spectroscopy, the sample is illuminated at a fixed incident wavelength while the measured light wavelength is varied.

The equipment used in these experiments was a Luminescence Spectrofluorometer from Edinburgh Instruments, UK, Model: F900. Set up used in fluorescence is similar as in UV-Vis measurements, but at this juncture, the emitted light intensity versus the incident light wavelength is measured. Also the emitted light has to pass through a monochromator so as to find out the intensity of particular emitted wavelengths. The Edinburgh Instruments, UK, Model: F900 exploited two Czerny-turner with a grating monochromator. The light source was a 450 W xenon short-arc lamp, along with an off-axis mirror for light collection and focusing. Detection was done by means of a photomultiplier tube.

### 2.3.6 Current Density-Voltage Characterization

Current density-voltage ( $J$ - $V$ ) curves give the most fundamental features regarding the solar cell performance.  $J$ - $V$  data were acquired using the Keithley 2420 source measurement unit. The ammeter can measure current from  $\pm 100$  pA to 3 A and can deliver a direct current (DC) voltage from  $\pm 5$   $\mu$ V to 60 V. The Keithley 2420

was controlled by a computer connected to the device with a standard interface cable. The remote instructions were specified using the programs written with the matlab 7.0.1 graphical language environment. The cell is placed under operating conditions (AM 1.5G solar illumination using Photo Emission Tech. (PET), Inc., Model SS150AAA solar simulator (Fig. 2.16) for all cells investigated in this work) and the current through the cell is measured as a function of voltage using a power source. The measured current is normalized by the active area of the cell, yielding the current density.

As illustrated in Fig. 1.7 (in previous chapter), the  $J$ - $V$  curve supplies the parameters worth for the cell comprising of the open-circuit voltage ( $V_{oc}$ ), the short-circuit current ( $J_{sc}$ ), the power at the maximum power point ( $P_{max}$ ), and the fill factor (FF). The fill factor is the ratio of  $P_{max}$  to  $V_{oc} * J_{sc}$ , and provides a measure of the rectification quality of the diode. The efficiency of the cell is simply the maximum power point divided by the total light-power incident on the cell. Current-voltage ( $I$ - $V$ ) measurements were taken using a two probe arrangement and the data was then used to compute the sheet resistance (resistance of thin film with uniform thickness) and resistivity of the film by the following methodology:

Ohm's Law ( $V = IR$ ) can be re-arranged to determine the resistance  $R = V/I$ , which is the slope of the  $I$ - $V$  graph and from the resistance, the resistivity ( $\rho$ ) can be calculated from equation 2.5 [22]:

$$\rho = \frac{RA}{L} = \frac{VA}{IL} \quad (2.5)$$

Where  $\rho$  is the resistivity in  $\Omega\text{cm}$ ,  $L$  is the distance between electrodes in the cell and  $A$  is the cross-sectional area of film (cross-sectional area split to width ( $w$ ) and thickness ( $t$ ) of the film).



**Figure 2.16:** A pictorial view of solar simulator (Model SS150AAA) alongwith computer controlled Keithley 2420 source measurement unit

Thus, equation 2.5 can be re-written in the following manner:

$$\rho = \frac{RWt}{L} \quad (2.6)$$

The sheet resistance ( $R_{sht}$ ) is generally accepted term for discussing the conductivity of uniform thin films which are being used as transparent electrodes. It has ohms units, but is usually expressed in  $\Omega/Sq$  (ohms per square). It is calculated by dividing the resistivity by the thickness of the film. Because the thickness of film was measured and the dimensions W, L and t are fixed by the aluminium layer deposited using the shadow mask calculating the sheet resistance and resistivity was trivial.



**References**

1. F. Kessler, D. Herrmann and M. Powalla, *Thin Solid Films*, 2005, 480, 491.
2. S. Wiedeman, R. G. Wendt and J. S. Britt, *AIP Conf. Proc.*, 1999, 17, 462.
3. A. G. Aberle, *Thin Solid Films*, 2009, 517, 4706.
4. M. Hoheisel, A. Mitwalsky and C. Mrotzek, *Phys. Status Solidi (A)*, 1991, 123, 461.
5. S. Lee, D. F. Yang and S. Nikumb, *Appl. Surf. Sci.*, 2007, 253, 4740.
6. M. Henry, P. M. Harrison and J. Wendland, *J. Laser Micro Nanoen.*, 2007, 2, 49.
7. J. Kim and S. Na, *Opt. Laser Technol.*, 2007, 39, 1443.
8. F. C. Chen, H. C. Tseng and C. J. Ko, *Appl. Phys. Lett.*, 2008, 92, 103316.
9. H. -L. Cheng, W. -Q. Lin and F. -C. Wu, *Appl. Phys. Lett.*, 2009, 94, 223302.
10. H. Yan and H. Okuzaki, *Synth. Met.*, 2009, 159, 2225.
11. F. C. Krebs, *Sol. Energy Mater. Sol. Cells*, 2009, 93, 394.
12. K. Norrman, A. Ghanbari-Siahkali and N. B. Larsen, *Annu. Rep. Prog. Chem., Sect. C.*, 2005, 101, 174.
13. R. V. Stuart, *Vacuum Technology, Thin Films and Sputtering, An Introduction.*, Academic Press Inc., London, 1983, 151.
14. N. Harris, *Modern Vacuum Practice, Third Edition*, Bell and Bain Ltd., Glasgow, 2007.
15. K. K. Murray, *Schematic of a Diffusion Pump*, 2008, Available from: [http://en.wikipedia.org/wiki/File:Diffusion\\_pump\\_schematic.gif](http://en.wikipedia.org/wiki/File:Diffusion_pump_schematic.gif).
16. D. K. Schroder, *Semiconductor Material and Device Characterization, Third Edition*, John Wiley and Sons, Hoboken, New Jersey, 2006.
17. Q. Overlord, *Atomic Force Microscope Block Diagram*, 2008, Available from: [http://en.wikipedia.org/wiki/File:Atomic\\_force\\_microscope\\_block\\_diagram.svg](http://en.wikipedia.org/wiki/File:Atomic_force_microscope_block_diagram.svg).
18. E. N. Kaufmann, *Characterization of Materials, Vol. 2.*, John Wiley and Sons, Hoboken, 2003, 1392.
19. D. F. Swinehart, *J. Chem. Educ.*, 1962, 39, 333
20. P. Dutta, *Curr. Sci.*, 2000, 78, 1478.

21. T. H. Gfroerer, Photoluminescence in Analysis of Surfaces and Interfaces, in Encyclopedia of Analytical Chemistry, (Ed: R.A. Meyers), John Wiley and Sons, Chichester, 2000, 9209.
22. M. J. Morgan, G. Jakovidis and I. McLeod, Phys. Educ., 1994, 29, 252.



# *Chapter 3*

*Effect of Different Cosolvents  
on the Photovoltaic  
Performance of an Inverted  
Organic Solar Cell*

## EFFECT OF DIFFERENT COSOLVENTS ON THE PHOTOVOLTAIC PERFORMANCE OF AN INVERTED ORGANIC SOLAR CELL

---

- 3.1 Introduction**
  - 3.2 Experimental**
    - 3.2.1 Materials
    - 3.2.2 Device fabrication
  - 3.3 Characterization**
  - 3.4 Results & discussion**
    - 3.4.1 Optical characteristics
    - 3.4.2 Structural characteristics
    - 3.4.3 Morphological characteristics
    - 3.4.4 Photovoltaic characteristics
  - 3.5 Conclusion**
- References**
- 

### 3.1 Introduction

While, visualizing the framework of different potential technological applications such as polymer solar cells (PSCs) or organic light emitting diodes (OLEDs), conjugated polymer electron donor and electron acceptor system is thought to be of most significance [1, 2]. Remarkable importance held by this polymer donor and acceptor combination is because this combination offers feasibility for large scale fabrication by simple solution processing by means of techniques like spin coating, inkjet printing, roller casting etc [3]. Soluble fullerene such as [6,6]-phenyl C<sub>61</sub>-butyric acid methyl ester (PCBM) has been the foremost choice for the electron accepting component on account of its higher electron affinity, while among the conjugated donor polymer with electronic and structural properties similar to semiconductors, poly(3-hexylthiophene) (P3HT) polymer is predominantly studied [4, 5]. Although, individually these components are

finest active materials in the current state-of-art for varied relevance however, mixing of these two potential components offer more attractive structural, electrical, and optical properties that can be exploited for advancement of existing technologies [6].

The use of solvent-cosolvent mixture for systematizing the P3HT:PCBM blend has led to improved photovoltaic performance with more defined control over the crystallinity and phase separation of the blended domains. The cosolvent, which is introduced in small quantity to the blend, controls the aggregation of P3HT in the blend mixture on account of the poor solubility of P3HT chains in this added cosolvent [7]. The nature and quantity of cosolvent added will drive the control over the crystallinity, domain size and orientation of polymer and also dictates the miscibility of donor and acceptor materials. So, the selection of solvent system utilized for active layer preparation is very important for building highly efficient OSCs based on poly(thiophene) polymer/fullerene blends [8, 9]. As different solvents have different intrinsic capacities to dissolve the P3HT component, there lies a chance of precise control over the interconnected percolated nanoscale phase separated domains of donor-acceptor with the exploitation of different solvents combination [10].

We intend to achieve a close perceptive of cosolvent addition during active layer preparation in inverted OSCs and its effect on the elementary parameters of device performance. Solvent-cosolvent mixture system primarily dissolves one component (mostly PCBM) of the blended mixture, avoiding interference of this component in the crystallization process of the other component, i.e., P3HT donor polymer. Moreover, study of four different cosolvents was completed so as to find the best solvent mixture for active layer preparation in the inverted architecture device.

## 3.2 Experimental

### 3.2.1 Materials

Poly(3-hexylthiophene) (P3HT) polymer ( $M_w = 87000$  g/mol and  $> 90\%$  head-to-tail RR) and [6, 6]-phenyl C<sub>61</sub>-butyric acid methyl ester (PCBM) were purchased from Sigma Aldrich, St Louis, MO, USA. *Ortho*-dichlorobenzene (*o*-DCB) and cyclohexanone solvents of analytical reagent grade were also procured from Sigma Aldrich. Benzaldehyde, anisole and toluene solvents were obtained from Merck India Ltd. Indium tin oxide (ITO) coated glass substrates with less than 20  $\Omega$ /sq sheet resistance were procured from Moserbaer India Ltd. Zinc acetate dihydrate, ethanolamine and 2-methoxyethanol for zinc oxide (ZnO) preparation were also obtained from Sigma Aldrich. Molybdenum oxide (MoO<sub>3</sub>) and silver (Ag) wire were procured from Central Drug House (CDH).

### 3.2.2 Device Fabrication

ITO coated glass substrates were first cleaned thoroughly for 20 min each in a soap solution at 50°C, demineralised water, acetone and isopropanol sequentially by ultrasonication. Subsequently, after nitrogen drying these substrates were treated in an UV-ozone chamber for 26 min. Inverted OSCs with a layer sequence of ITO/ZnO/P3HT:PCBM/ MoO<sub>3</sub>/Ag were fabricated. Firstly, a 30 nm thick ZnO film was deposited from a 0.5M ZnO solution which has been prepared from zinc acetate dihydrate, 2-methoxyethanol (solvent) and ethanolamine (stabilizer). The deposited layer was then annealed at 250°C to promote ZnO crystallization. The substrates were then moved to a glove box for active layer deposition. The spin coating solution for active layer deposition was prepared by dissolving 37.5 mg P3HT and 22.5 mg PCBM per 2 mL of good solvent *ortho*-dichloro benzene (*o*-DCB) by stirring

overnight on a hot plate at 50°C. Further, 5 vol % of each of the cosolvents cyclohexanone, benzaldehyde, anisole and toluene were then individually added to the above solution of P3HT:PCBM in *o*-DCB and stirred for 2 h prior to spin coating. The active layer was spin coated at 600 rpm for 2 min using the above prepared P3HT:PCBM solution followed by mild annealing for 30 min at 85°C. To complete the inverted OSC device preparation, a 7 nm thick hole transporting layer (HTL) of MoO<sub>3</sub> and a top layer of 150 nm thick Ag were thermally deposited so as to prepare a device having four cells, each with an active area of 0.09 cm<sup>2</sup>.

### **3.3 Characterization**

The photovoltaic performance of devices of area 0.09 cm<sup>2</sup> under a solar simulator (Model SS150AAA Photo Emission Technology Inc.) was obtained using a Keithley (Model 2420) source meter. P3HT:PCBM films prepared with different solvent mixture were studied by using various techniques. The absorption measurements were done using a Perkin Elmer 35 lambda UV-Vis spectrophotometer. Surface morphology was studied using atomic force microscope (AFM) (Model: VEECO DI-3100) with Nanoscope (III) in tapping mode. GIXRD (grazing incidence X-ray diffraction) measurements were done using Rigaku Ultima IV X-ray diffractometer with Cu-K<sub>α</sub> radiation source. Photoluminescence (PL) spectra were recorded at an excitation wavelength of 470 nm using a Luminescence Spectrofluorometer (M/s Edinburgh Instruments, UK, Model: F900).

### **3.4 Results and Discussion**

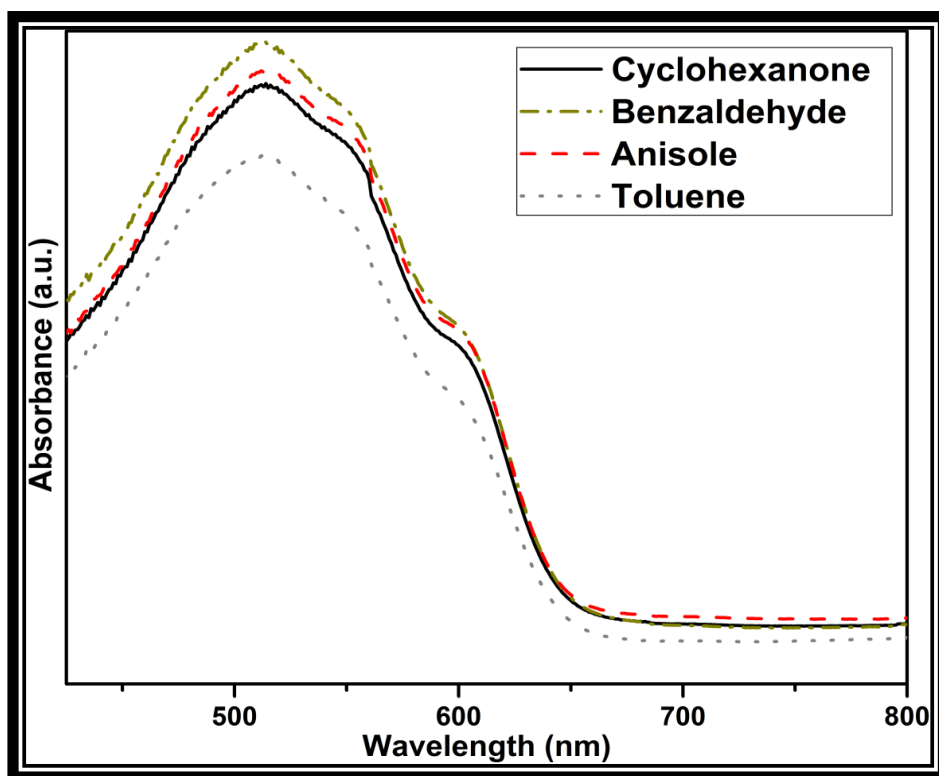
#### **3.4.1 Optical Characteristics**

Fig. 3.1 illustrates the comparative absorption spectra of P3HT:PCBM (1:0.6) layer which is casted using different solvent mixtures. All films characteristically

show one prominent peak at 512 nm proportionate to intrachain transition in P3HT chains, along with two vibronic shoulders attributable to extended conjugated chain length resulting from the disorder-order transformation and interchain stacking interactions, respectively [11]. These absorptions are typical characteristics of a solid state well structured P3HT aggregates. The creation of such ordered aggregates of P3HT progresses by transformation from random coiled phase of polymer chains present in its well dissolved solution (like in *o*-DCB) to extended rod like polymer phases through its solvophobic interaction associated with the addition of a marginal solvent. The extended coplanar polymer chains then arrange themselves in a most organized manner with their hexyl side chains positioned in the interlayer spacing in between these stacked lamellar chains [12].

Again, a difference in absorption intensities in the absorption spectra is found due to the differences in the dissolution of polymer chains in solution mixtures, varying with the polarity and other interactions intrinsic to the solvent. The solubility is expressed in terms of Hansen solubility parameters (HSP) which is mainly having three contributions, specifically, (atomic) dispersive forces ( $\delta$  D), (molecular) permanent dipole-dipole (polar) interactions ( $\delta$  P), and (molecular) hydrogen-bonding interactions ( $\delta$  H). In principle, the solubility parameter of solvent should not differ much from the solubility parameter of solute. In case of P3HT, though the magnitude of Hansen non-dispersive (polar, hydrogen) component  $\delta$  is much smaller than the dispersive component but the magnitude of this non-dispersive component is affecting the solubility of polymer in different solvents. Perhaps this is because of the magnitude of  $\delta$  D of different selected cosolvents which do not differ much from *o*-DCB and chloroform (known good solvents for P3HT) solvents (Table 3.1).





**Figure 3.1: Absorption spectra of P3HT:PCBM films casted from different solvent mixtures**

Addition of benzaldehyde cosolvent (with P3HT ( $S_{P3HT}$ ) and PCBM ( $S_{PCBM}$ ) solubility of 0.1 and 20.8 mg/mL, respectively) resulted in maximum absorption enhancement as suggested by the highest absorption intensity of its 512 nm main peak and (550 and 610 nm) shoulder peaks [13]. This increase in absorption intensity is due to the most ordered growth of P3HT domains in *o*-DCB-benzaldehyde solvent admixture. Such enhanced absorption characteristics in *o*-DCB-benzaldehyde admixture solvent can be explained in terms of poor solubility of P3HT chains in this mixture solvent realized via its solubility parameters. This unfavourable solvophobic interaction between P3HT chains and benzaldehyde solvent promotes the P3HT crystallization in the solution and concurrently, the casted film inherits this organized structure.

Table 3.1: Hansen solubility parameters (HSP) of different solvents

Solvents	<sup>a</sup> $\delta$ D (MPa <sup>1/2</sup> )	$\delta$ P (MPa <sup>1/2</sup> )	$\delta$ H (MPa <sup>1/2</sup> )	S <sub>P3HT</sub> (mg/mL)	S <sub>PCBM</sub> (mg/mL)
CB	19.0	4.3	2.0	15.9	59.5
<i>o</i> -DCB	19.2	6.3	3.3	14.7	42.1
Chloroform	17.8	3.1	5.7	14.1	28.8
Toluene	18.0	1.4	2.0	0.7	15.6
Cyclohexanone	17.8	8.4	5.1	0.2	23.6
Benzaldehyde	19.4	7.4	5.3	0.1	20.8
Anisole	17.8	4.0	7.0	0.1	22.0

<sup>a</sup> $\delta$  D,  $\delta$  P,  $\delta$  H represent dispersive forces, (molecular) permanent dipole-permanent dipole (polar) interactions, and (molecular) hydrogen-bonding interactions, respectively

However, the minimum absorption intensity in case of *o*-DCB-toluene solvent mixture casted layer most likely associates with P3HT chains taking up a randomly coiled conformation and hence restricting its interchain stacking. This variation in conformation is owing to the solubility index of the toluene solvent (S<sub>P3HT</sub>=0.7 mg/mL and S<sub>PCBM</sub>=15.6 mg/mL) that directs more solubility to P3HT chains and lesser solubility to PCBM when compared to other selected cosolvents, restricting the ordered growth of P3HT domains and hence, preventing it from efficient photon absorption [14]. The absorption intensities of anisole and cyclohexanone casted layers are lying in between these benzaldehyde (highest intensity) and toluene (lowest intensity) casted films. Anisole solvent being a more poor solvent for P3HT polymer chains than cyclohexanone cosolvent, P3HT chains undertake faster transition from solvation to aggregation phase or self-assembly process is faster in anisole cosolvent [15]. This rapid disorder-order conversion implies greater intensity of absorption peaks in case of *o*-DCB-anisole casted film compared to *o*-DCB-cyclohexanone film.

The solubility of P3HT in different solvents is recorded in the order: Chlorobenzene > *o*-DCB> chloroform> toluene> cyclohexanone> benzaldehyde> anisole. This suggests that with decrease in solubility, aggregation in solution becomes faster which in turn, increases the absorption by the casted films (excluding their disparity in terms of boiling points).

Again, a comparison of the Hansen parameters of four selected cosolvents with the best available solvents (*o*-DCB, chlorobenzene, chloroform) for P3HT implies that disparity in solubility is mainly caused by difference in their non-dispersive (polar, hydrogen) components. So, while selecting the cosolvent for active layer preparation, the solvent with balanced polar and hydrogen bonding character is best for overall performance of solar device. Though, benzaldehyde and anisole could result in maximum photon absorption among all the solvent mixtures owing to faster aggregation of P3HT but only improved absorption feature cannot guarantee good solar cell performance as other processes such as excitons separation and charge transport are equally important. So, cyclohexanone cosolvent with optimum  $\delta P$ ,  $\delta H$  and  $S_{P3HT}$  provides the intermediate photon absorption but the best device performance.

Fig. 3.2 shows the photoluminescence (PL) spectra of P3HT:PCBM (1:0.6) layer formed using different solvent mixtures. PL emission quenching is suggestive of successful exciton dissociation at donor-acceptor interface in BHJ blend and subsequent charge generation. A higher PL intensity or a noticeable reduction in the PL quenching in anisole casted film reveals larger size of phase separated domains and recombination of photoinduced excitons ahead of it turning up to the interface for dissociation. This is agreeing with the calculation of crystallite size in GIXRD

measurements which showed the P3HT domain size as large as 16 nm in anisole casted film and hence, results in inefficient exciton dissociation. However, comparatively more quenched PL signals in cyclohexanone and toluene casted films indicate closely contacted phase separated domains of small size with larger interface

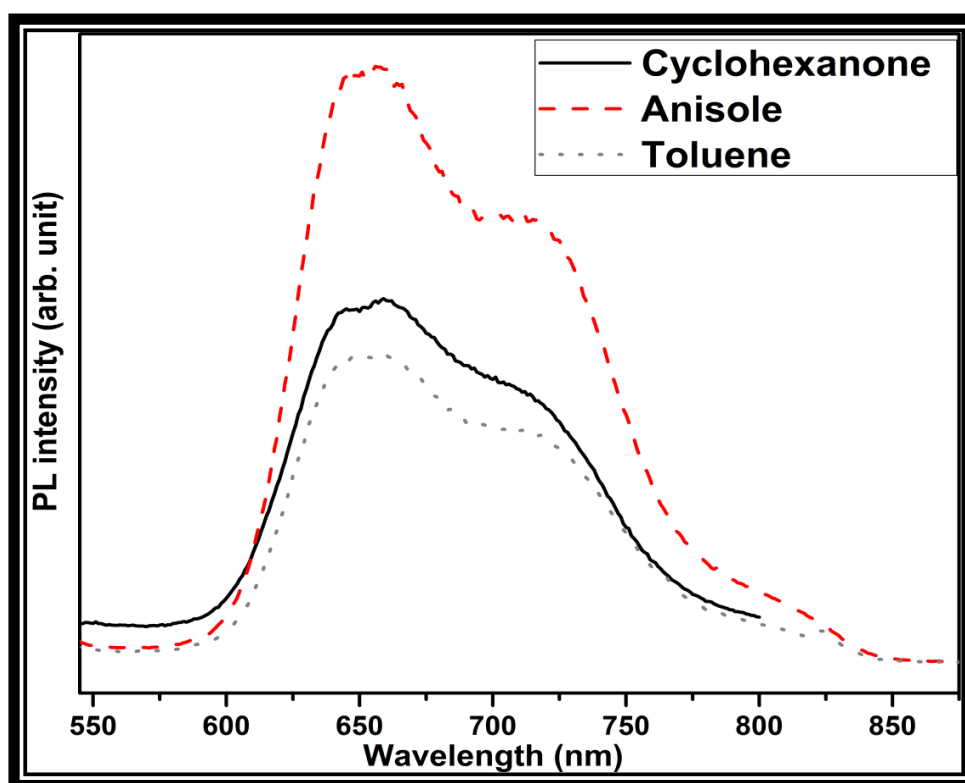


**Figure 3.2: Photoluminescence spectra of P3HT:PCBM films casted of different solvent mixtures**

area for dissociation. Thus, converting excited energy stored in excitons to successive photocurrent rather than passing on useless PL emission. It is presumed that for efficient excitons dissociation, the domain size have to be within the excitons diffusion limit (of the order of 8-10 nm). However, distant PL quenching seen with larger grain sized (~ 12 nm) cyclohexanone cosolvent casted film can be manifested in as the self quenching mechanism in the well organized planar P3HT chains formed [16]. Such efficient polymer structure presents the interchain excitons formed within

the blend structure with an easy energy dissipation channel at a diffusion length farther than the normal excitons diffusion length (8-10 nm) in organic polymers and consequently, deteriorating the prospects of radiative loss (photoluminescence).

### 3.4.2 Structural Characteristics

GIXRD measurements were carried out at a grazing incidence angle of  $0.3^\circ$  to verify the structural order in the casted layers of P3HT:PCBM. In order to have more intense diffraction peaks, the grazing incidence angle was set above the critical angle of P3HT and below the critical angle of the substrate so that X-ray can go through the entire volume of the film. GIXRD confirmed two types of peaks, one of (h00) type and other of the (0h0) type where h can be 1, 2, 3 etc., as indexed in Fig. 3.3.

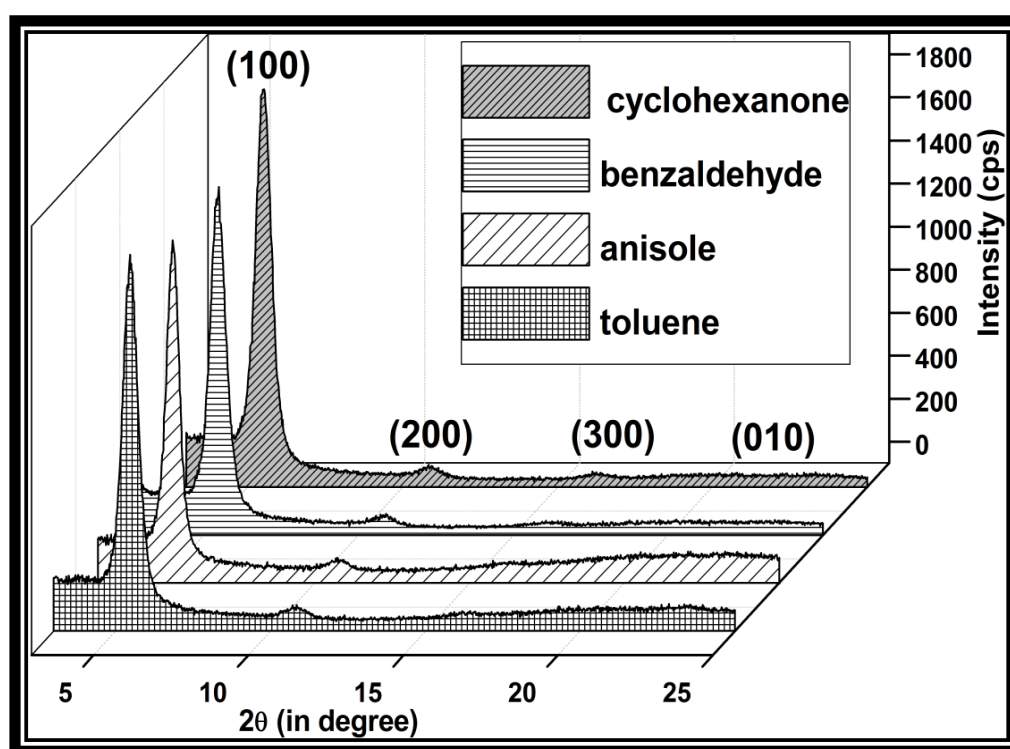


**Figure 3.3: GIXRD profile of P3HT:PCBM films casted from blend solution modified with different cosolvents**

Former type of peaks signifies lamellar intrachain orientation in P3HT chains and other type of peak indicates definite interchain stacking orientation among the

ordered P3HT chains [17]. However, later peaks of planar interchain stacking were less prominent in these cases. These well resolved reflection peaks in the diffraction pattern are characteristics of ordered packing in P3HT crystallites. Comparison of the intensities of (100) reflection peak from different P3HT:PCBM layer could be used as a useful means to correlate the extent of overall crystallinity in the different solvent mixture casted films. Intense (100) reflection peak and higher order reflection peaks of the type (h00) from different solvent mixture casted films recommend preferable molecular orientation of P3HT lamellar structure along the a-axis of the crystallographic plane.

**Table 3.2: Interlayer spacing ( $d_{100}$ ) and P3HT crystallite sizes determined from the (100) diffraction peak in GIXRD pattern**

S.No.	Device	$2\theta$ (in degree)	Interlayer distance ( $d_{100}$ ) (Å)	FWHM	Grain size (nm)
1.	Cyclohexanone modified	5.3	16.48	0.654	12.0
2.	Benzaldehyde modified	5.4	16.26	0.588	13.4
3.	Anisole modified	5.4	16.30	0.491	16.0
4.	Toluene modified	5.4	16.31	0.600	13.1

The most favoured crystal structure of P3HT chains is specific of packing its extended polymer  $\pi$ -system backbone parallel to each other and to the substrate, with their perpendicular hexyl lateral chains in between these stacked layers. Interdigitation among the hexyl side chains from parallel polymer backbone happens inducing the interlayer spacing between the polymer layers [18]. Intensity of (100)

reflection peaks of different casted films were found relatively the same. However, variation was noted in the crystallite sizes and interlayer spacing in the donor molecule. By employing the Debye-Scherrer equation,  $T = K\lambda/\beta \cos \theta$  (where,  $\beta$  = full width half maximum (FWHM),  $\lambda$  = wavelength of X-ray and  $T$  = size of crystal) we could find out the mean P3HT crystallite size in the cyclohexanone casted film as 12.0 nm with interlayer spacing of 16.48Å. Table 3.2 presents the summary of the interlayer spacing ( $d_{100}$ ) intended of (100) reflection peak and crystallite sizes of P3HT in the blend film casted of different solvent mixtures.

All casted films though have the same intensity of the (100) reflection peak, however, the largest P3HT crystallites of size 16 nm was found out from (100) reflection peak at  $2\theta = 5.4^\circ$  in anisole cosolvent with interlayer spacing of 16.30Å. This bigger crystallite size is due to least solubility of the P3HT chains in the *o*-DCB-anisole solvent mixture, which increases the interaction among the P3HT chains in turn. In case of benzaldehyde and toluene solvents, P3HT crystallite size was found to be of the order of 13.4 and 13.1 nm, respectively with interlayer spacing of 16.26 and 16.31 Å. Benzaldehyde cosolvent also being a non-solvent for P3HT chains compared to cyclohexanone and toluene cosolvent, supports faster self assembly process in P3HT and hence, P3HT aggregates of large sizes were formed. So, anisole and benzaldehyde solvent could form larger and closely packed P3HT crystallites while, in case of cyclohexanone solvent smaller P3HT crystallites are covering the surface of film. So, ordered active layer precursor solution produced on account of marginal solvent addition can improve the crystallization of donor molecule in the casted film. Extent of crystallinity in the casted film is controlled by evaporation rate and solubility index of the solvent.



### 3.4.3 Morphological Characteristics

Morphological behaviour of the P3HT:PCBM layer was studied using AFM. Fig. 3.4 illustrates the surface morphology of P3HT:PCBM layers casted by using different solvent mixtures. There is a clear distinction between the characteristic features of brighter P3HT phases and darker PCBM phases.

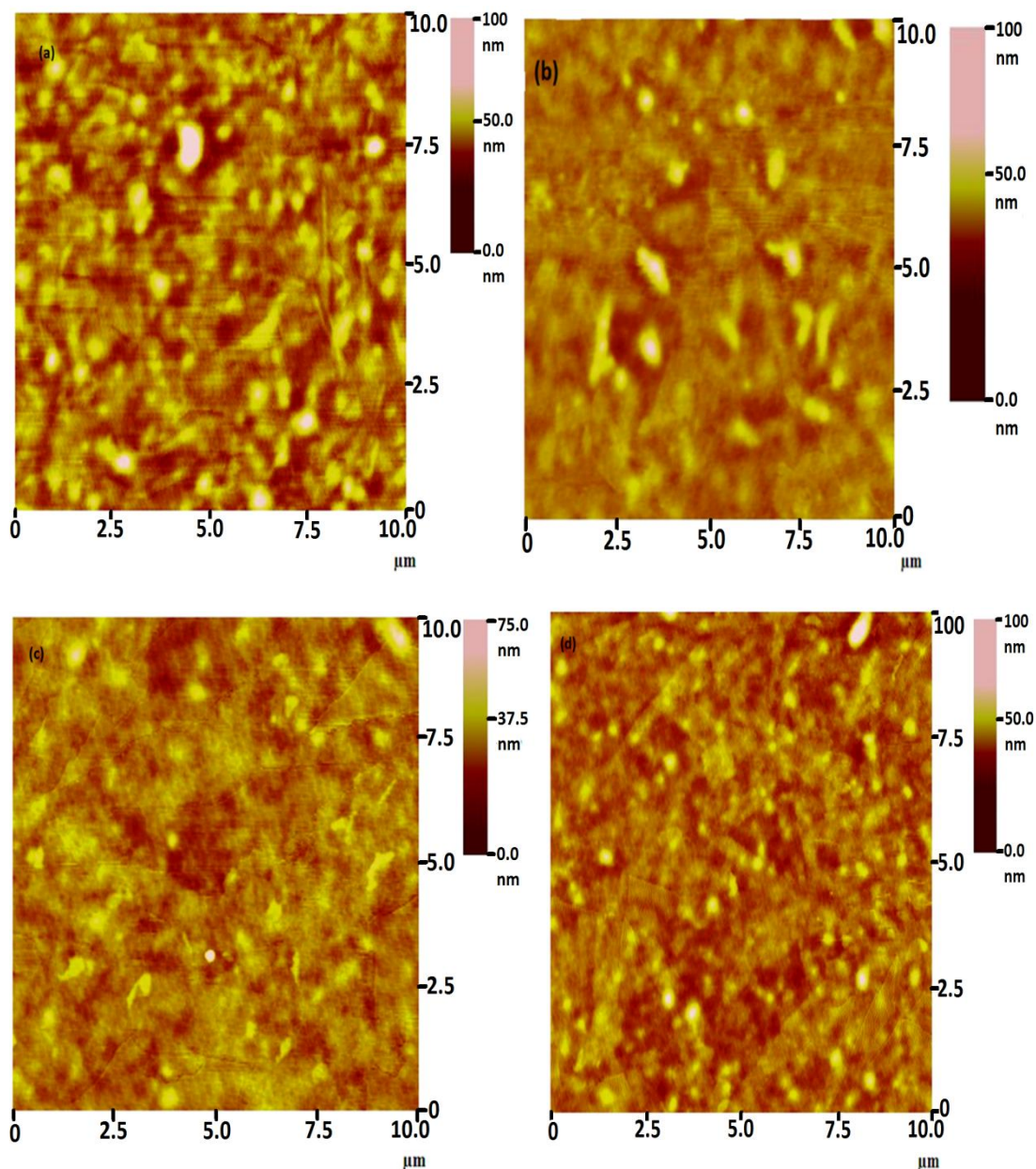


**Figure 3.4:** AFM topographic image scans of P3HT:PCBM films casted of different cosolvents (a) anisole (b) benzaldehyde (c) cyclohexanone and (d) toluene



AFM images reveal that there is a strong influence of solvents used for spin coating on the surface topography of the casted films. The surface of *o*-DCB-anisole casted film features larger P3HT crystallites supporting our data of crystallite size. Benzaldehyde casted film depicts the closely packed larger P3HT crystallites with no apparent phase separation showing smaller interlayer spacing between P3HT chains which is in conformity with GIXRD data while, *o*-DCB-cyclohexanone casted film displays dense coverage of well developed P3HT crystallites [19]. In contrast, toluene casted film has greatly intermixed domains of P3HT:PCBM all through the surface of film also verified by highly quenched PL signals. Ordered structure formation in the active layer is required for presenting improved pathways to carrier transport and simultaneously for gaining higher device efficiency.

#### 3.4.4 Photovoltaic Characteristics

Fig. 3.5 illustrates the current density ( $J_{sc}$ )-voltage ( $V$ ) characteristics of inverted OSCs prepared from different solvent mixtures. Table 3.3 shows the cell characteristics of the devices. The devices primed with cyclohexanone cosolvent showed the excellent performance with an open circuit voltage ( $V_{oc}$ ) of 0.61 V, short circuit current density ( $J_{sc}$ ) of  $8.04 \text{ E-}03 \text{ A/cm}^2$  and fill factor ( $FF$ ) of 61%, following in a power conversion efficiency (PCE)  $3.01 \pm 0.05\%$ . This improvement in PCE is attributed to the increase in photocurrent caused by a combined effect of ordered P3HT crystallite growth, and precise size and phase separation of domains [20]. Although benzaldehyde and anisole casted devices had a greater share of photon absorption, still they demonstrated poor device performance by reason of inefficient photoconversion caused by higher series resistance ( $R_s$ ) and lower shunt resistance

( $R_{sh}$ ) in their devices owing to their large sized P3HT crystallites and larger phase separation.

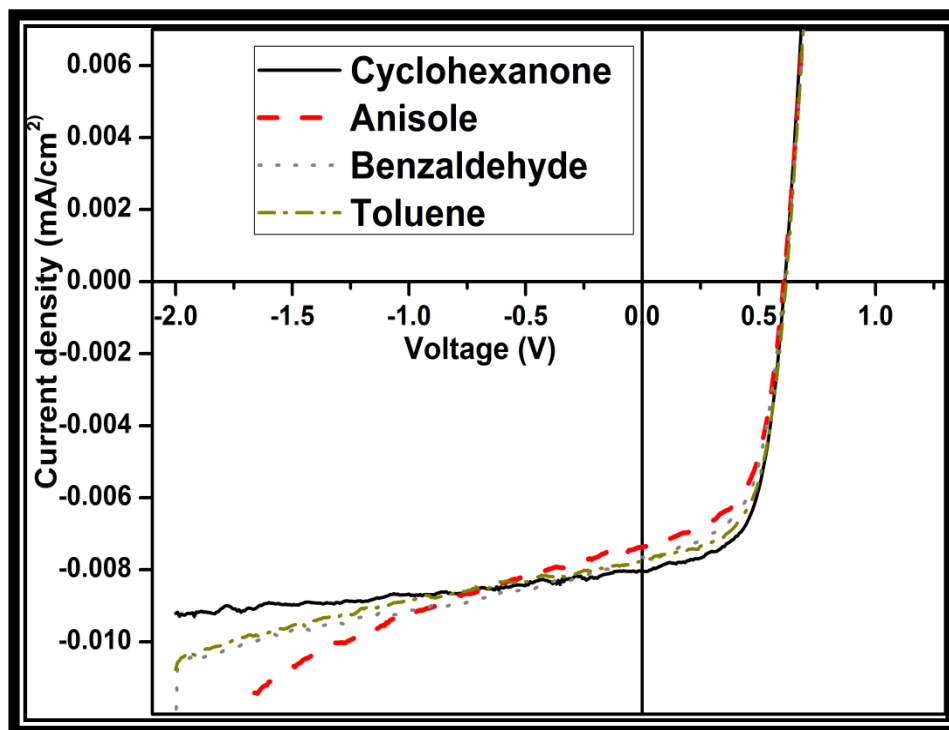


**Figure 3.5: Current density-voltage ( $J$ - $V$ ) characteristic of devices fabricated with active layer casted from different solvent mixtures**

Thus, merely the use of a non-solvent or marginal solvent for active layer preparation may not be enough to raise the efficiency of the device. This particular non-solvent should have an appropriate solubility index so as to produce well crystallized nanoscale separated domains of appropriate sizes for efficient photon harvesting. Also, in toluene casted device  $J_{sc}$  was the limiting factor that can be related to insufficient crystallization of P3HT and hence limited photo absorption due to interference by fullerene.

In contrast to other employed cosolvents, toluene solvent dissolves more P3HT chains and lesser of PCBM so, co-precipitation of both components may lead to intermixed domains of donor-acceptor that limits the apparent crystallization of P3HT

chains in the blend film due to the interference by PCBM. So, the photon absorption and harvesting would be limited as P3HT is the foremost absorber of the photo radiation. Studies carried out in this direction made us to realize the importance of the active layer casting solvent on the crystallinity of the blended domains, photon absorption, charge transport, and final efficiency of the inverted device. *o*-DCB-cyclohexanone solvent mixture was found to be the best combination among the four studied combination of solvent mixtures for active layer preparation. An increased efficiency is due to the optimum solubility of blend materials which leads to efficient crystallization and enhanced photon absorption by the casted layer along with fine separation between the phases for charge generation and transport.

**Table 3.3: Photovoltaic device parameters under AM 1.5 G white light illumination for inverted polymer solar cell with active layer casted with different solvent mixtures**

Substrate	Device	$V_{oc}$ (V)	$J_{sc}$ (A/cm <sup>2</sup> )	FF	%E	$R_{sh}$ ( $\Omega$ cm <sup>2</sup> )	$R_s$ ( $\Omega$ cm <sup>2</sup> )
1	Cyclohexanone	0.61	8.04E-03	0.61	3.01±0.05	700	12
2	Anisole	0.60	7.37E-03	0.57	2.56±0.04	477	15
3	Benzaldehyde	0.61	7.66E-03	0.58	2.72±0.05	600	16
4	Toluene	0.62	7.78E-03	0.59	2.85±0.04	667	13

### 3.5 Conclusion

The effect of different solvent mixtures on parameters inherent to photovoltaic performance of an inverted OSC was studied thoroughly. The solvent mixture

consisting of *o*-DCB and cyclohexanone was realized to provide optimal polymer crystallinity and proportionate lateral phase separation between the blended domains in the BHJ blend of inverted OSC. This results in an increase in the generated photocurrent density  $8.04\text{E-}03 \text{ A/cm}^2$  ensuing in an efficiency as high as  $3.01\pm 0.05\%$ . This increase in efficiency of the inverted device was associated to the collective effect of increased photocurrent generation and improved fill factor. Increased photocurrent generation was ascribed to increased crystallinity and enhanced photoabsorption with cyclohexanone addition to the main solvent.

**References**

1. A. Facchetti, *Chem. Mater.*, 2011, 23, 733.
2. J. -T. Chen and C. -S. Hsu, *Polym. Chem.*, 2011, 2, 2707.
3. F. C. Krebs, *Sol. Energy Mater. Sol. Cells*, 2009, 93, 394.
4. B. Kraabel, D. McBranch, N. S. Sariciftci, D. Moses and A. J. Heeger, *Phys. Rev. B*, 1994, 50, 18543.
5. M. He, J. Ge, M. Fang, F. Qiu and Y. Yang, *Polymer*, 2010, 51, 2236.
6. Y. Wang, W. Wei, X. Liu and Y. Gu, *Sol. Energy Mater. Sol. Cells*, 2012, 98, 129.
7. J. -H. Kim, J. H. Park, J. H. Lee, J. S. Kim, M. Sim, C. Shim and K. Cho, *J. Mater. Chem.*, 2010, 20, 7398.
8. Y. Shao-Peng, L. Na, L. Guang, S. Jiang-Bo, L. Xiao-Wei and F. Guang-Sheng, *Acta Phys. Sin.*, 2013, 62, 014702.
9. M. T. Dang, G. Wantz, H. Bejbouji, M. Urien, O. J. Dautel, L. Vignau and L. Hirsch, *Sol. Energy Mater. Sol. Cells*, 2011, 95, 3408.
10. Y. Yao, J. Hou, Z. Xu, G. Li, and Y. Yang, *Adv. Funct. Mater.*, 2008, 18, 1783.
11. N. Kiriy, E. Ja'hnke, H. J. Adler, M. Schneider, A. Kiriy, G. Gorodyska, S. Minko, D. Jehnichen, P. Simon, A.A. Fokin and M. Stamm, *Nano Lett.*, 2003, 3, 707.
12. W. Xu, L. Li, H. Tang, H. Li, X. Zhao and X. Yang, *J. Phys. Chem. B*, 2011, 115, 6412.
13. F. Machui, S. Langner, X. Zhu, S. Abbott and C. J. Brabec, *Sol. Energy Mater. Sol. Cells*, 2012, 100, 138.
14. F. Reisdorffer, O. Haas, P. L. Rendu and T. P. Nguyen, *Syn. Met.*, 2012, 161, 2544.
15. S. Sun, T. Salim, L. H. Wong, Y. L. Foo, F. Boey and Y. M. Lam, *J. Mater. Chem.*, 2011, 21, 377.
16. A. L. Ayzner, C. J. Tassone, S. H. Tolbert and B. J. Schwartz, *J. Phys. Chem. C*, 2009, 113, 20050.
17. F. C. Chen, C. J. Ko, J. L. Wu and W. C. Chen, *Sol. Energy Mater. Solar Cells*, 2010, 94, 2426.
18. Y. Kim, S. Cook, S. M. Tuladhar, S. A. Choulis, J. Nelson, J. R. Durrant, D. D. C. Bradley, M. Giles, I. McCulloch, C. -S. Ha and M. Ree, *Nat. Mater.*, 2006, 5, 197.

19. L. Dan, X. Y. Dong, Y. He, Z. J. Ping and A. X. Cheng, *Chin. Sci. Bull.*, 2012, 57, 3436.
20. J. Liu, S. Shao, H. Wang, K. Zhao, L. Xue, X. Gao, Z. Xie and Y. Han, *Org. Electron.*, 2010, 11, 775.



# *Chapter 4*

*Optimization of Processing  
Conditions of Cosolvent  
Addition in the Active Blend  
of Inverted Organic Solar Cell*

# 4

## OPTIMIZATION OF PROCESSING CONDITIONS OF COSOLVENT ADDITION IN THE ACTIVE BLEND OF INVERTED ORGANIC SOLAR CELL

---

- 4.1 Introduction**
  - 4.2 Experimental**
    - 3.2.1 Materials
    - 3.2.2 Device preparation
  - 4.3 Characterization**
  - 4.4 Results & discussion**
    - 4.4.1 Effect of ageing of precursor solution
    - 4.4.2 Morphological characterization
    - 4.4.3 UV-Visible absorption measurements
    - 4.4.4 Grazing incidence X-ray diffraction measurements
    - 4.4.5 Photovoltaic characteristics
  - 4.5 Conclusion**
- References**
- 

### 4.1 Introduction

The discovery of semiconducting conjugated polymers by Heeger, Shirakawa and Mac Diarmid set the route for the growth and development of research on organic solar cells (OSCs) based on a semiconducting polymer donor and fullerene acceptor combination [1]. Compared to their inorganic semiconductor counterparts, organic semiconductors such as conjugated polymers have the advantage of low cost solution processing, simple large scale production and also present the possibility of flexible device fabrication. However, to achieve a competitive space in the energy sector and to become a promising replacement to the expensive silicon technology, organic semiconductors still have a long way to go [2, 3].

The issues of limited life time and smaller power conversion efficiency related with the polymer based solar cells limit their prospects of commercialization. At the



beginning of organic solar cells research and development, an efficiency of 1% was accounted for the bilayer organic donor-acceptor combination. This structure however, suffered from high photocurrent loss caused by insufficient donor-acceptor interfaces in the vicinity of the photo generation point, as the photo generated excitons in organic materials can diffuse only short distances of up to 8-10 nm before they undergo a radiative or non-radiative decay. To overcome this limitation of reduced donor-acceptor interfaces in a bilayer structure, a new structure with homogeneously distributed donor-acceptor interfaces throughout the active layer was investigated [4].

With the advent of bulk heterojunction (BHJ) concept in the photoactive layer composed of conjugated polymer donor and soluble fullerene acceptor, advantage of thicker photoactive layer implementation can be extended to organic solar cells (OSCs). Also, distinct from their inorganic counterparts, organic materials need external driving force for excitons separation and charge generation from their strongly bounded electron-hole pair (excitons). So, BHJ model with intermixed domains presents extended interfacial area between the blended photoactive nanophases for bulk separation of photogenerated excitons [5]. As a whole, the BHJ blend of poly(3-hexylthiophene) (P3HT) donor and [6, 6]-phenyl C<sub>61</sub>-butyric acid methyl ester (PCBM) acceptor has been the most commonly proposed system for photocurrent generation.

In the recent past, there has been a great improvement in the efficiency of OSC with this donor-acceptor mixture in its photoactive layer [6]. One of the key parameters which is continuously explored for further possible improvements in the performance of solar devices prepared with this donor-acceptor pair is the morphology transformation with the changes in processing parameters. Best possible

morphology pertaining to the donor-acceptor pair corresponds to the balanced equilibrium between the crystallinity (molecular ordering) within each phase and nanoscale phase separation between its intermixed domains [7, 8]. Definite order in the donor and acceptor moieties dictates photoabsorption and carrier mobility. Furthermore, bi-continuous interpenetrating phases separating the nanoscale donor-acceptor domains contribute to the successful exciton dissociation and bidirectional pathways for carriers transport to their corresponding electrodes [9].

Solution processing method for active layer preparation allows control over many process parameters including blending ratios of the two components, solvent system employed; post treatment processes such as thermal and solvent annealing etc., for organizing the photoactive blend morphology [10]. Though, post treatment methods such as solvent vapour annealing and thermal annealing have shown to be beneficial for improving the morphology and hence, the efficiency of OSCs. However, such post treatment processes may not be effective for large scale manufacturing practices.

Further, solvent system engaged in preparing active layer spin coating solution has enormous effects on the morphology of the casted thin film. Earlier practice was used to get a single solvent solubilising for both the components of blend. Such a practice though may appear straightforward however; it is allied with the difficulties of intervention from one component in the crystallization process of the other component in the blend. Moreover, the different materials have different solubilities in a particular solvent, so single solvent may not be suitable to accomplish the required part.

Recently, solvent-cosolvent mixture approach has been recognized to provide the desired morphology to the photoactive blend. In this approach, a host solvent dissolving both the components of the mixture evenly, and the second solvent is also added which presents incomplete solubility to one of the component (predominantly P3HT component) [11]. As a result, PCBM can remain dissolved in the solution mixture so that undissolved P3HT chains start to crystallise out first in the solution without being hindered by the completely dissolved component (PCBM).

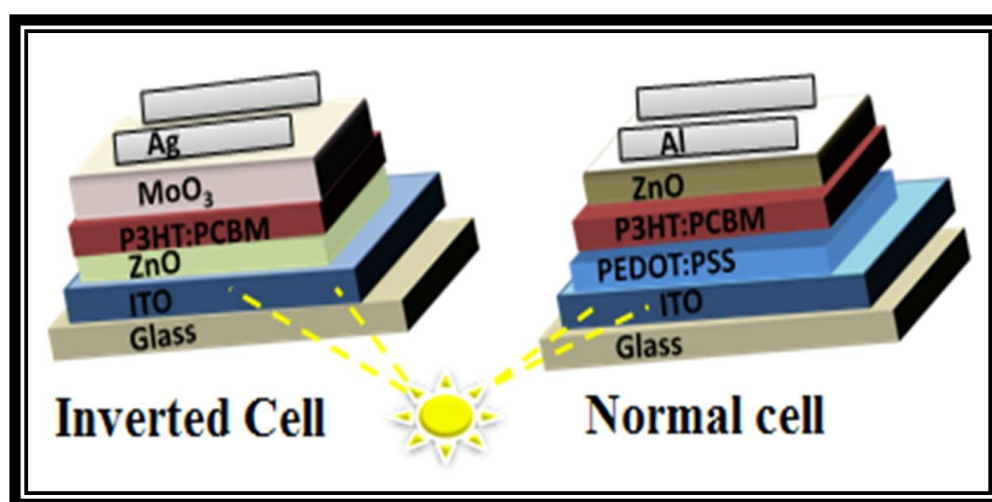


**Figure 4.1:** Schematic representation of inverted and normal architecture of polymer based solar cell

Until now, this solvent-non-solvent mixture approach has been opted to practice for modifying the morphology of the active layer in normal architecture of OSCs [12]. However, declining prospects of the normal architecture in OSCs as a result of its non-stability and degradation from oxygen and moisture in the atmosphere shifted the focus towards inverted configuration. This non-stability is attributable to the existence of low work function reactive metal like aluminium at the top, interfacing with the air. Replacement of low work function metal by a high work function metal like silver (Ag) or gold (Au) can work to stabilize the overall system

from the damaging effect of moisture or air [13]. Fig. 4.1 shows a recognized layer sequence in inverted and normal architecture of polymer based solar cells.

As, there has been very limited reports on morphological modification of the photoactive blend in inverted OSC via solvent mixture approach therefore, we considered performing a detailed study on the effect of *ortho*-dichlorobenzene (*o*-DCB)-cyclohexanone solvent mixture on P3HT:PCBM layer in case of inverted OSC. Such a modification is worth considering, as the underlying and overlying layers placed with the active layer in inverted configuration will cause the P3HT:PCBM mixture to act in a different way to the solvent mixture modification from that of the normal configuration OSCs.

## 4.2 Experimental

### 4.2.1 Materials

Poly(3-hexylthiophene) (P3HT) polymer ( $M_w=87000$  g/mol), [6, 6]-phenyl  $C_{61}$ -butyric acid methyl ester (PCBM), *ortho*-dichlorobenzene (*o*-DCB), cyclohexanone, zinc acetate dihydrate, ethanolamine and 2-methoxyethanol were procured from Sigma Aldrich. Solvents used in this study like were of analytical grade. Indium tin oxide (ITO) coated glass substrates ( $5 \times 5$  cm) with sheet resistance of less than  $20 \Omega/\text{sq}$  were purchased from Moserbaer India Ltd. Both, molybdenum oxide ( $\text{MoO}_3$ ) and silver (Ag) wire were obtained from Central Drug House (CDH), India.

### 4.2.2 Device Preparation

Constituent layer structure in inverted polymer based solar cells comprises of ITO/ ZnO/P3HT:PCBM/ $\text{MoO}_3$ /Ag. ITO coated glass substrates were first patterned using a laser scribe and cleaned thereafter via ultrasonication for 20 min each in a

soap solution at 50°C, demineralised water, acetone and isopropanol in succession. The cleaned substrates were then dried using nitrogen and treated further in an UV-ozone chamber for 26 min. Firstly, a ZnO (30 nm) layer was deposited on ITO using a 0.5M ZnO solution prepared by mixing (0.46 g) zinc acetate dehydrate with ethanolamine (stabilizer) and 2-methoxyethanol (solvent). Subsequent curing of the deposited ZnO layer was carried out at 250°C for 10 min. Active layer spin coating solution was prepared by dissolving 18.7 mg of P3HT polymer and 11.3 mg of PCBM in 1 mL of good solvent, i.e., *o*-DCB by means of stirring overnight at 50°C on a hot plate. For active layer modification, cyclohexanone cosolvent (5 vol %) was added to the above prepared active layer spin coating solution and stirred further for 2 h. Active layer was then spin coated using the solution and deposited layer was cured at 85°C for 30 min. Thereafter, 7 nm thick molybdenum oxide (MoO<sub>3</sub>) and 150 nm thick silver (Ag) layers were thermally deposited at a deposition rate of 0.5 and 1.0 Å s<sup>-1</sup>, respectively, in a vacuum chamber maintained at a base pressure of 5 × 10<sup>-6</sup> mbar. Final photovoltaic devices with an active area of 0.09 cm<sup>2</sup> were prepared with and without cosolvent modification in the active layer. Further, a comparison of the performance of these devices with and without cosolvent modification was made.

### 4.3 Characterization

Device preparation was carried out in the nitrogen environment within a glove box from Jacomex with pressure gradient of 3.0 mbar and oxygen level of 0.3 ppm. The current density (*J*)–voltage (*V*) characteristics of the photovoltaic devices were measured using a Keithley (Model 2420) source meter under a solar simulator (Model SS150AAA Photo Emission Technology Inc.) equipped with AM 1.5 G filter with an illumination intensity of 100 mW cm<sup>-2</sup>. The UV–Visible absorption measurements

were carried out using a Perkin Elmer 35 lambda UV–Visible spectrophotometer. Surface morphology studies were done using atomic force microscope (AFM) (VEECO DI-3100) with Nanoscope (III) in tapping mode. Grazing incidence X-ray diffraction (GIXRD) measurements were carried out using Rigaku ultima IV X-ray diffractometer ( $\lambda=1.54 \text{ \AA}$ ) with Cu-K $_{\alpha}$  radiation source at grazing incidence angles of  $0.11^{\circ}$  and  $0.3^{\circ}$ .

## 4.4 Results and Discussion

### 4.4.1 Effect of Ageing of Precursor Solution

P3HT:PCBM blend solution in solvent-non solvent mixture assumes P3HT aggregation like a pure P3HT bulk solution in a non-solvent or marginal solvent. The aggregation of P3HT is identified by conversion of P3HT from coil to extended rod on account of solvophobic interaction with a marginal solvent and subsequently,  $\pi$ - $\pi$  stacking of these extended chains [14]. Aggregation can be settled as disordered to ordered transformation of crystallizing P3HT chains in a marginal solvent. Cosolvent used in this work is cyclohexanone. This solvent is a marginal solvent for P3HT providing limited or poor solubility to P3HT chains and more solubility to PCBM aggregates.

Aggregation process of P3HT in P3HT:PCBM blend solution in *o*-DCB-cyclohexanone solvent mixture will be different from the aggregation of P3HT chains in pure P3HT solution caused by intervention from the dissolved PCBM portions in the former [15]. Such an aggregation on marginal solvent addition in P3HT:PCBM solution is manifested in terms of increased absorption and better P3HT crystallinity together with changes in the colour of the solution from orange to purple. This process of aggregation is more pronounced with ageing, i.e., retaining the solution for

an adequate period at room temperature, marked by increased viscosity and darkening of solution colour attributable to growing amount of non-dissolved P3HT segments in the solution [16]. But, an extensive ageing and higher fraction of cosolvent can result in gelling of the solution accordingly, making the solution unsuitable for the spin coating process [17]. Thus, an optimization of the ageing period and cosolvent amount is required for efficient casting of the active layer.

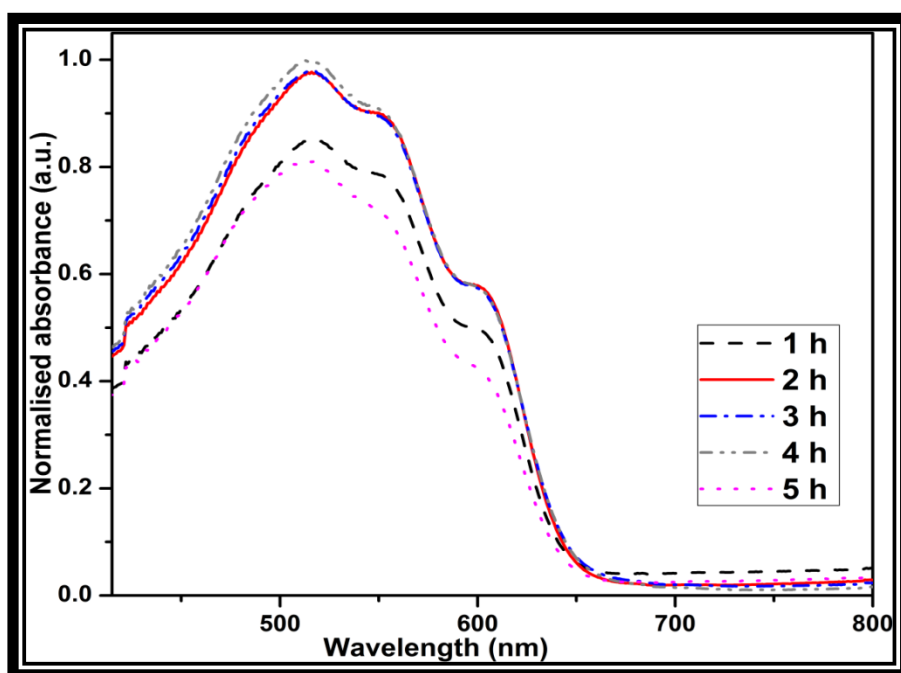


**Figure 4.2:** Absorption spectra of P3HT:PCBM films casted of precursor solutions aged for different time periods in *o*-DCB-cyclohexanone mixture

The absorption spectra of P3HT:PCBM films casted from *o*-DCB-cyclohexanone solvent mixture aged for different time period was measured (Fig. 4.2) for establishing the dependence of ageing time on aggregation and successive absorption enhancements. The absorption spectra of the P3HT:PCBM films were characterized by main peak around 512 nm, with two “shoulders” towards the higher wavelength region. The main peak is distinctive of intrachain transitions in P3HT chains supporting decreased chain entanglement. Absorption shoulders in the higher

wavelength are inter-related to extended chain length absorption and interchain lamella stacking [18]. With ageing, these spectral features seem to be more prominent. From the absorption spectra, it's evident that there is a substantial improvement in absorption with ageing for 1 to 4 h at room temperature representing growth of ordered P3HT structures. However, a decrease in the absorption was perceived in the solution aged for 5 h probably due to larger aggregate formation with no further development of ordered P3HT chains [19]. Again, as the variation in absorption intensity between 2, 3 and 4 h aged solution was modest. So, for our study, we optimized the ageing period to be 2 h, as longer treatment time may not be a realistic proposal for large scale production practice.

To attain better viewpoint on the effect of ageing and crystallinity improvement, grazing incidence X-ray diffraction (GIXRD) measurements were performed for P3HT-PCBM films at a grazing incidence angle of  $0.3^\circ$  as shown in Fig. 4.3. GIXRD can give important facts about the crystallinity of P3HT in the blend film. An indication of crystallinity in P3HT:PCBM films casted from precursor solution aged for different times (1-5 h) was evaluated by comparing the (100) reflection peak intensities observed at  $2\theta$  value of  $5.426^\circ$ . Further, 2 h aged precursor solution with highest (100) peak intensity reveals most well organized arrangements of P3HT chains [20]. Also, equally intense higher order diffractions in films prepared from 2 h aged solution suggest higher crystallinity and self organization ability in the blend film. So, aging time could be used as a management control towards attaining highly oriented crystals of P3HT in P3HT:PCBM blend films via solvent mixture approach. Such a molecularly ordered film of P3HT:PCBM can be taken advantage of, as an active layer of OSCs.



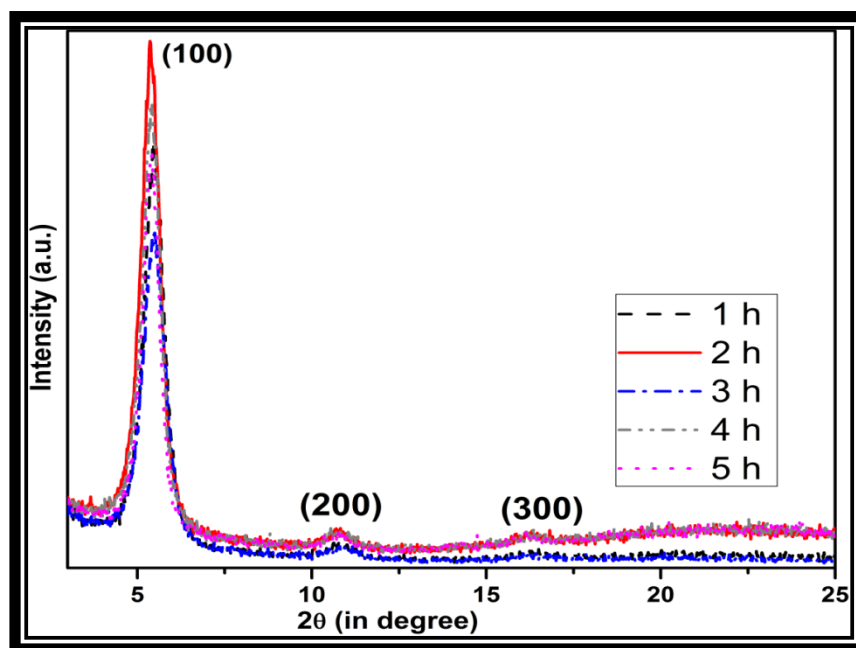


**Figure 4.3:** GIXRD patterns for P3HT:PCBM films casted of precursor solutions aged for different time periods in *o*-DCB-cyclohexanone mixture

Again, the amount of marginal solvent was also optimized to be 5 vol %. It is noticed that cosolvent amount lesser than 5 vol % could not lead to significant crystallization in the blend film. And also, larger amount of the cyclohexanone cosolvent would give rise to greater non-dissolved P3HT crystallites in the precursor solution and subsequent gelling of the solution occurs on keeping the same for few hours. The detailed studies have been carried out to see the effect of introducing modified P3HT:PCBM layer as an active layer in case of inverted OSC with an optimized ageing time (2 h) and cosolvent amount (5 vol %).

#### 4.4.2 Morphological Characterization

Fig.4.4 a & b shows the topographical AFM image of P3HT:PCBM film without any modification and with cyclohexanone addition, respectively. Surface images confirm the significant dependence of film morphology on solvent mixture used to dissolve the blend materials.

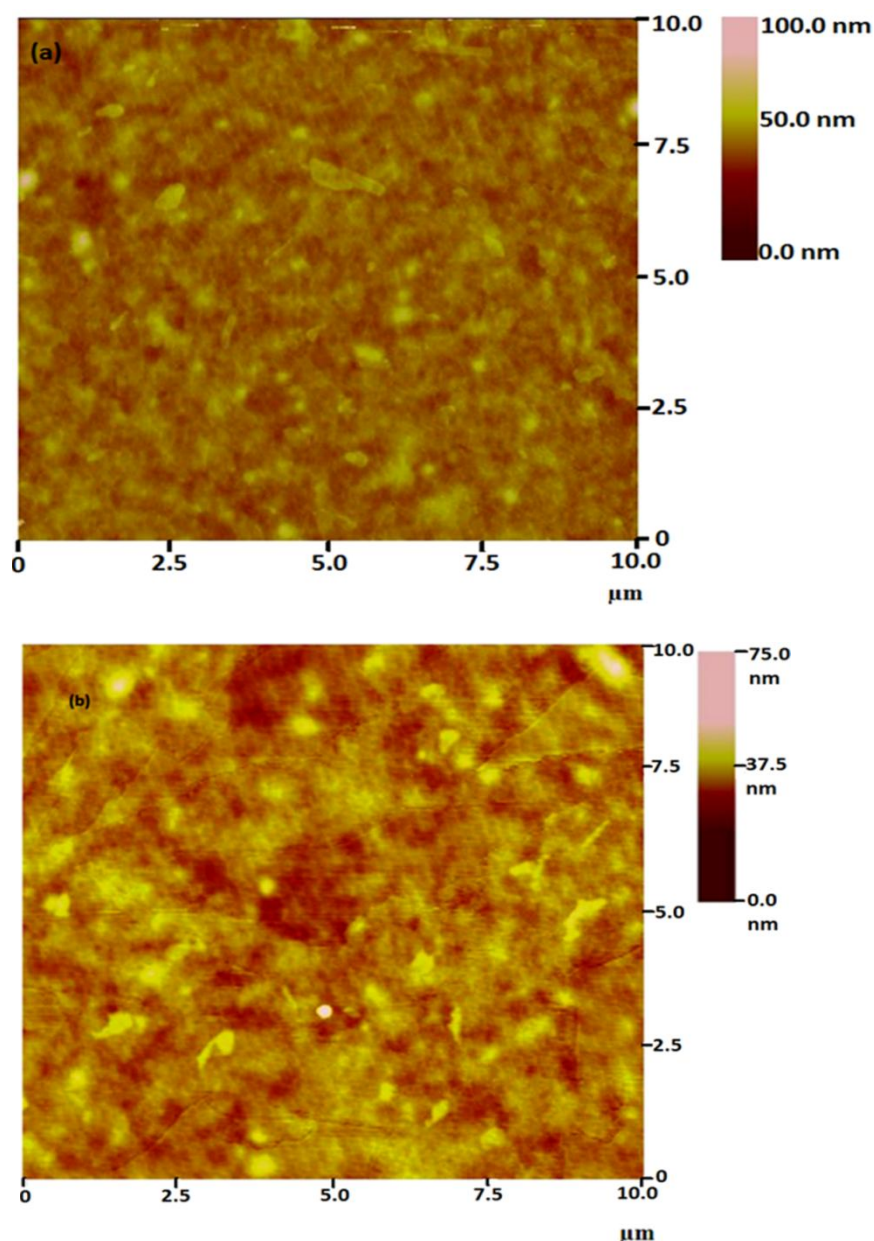


**Figure 4.4: Tapping mode AFM image scans of P3HT:PCBM films (a) without modification (b) with cyclohexanone addition**

In case of conventional film prepared with single good solvent (*o*-DCB) dissolving both the components of the mixture, no apparent separation between P3HT (brighter region) and PCBM (darker regions) phases was noticeable from AFM micrographs. Such a homogenous feature all through the conventional film could possibly be resulting from co-precipitation of both components from the mixture at

the same time. However, with further addition of cyclohexanone, the extent of phase separation between two components seems to be improved. Such a phase separation could be a result of preferential crystallization and aggregation of P3HT component directing further demixing of the phases on spin casting [21]. Such a lateral phase separation between the components of the blend at all depths of the film is required for efficient dissociation of the photoinduced exciton for charge generation. So, cyclohexanone addition seems to be beneficial for giving the desired morphology in the blend film.

#### 4.4.3 UV-Visible Absorption Measurements

The absorption spectra of P3HT:PCBM films were assessed to understand the effect of cyclohexanone addition on the relative light absorption properties and crystal structure arrangement of P3HT chains in the active layer. Fig. 4.5 shows the UV-Visible absorption characteristics of P3HT:PCBM layer from a solution with and without cyclohexanone addition. As discussed earlier, the absorption spectra feature one main peak at around 512 nm and two absorption shoulders in the lower energy region equivalent to the absorption by highly organized solid P3HT aggregates. Upon cyclohexanone addition, a small shift in the peak to higher wavelength side and an increase in intensities of absorption peaks (main absorption peak and low energy vibronic bands) were seen.

Absorption spectra of modified film identify the growth of well ordered P3HT crystals. This well controlled growth in P3HT crystals is sustained by coil to extended rod spontaneous transition which is induced by the poor interaction between polymer and solvent. This transformation leads to aggregation in polymer domains by stronger  $\pi$ - $\pi$  interaction set among these extended P3HT chains [22]. However, in case of

conventional P3HT:PCBM film, a transformation from coil to rod does not seem to be reasonable due to the well dissolved P3HT chains in *o*-DCB which is a good solvent.

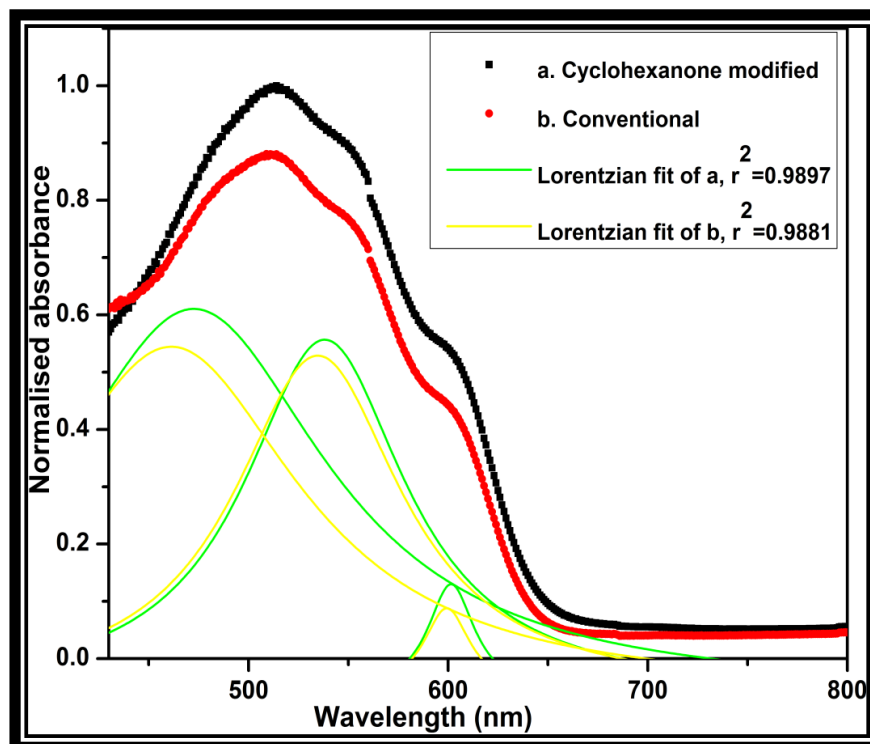


Figure 4.5: Absorption spectra of P3HT:PCBM films with and without cosolvent

#### 4.4.4 Grazing Incidence X-ray Diffraction (GIXRD) Measurements

To study the effect of cyclohexanone addition on the crystalline structure and molecular ordering in the active layer of inverted OSC, GIXRD measurements were carried out on spin coated films of P3HT:PCBM. GIXRD measurements were done at two grazing incidence angles for outlining the structural attributes via depth profiling of P3HT:PCBM thin film. As per the recent literature available on GIXRD measurements using lab instruments for stronger scattering films, it is suggested to carry out the depth profiling of P3HT:PCBM thin film with laboratory source GIXRD instrument [23]. Total exterior reflection takes place with X-ray penetrating to merely ~10-12 nm underneath the surface of film at grazing incidence angle less than the

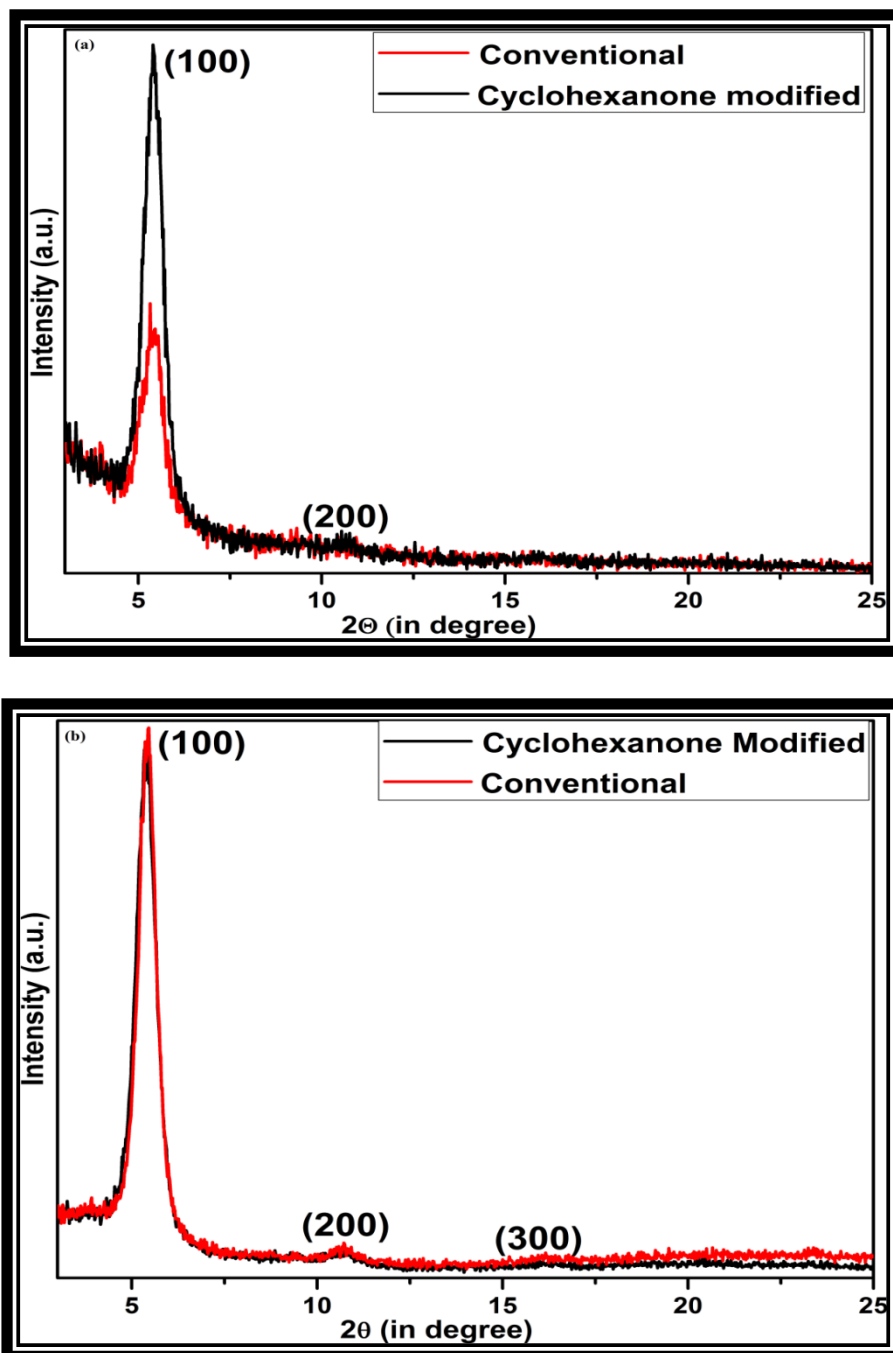
critical angle (i.e., at  $0.11^\circ$ ) for P3HT:PCBM film. So, diffraction patterns at  $0.11^\circ$  grazing incidence angle consist of reflections mainly occurring from the interlayer spacing between P3HT crystallites present at the surface of the film [24]. While, continuing with an incidence angle greater than the critical angle for P3HT:PCBM film but less than the critical angle of the substrate (i.e., at  $0.3^\circ$ ), X-ray can be made to penetrate the entire thin film. So, at  $0.3^\circ$  grazing incidence angle, reflections from the whole bulk of the film can be obtained.

Fig. 4.6 a & b represents the X-ray diffractograms of P3HT:PCBM film at grazing incidence angles  $0.11^\circ$  and  $0.3^\circ$ , respectively. Interlayer distances ( $d$ ) and crystallite sizes of P3HT domains calculated of the (100) diffraction peaks are presented in Table 4.1. The crystallite sizes are calculated using the Scherrer's formula from the peak broadening in the corresponding diffraction patterns.

$$T = \frac{K\lambda}{\beta \cos\theta}$$

where,  $\beta$  = full width half maximum (FWHM),  $\lambda$  = wavelength of X-ray ( $1.54 \text{ \AA}$ ) and  $T$  = crystallite size. It is noticed that both the diffractograms mainly show three peaks corresponding to reflections from (100), (200) and (300) axis orientation of lamellar P3HT chains [25]. A comparison of the (100) reflection peak intensities at  $0.11^\circ$  grazing incidence angle from unmodified and cyclohexanone modified P3HT:PCBM films were done to analyse the crystalline characteristic of P3HT phase at the film surface. An increase in the intensity of (100) reflection peak observed at  $2\theta = 5.4^\circ$  in the cyclohexanone modified film as compared to unmodified film signifies higher level of ordering and orientation of P3HT chains at the surface of the film on cyclohexanone addition. However, higher order diffraction peaks of two films were

less pronounced as only a transient beam of X-ray was made to fall on a smaller depth of P3HT:PCBM film at  $0.11^\circ$  incidence angle.



**Figure 4.6:** (a) Grazing incidence X-ray diffraction (GIXRD) profiles of P3HT:PCBM composite films at grazing incidence of  $0.11^\circ$  and (b)  $0.3^\circ$

A comparison of the crystallite sizes and interlayer spacing between P3HT chains reveals larger well developed closely spaced P3HT crystallites in

cyclohexanone modified sample as compared to smaller crystallites at the surface of unmodified sample. The reason for such a unique feature observed with mixed solvent approach is associated with the cyclohexanone (poor solvent for P3HT) induced preferential self assembly of P3HT in the solvent mixture.

**TABLE 4.1: Interlayer distances (d) and the size of P3HT crystallites of (100) diffraction peak at two grazing incidences  $0.11^\circ$  and  $0.3^\circ$  in the XRD pattern**

S.No.	Device	Grazing incidence angle (degree)	$2\Theta$ value (degree)	Interlayer distance $d_{100}(\text{\AA})$	FWHM	Grain size (nm)
1.	Cyclohexanone modified	$0.11^\circ$	5.4	16.27	0.608	13.0
2.	Cyclohexanone modified	$0.3^\circ$	5.3	16.48	0.654	12.0
3.	Conventional	$0.11^\circ$	5.4	16.29	0.654	12.0
4.	Conventional	$0.3^\circ$	5.4	16.37	0.585	13.4

Again, a comparison of (100) diffraction peak intensity at grazing incidence angle of  $0.3^\circ$  revealed slightly more number of better crystallized P3HT domains in the bulk of conventional unmodified film as compared to cyclohexanone modified P3HT:PCBM film. Higher order diffraction peaks (200) and (300) were also more pronounced in the bulk of conventional unmodified sample than the cyclohexanone modified sample. As, the blend films with identical thickness and concentration have same number of P3HT chains so, it can be stated that the solvent-non-solvent mixture method not only brings about the preferential crystallization of P3HT domains but also, stimulates upward distribution of P3HT fractions. Although, it is known that in a

solution processing technique such as spin coating, the P3HT fractions with the lower surface energy factor have a tendency to occupy surface of the film [26]. Such a probability is however, found to be more enhanced with the practice of solvent-non-solvent mixture for spin coating.

This vertical concentration gradient in the blend film with cyclohexanone modification must benefit the inverted device prepared thereof with the modified P3HT:PCBM layer being employed as active layer for photoabsorption. In case of cyclohexanone modification, the crystallized P3HT domains occupy the surface of active layer in contact with MoO<sub>3</sub> (hole transporting layer, HTL) layer so, hole transport to the silver anode would be enhanced. In addition, leakage current due to the wrong carrier ion transport to anode would be minimised. GIXRD measurement thus confirms favourable vertical concentration gradient of P3HT fractions with cyclohexanone addition.

#### 4.4.5 Photovoltaic Characteristics

We have designed an inverted device with layer sequence of glass/ITO/ZnO/P3HT:PCBM/MoO<sub>3</sub>/Ag, to evaluate the effect of cyclohexanone addition to active layer, on the photovoltaic performance. Each photovoltaic device consists of four cells each with an active area of 0.09 cm<sup>2</sup> and device properties were measured underneath solar simulator with an illumination intensity of 100 mW cm<sup>-2</sup> and AM 1.5 G condition. Fig. 4.7 illustrates the current density-voltage (*J-V*) characteristics of the devices prepared with and without cyclohexanone modification. Photovoltaic parameters of these prepared inverted devices are summarised in the following Table 4.2.



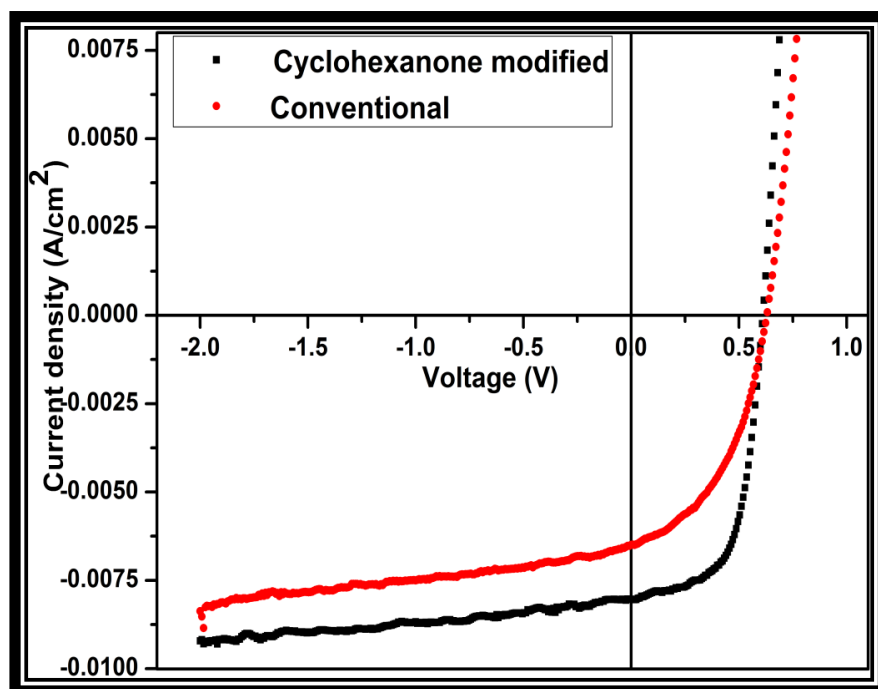


**Figure 4.7: Current density-voltage ( $J$ - $V$ ) characteristic of devices fabricated with and without cosolvent modification**

It is seen from the figure that a power conversion efficiency (PCE) of 2.77% resulting from the short circuit current density ( $J_{sc}$ ) in order of 7.41E-03 A cm<sup>-2</sup>, open circuit voltage ( $V_{oc}$ ) 0.61 V and fill factor (FF) 0.61 is achieved from the conventional photovoltaic device fabricated with active layer casted from a single good solvent. However, *o*-DCB-cyclohexanone mixed solvent casted active layer in a typical inverted device could result in a PCE of 3.09% with a  $J_{sc}$  value of 8.14E-03 A cm<sup>-2</sup>,  $V_{oc}$  0.61V and FF 0.62. This increase in efficiency from 2.74±0.05% to 3.01±0.05% with the addition of poor solvent (cyclohexanone) to the main solvent (*o*-DCB) during the preparation of active layer could possibly be attributable to the increase in photocurrent generation and also increasing fill factor of the device. Improved crystallization in the polymer donor could be the reason for realising increased current density in the modified devices as evident from the UV-Vis and GIXRD measurements [27].

**TABLE 4.2: Photovoltaic device parameters for ITO/ZnO/P3HT:PCBM/MoO<sub>3</sub>/Ag polymer solar cell**

Substrate	Cell No.	Device	$V_{oc}$ (V)	$J_{sc}$ (Acm <sup>-2</sup> )	FF	%E	$R_{sh}$ ( $\Omega$ cm <sup>2</sup> )	$R_s$ ( $\Omega$ cm <sup>2</sup> )
1	1	cyclohexanone modified	0.61	8.04E-03	0.61	3.01	700	12
1	2	cyclohexanone modified	0.61	8.14E-03	0.62	3.09	600	12
1	3	cyclohexanone modified	0.62	7.94E-03	0.61	3.00	1167	12
1	4	cyclohexanone modified	0.62	7.62E-03	0.64	3.01	1391	12
2	1	Conventional	0.61	7.41E-03	0.61	2.77	1123	14
2	2	Conventional	0.61	7.66E-03	0.58	2.72	634	15
2	3	Conventional	0.61	7.45E-03	0.60	2.74	489	13
2	4	Conventional	0.62	7.28E-03	0.60	2.69	654	14

<sup>a</sup>Conventional device = device with active layer prepared from a good solvent (*o*-DCB)

cyclohexanone modified = device with active layer prepared by cyclohexanone addition

<sup>b</sup>Substrate = 5cm × 5cm ITO glass with inverted cell layer sequence comprising 4 cells each of area 0.09 cm<sup>2</sup>

<sup>c</sup> $R_{sh}$  &  $R_s$  = shunt and series resistances of the device, respectively

Favourable upright concentration gradient must have brought about the observed increase in FF of the device. As the fractions of P3HT near the HTL layer increases, series resistance in the device decreases which provides efficient pathway for hole transport. So, cyclohexanone addition in the active layer preparation of

inverted OSC benefits the device in two ways. Firstly, the improved crystallization of the donor polymer enhances both the photo-absorption and hole transport. Secondly, hole transport to anode is enhanced by favourable upright concentration gradient in the active layer with better crystallized P3HT at the top in close contact with HTL.

#### **4.5 Conclusion**

The work presented in this chapter is describing the optimization of amount of non-solvent addition and ageing period of the precursor solution for obtaining the best possible crystallization in the donor phase. Increasing the order of precursor solution by addition of poor solvent (cyclohexanone) appreciably enhances the crystallinity in the P3HT:PCBM films as compared to films prepared from disordered precursor solution. Practice of the cyclohexanone modified P3HT:PCBM film as active layer of inverted OSC improves the PCE to a value of  $3.01\pm 0.05\%$  as compared to  $2.74\pm 0.05\%$  in the unmodified device. This improvement is related to the increased current density and fill factor of the device with cyclohexanone addition. Characteristics of well ordered donor phase in the active layer and favourable concentration gradient with encouraging distribution of donor domains closer to hole transport layer are being introduced to the inverted OSC.

**References**

1. A. G. MacDiarmid, *Angew. Chem. Int. Ed.*, 2001, 40, 2581.
2. A. J. Heeger, *Angew. Chem. Int. Ed.*, 2001, 40, 2591.
3. J. D. Strenger-Smith, *Prog. Polym. Sci.*, 1998, 23, 57.
4. J. -T. Chen and C. -S. Hsu, *Polym. Chem.*, 2011, 2, 2707.
5. J. J. M. Halls, C. A. Walsh, E. A. Marseglia, R. H. Friend, S. C. Moratti and A. B. Holmes, *Nature*, 1995, 376, 498.
6. B. C. Thompson and J. M. J. Frechet, *Angew. Chem. Int. Ed.*, 2008, 47, 58.
7. L. -M. Chen, Z. Hong, G. Li and Y. Yang, *Adv. Mater.*, 2009, 21, 1434.
8. Y. Wang, W. Wei, X. Liu and Y. Gu, *Sol. Energy Mater. Sol. Cells*, 2012, 98, 129.
9. H. Hoppe, M. Niggemann, C. Winder, J. Kraut, R. Hiesgen, A. Hinsch, D. Meissner and N. S. Sariciftci, *Adv. Funct. Mater.*, 2004, 14, 1005.
10. G. Li, V. Shrotriya, Y. Yao, J. Huang and Y. Yang, *J. Mater. Chem.*, 2007, 17, 3126.
11. F. Reisdorffer, O. Haas, P. Le Rendu and T. P. Nguyen, *Synth. Met.*, 2012, 161, 2544.
12. M. N. Yusli, T. W. Yun and K. Sulaiman, *Mater. Lett.*, 2009, 63, 2691.
13. F. Zhang, X. Xu, W. Tang, J. Zhang, Z. Zhuo, J. Wang, J. Wang, Z. Xu and Y. Wang, *Sol. Energy Mater. Sol. Cells*, 2011, 95, 1785.
14. W. Xu, L. Li, H. Tang, H. Li, X. Zhao and X. Yang, *J. Phys. Chem. B*, 2011, 115, 6412.
15. J. Liu, S. Shao, H. Wang, K. Zhao, L. Xue, X. Gao, Z. Xie and Y. Han, *Org. Electron.*, 2010, 11, 775.
16. U. Bielecka, P. Lutsyk, K. Janus, J. Sworakowski and W. Bartkowiak, *Org. Electron.* 2011, 12, 1768.
17. W. Y. Huang, P. T. Huang, Y. K. Han, C. C. Lee, T. L. Hsieh and M. Y. Chang, *Macromolecules*, 2008, 41, 7485.
18. J. S. Kim, J. H. Lee, J. H. Park, C. Shim, M. Sim and K. Cho, *Adv. Funct. Mater.*, 2011, 21, 480.
19. Y. D. Park, S. G. Lee, H. S. Lee, D. Kwak, D. H. Lee and K. Cho, *J. Mater. Chem.*, 2011, 21, 2338.

20. J. H. Jeon, H. K. Lee, D. H. Wang, J. H. Park and O. O. Park, *Sol. Energy Mater. Sol. Cells*, 2012, 102, 196.
21. L. Li, H. Tang, H. Wu, G. Lu and X. Yang, *Org. Electron.*, 2009, 10, 1334.
22. A. J. Moulé and K. Meerholz, *Adv. Mater.*, 2008, 20, 240.
23. D. J. Gundlach, J. E. Royer, S. K. Park, S. Subramanian, O. D. Jurchescu, B. H. Hamadani, A. J. Moad, R. J. Kline, et al., *Nat. Mater.*, 2008, 7, 216.
24. N. D. Treat, M. A. Brady, G. Smith, M. F. Toney, E. J. Kramer, C. J. Hawker and M. L. Chabiny, *Adv. Energy Mater.*, 2011, 1, 82.
25. F. -C. Chen, C. -J. Ko, J. -L. Wu and W. -C. Chen, *Sol. Energy Mater. Sol. Cells*, 2010, 94, 2426.
26. P. G. Karagiannidis, D. Georgiou, C. Pitsalidis, A. Laskarakis and S. Logothetidis, *Mater. Chem. Phys.*, 2011, 129, 1207.
27. Y. Zhao, S. Shao, Z. Xie, Y. Geng and L. Wang, *J. Phys. Chem. C*, 2009, 113, 17235.

# *Chapter 5*

*Investigation on Processing  
Pathway for Cosolvent Addition  
in Active layer Preparation of  
Inverted Organic Solar Cell*

## INVESTIGATION ON PROCESSING PATHWAY FOR COSOLVENT ADDITION IN ACTIVE LAYER PREPARATION OF INVERTED ORGANIC SOLAR CELL

---

- 5.1 **Introduction**
  - 5.2 **Experimental**
    - 5.2.1 *Materials*
    - 5.2.2 *Device preparation*
  - 5.3 **Characterization**
  - 5.4 **Results & discussion**
    - 5.4.1 *UV-Visible absorption measurements*
    - 5.4.2 *Grazing incidence X-ray diffraction (GIXRD) measurements*
    - 5.4.3 *Surface characteristic*
      - 5.4.3.1 *Atomic force microscopy*
      - 5.4.3.2 *Contact angle measurement*
    - 5.4.4 *Photoluminescence emission*
    - 5.4.5 *Photovoltaic properties*
  - 5.5 **Conclusion**
- References**
- 

### 5.1 Introduction

The trend of organic semiconducting molecules (donor/acceptor mixture) to act as the active layer in polymeric solar cell has been extensively progressing these days [1]. The barriers of vertical phase separation and device instability of normal architectures suggest taking up an inverted configuration as a reliable option. Inclination towards the inverted configuration with reversed polarity is favourable because this architecture offers air stability in such devices [2]. This inverted architecture offers the complimentary advantage of favourable vertical phase separation for charge carrier transport which affects negatively in case of normal device configuration [3]. Also, with the recent bridging of the efficiency gap between normal and inverted architectures, inverted device with better lifetime is practised more [4]. But, in both of these configurations, morphology of photoactive

organic thin film has a crucial role to play for successful performance of the solar device.

Disparity between the hole and electron mobility is responsible for low power conversion efficiency in OSC. The hole mobility is also unfavourably affected in donor-acceptor composite films, as thin film coating technique such as spin coating do not sustain ordered growth of P3HT crystals on account of fast solvent evaporation [5]. Previous reports have shown that the solubility of acceptor molecules does influence the crystallinity of donor in the composite. So, the acceptor present in the composite material produces amorphous P3HT domains and the amorphous segment so produced restricts the charge carrier mobility due to the hopping movement. This structural growth defect limits the hole transport and consequently producing low efficiency in devices based on the crystallisable polymer like P3HT in the presence of PCBM [6]. To overcome such problems, few reports in literature also suggest the mixing of pre-organized fibrillar poly(3-alkylthiophene) (P3AT) with the acceptor. However, such devices had low efficiency because of larger phase separation between the donor and acceptor domains in the composite mixture. Therefore, they recommended mixing certain quantity of low molecular weight amorphous P3HT again into the sorted P3HT nanofibers solution to have the connectivity between its crystalline domains resulting an interpenetrating network structure for improved device efficiency [7].

Several processing methods initiated to improve the device efficiency in the course of achieving appropriate active layer morphology, using thermal annealing [8], solvent annealing [9], solvent-non-solvent mixture method [10], etc. Treatments such as thermal and solvent annealing though doing well to certain point for modifying the



morphology of the active layer are difficult to give to practice taking into consideration their incompatibility with flexible substrates and the probable danger of explosive solvent vapours. The solvent-non-solvent mixture method has been developing even with flexible substrates, and combination of solvents can offer better solubility of the components in the composite mixture [11]. Alkane dithiol non-solvent has been used for modifying the morphology of polymers including classical P3HT polymer as well as group of some low band gap polymers. A significant enhancement in the photovoltaic device efficiency is seen on incorporating 1,8-octanedithiol as a result of change in the morphology of the active layer. The non-solvent was found to dissolve the fullerene phase selectively, providing freedom for the poly[2,6-(4,4-bis(2-ethylhexyl)-4H-cyclopenta[2,1-b;3,4-b']-dithiophene)-alt-4,7-(2,1,3 benzothiadiazole)] (PCPDTBT) polymer to crystallize sufficiently in the composite mixture [12]. Further, efforts were made by many other researchers providing a means for exploring other solvent mixtures such as 1, 8-diiodooctane/chlorobenzene for active layer preparation [13].

Nevertheless, we are still far away from the optimal composite morphology and from the realm of commercialization. A precise control over the morphology of the composite in the solvent mixture was complex as the P3HT crystallization and basic phase separation of components happen in a single stage. The different solvents offer variation in solubility to P3HT polymer and PCBM acceptor consequently, the solvent mixture method resulting a large number of arrangements among the components of the composite. Hence, this method can be useful in transforming the donor-acceptor interface areas and charge carrier mobility in P3HT:PCBM composites as a function of solvent system [14, 15]. Since, there have not been many

reports on utilization of solvent-cosolvent mixture method for transforming the active layer (P3HT:PCBM) morphology in an inverted device so, we have considered the processing techniques for cosolvent addition. Our main aim is to improve the P3HT reorganization or self assembly by nullifying the influence of the acceptor component to enhance the device performance. In order to have an efficient P3HT crystallization and simultaneously maintaining the effectual connectivity between these crystalline P3HT domains, amorphous P3HT segments are dispersed among them which results in interpenetrating donor-acceptor networks.

In comparison to one step conventional process of direct marginal solvent addition to the P3HT:PCBM solution in good solvent (like *o*-dichloro benzene), the two step process is found to be better. The two step process consists of crucial P3HT crystallization by marginal solvent addition (like cyclohexanone) to a solution of P3HT in good solvent followed by second step where mixing of PCBM solution in good solvent to the same takes place. And, ultimately mild thermal annealing of the casted films was done for further phase separation of both the domains in the composite film.

## 5.2 Experimental

### 5.2.1 Materials

In this work, we have fabricated inverted BHJ polymer solar cells with a constituent layer structure of indium tin oxide (ITO)/ zinc oxide (ZnO)/ poly(3-hexylthiophene) (P3HT):[6,6]-phenyl-C<sub>61</sub>-butyric acid methyl ester (PCBM) blend (P3HT:PCBM)/MoO<sub>3</sub>/Ag. Poly(3-hexylthiophene)(P3HT) ( $M_w = 87000$  g/mol and > 90% head-to-tail RR), [6,6] phenyl C<sub>61</sub> butyric acid methyl ester (PCBM), zinc

acetate dihydrate ( $C_4H_{10}O_6Zn$ ), 2-methoxyethanol ( $C_3H_8O_2$ ) and ethanolamine ( $C_2H_7NO$ ) have been procured from Sigma Aldrich.

### 5.2.2 Device Preparation

Inverted polymeric solar cells were assembled over the patterned ITO coated glass substrate with less than  $20 \Omega/\text{sq}$  sheet resistance. ITO glass substrates were cleaned via ultrasonication for 20 min each sequentially in a boiling soap solution, deionised water, acetone, and isopropanol, followed by drying with nitrogen and then 26 min of UV-ozone exposure. A 30 nm thin ZnO film was deposited by spin coating on the cleaned ITO substrate using a 0.5M ZnO solution prepared by mixing zinc acetate dihydrate, ethanolamine and 2-methoxyethanol. The curing of coated film was carried out at  $250^\circ\text{C}$  for 10 min to crystallize the ZnO. For active layer preparation, P3HT and PCBM (1:0.6 weight ratio) were dissolved in 1 mL of good solvent, i.e., *ortho*-dichlorobenzene (*o*-DCB) by means of continuous stirring overnight at  $50^\circ\text{C}$ , and it was spin coated over the ZnO coated substrate. Thereafter, the substrates were transferred to nitrogen ambient and annealed at  $85^\circ\text{C}$  for 30 min. Molybdenum oxide ( $\text{MoO}_3$ ) and silver (Ag) layers were thermally deposited in a vacuum chamber at a pressure of  $5 \times 10^{-6}$  mbar. A 7 nm thick  $\text{MoO}_3$  layer (hole transporting layer, HTL) was deposited with a deposition rate of  $0.5 \text{ \AA s}^{-1}$  which is followed by deposition of 150 nm Ag as a top electrode with a deposition rate of  $1.0 \text{ \AA s}^{-1}$ .

The performance of devices was studied under illumination using a solar simulator AM 1.5G with intensity of  $100 \text{ mW cm}^{-2}$ . In order to understand the effect of cosolvent addition on the active layer preparation, a comparison of two different methods of cosolvent addition was studied in detail. The cyclohexanone having a boiling point of  $155^\circ\text{C}$  was used as cosolvent in this study. The choice of

cyclohexanone cosolvent was made keeping in mind the solubility index of the solvent that implies more solubility of PCBM than P3HT. The amount of cosolvent for active layer preparation was optimized to 5 vol %, as an amount higher than 5 vol % results in gel formation in precursor solution over a period of time at room temperature while, lesser than 5 vol % cosolvent did not result in significant improvement. For all these modifications, cosolvent was added and the solution was stirred for 2 h in nitrogen atmosphere before further processing. The composite films have been referred here as BLND in case of blended addition, where films were prepared from solution with cyclohexanone added directly to P3HT:PCBM blended solution in *o*-DCB solvent and individual where films were prepared from solutions firstly, with cyclohexanone added to a P3HT solution in *o*-DCB, followed by stirring for 2 h and mixing of PCBM solution.

### 5.3 Characterization

The current density ( $J$ ) – voltage ( $V$ ) characteristics of the photovoltaic devices were measured using a Keithley (Model 2420) source meter under illumination intensity of  $100 \text{ mW cm}^{-2}$  from a solar simulator (Model SS150AAA Photo Emission Technology Inc.) with AM 1.5 G filter. The device was prepared in nitrogen atmosphere (which was maintained inside a glove box from Jacomex with  $\Delta P = 3.0 \text{ mbar}$  and oxygen level of  $0.3 \text{ ppm}$ ). The UV–Visible absorption measurements were performed using a Perkin Elmer 35 lambda UV–Visible spectrophotometer. The surface morphology was studied by using an Atomic Force Microscope (AFM) (Model VEECO DI-3100) with Nanoscope (III) in tapping mode. Grazing incidence X-ray diffraction (GIXRD) measurements were done at three grazing incidence angles of  $0.11^\circ$ ,  $0.13^\circ$  and  $0.3^\circ$  using a Rigaku ultima IV X-ray

diffractometer ( $\lambda = 1.54 \text{ \AA}$ ) employing Cu-K $_{\alpha}$  radiation source. Contact angle measurements were made on Drop Shape Analysis System (Model DSA10MK2) from Kruss GmbH, Germany. These measurements are based on sessile drop method which employed to evaluate the hydrophobic/hydrophilic nature of the surface. The picture of the drop placed on the P3HT:PCBM coated glass substrate surface was taken using a video camera and image-analysis system then records the contact-angle ( $\theta$ ), based on the shape profile of the drop.

## 5.4 Results and Discussion

### 5.4.1 UV-Visible Absorption Measurements

Fig. 5.1 shows the comparative UV-Visible absorption spectra of both the P3HT:PCBM composite films prepared using two different methods (blended addition and individually mixed addition). We have studied the effect of cosolvent addition pathway on the radiation absorbed by the polymer chains in the composite mixture. Spectra of both these films consist of an absorption peak at around 512 nm, with shoulders at 550 and 610 nm, noticeably proving the presence of strictly controlled P3HT chains in the composite mixture. The absorption peaks at 512, 550, and 610 nm indicate intrachain  $\pi$ - $\pi^*$  transition, extensive conjugated chain absorption and interchain transition, respectively in the highly ordered solid state P3HT [16]. An increase in the intensity of the absorption peak at 512 and 550 nm in case of individually mixed modified (Individual) sample as compared to blended (BLND) cosolvent modified film suggests a well organized growth of P3HT crystals. This improved crystallization of P3HT in individual cosolvent modified sample is because of the diminishing interruption of PCBM next to P3HT crystallization.

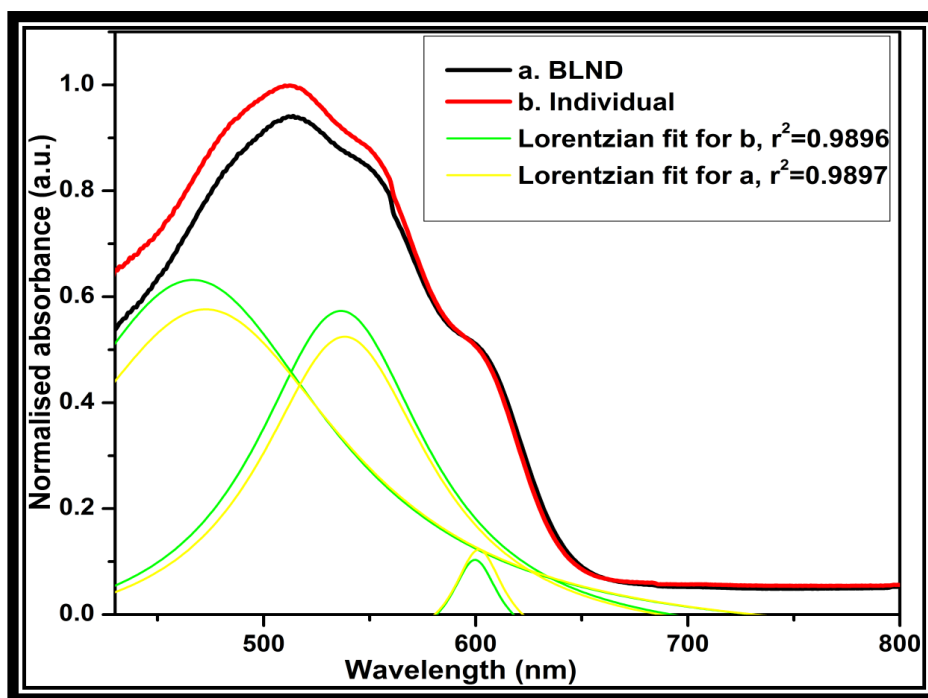


**Figure 5.1:** UV-Visible absorption spectra of P3HT:PCBM composite films

The growth of P3HT crystals in P3HT solution occurs by self organization from random coil conformation to rod like conformation [17]. A similar transition is responsible for the crystallization of P3HT in composite (P3HT:PCBM) film also. However, such a transition is restricted to some extent due to the co-precipitating (or co-existing) PCBM content in the composite.

The coil to rod transition was found to be more favoured in an individual cosolvent modified sample consistent with an increased intensity of 512 and 550 nm absorption peaks. So, the sufficient P3HT precipitation must have occurred in the individual cosolvent modified solution prior to introduction of PCBM. The crystallization step is followed by diffusion of PCBM to the amorphous phases of some fully dissolved (un-precipitated) polymer in *o*-DCB/cyclohexanone mixture to form an interpenetrating network and achieving the best P3HT crystallization in the composite mixture. However, such a route would have resulted in a bit larger sized

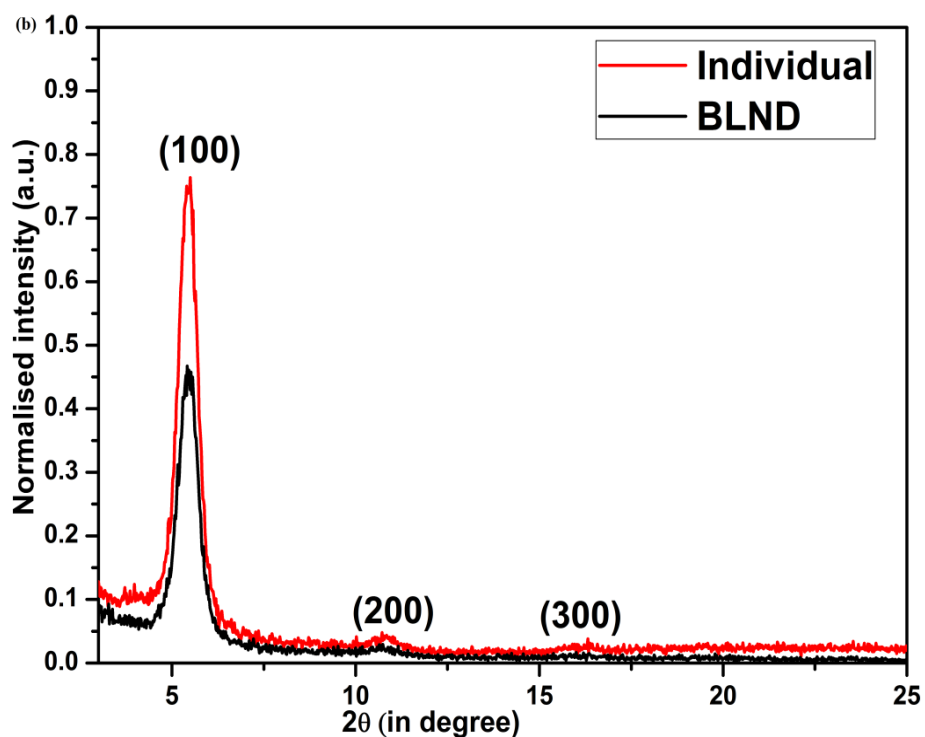
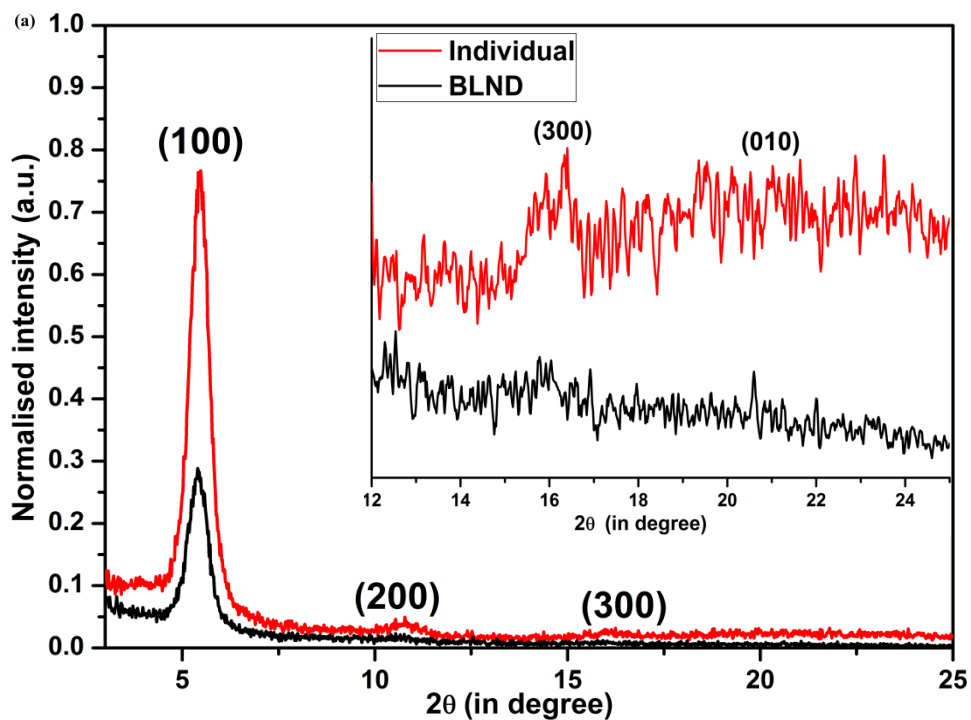
P3HT domains, causing larger phase separation between the components of the composite mixture as recommended by Kozub et al [18].

A decreased P3HT absorption in the BLND film reveals that the intra-chain transition of P3HT chains is not achieved up to the mark. Though, the cyclohexanone addition must have influenced the precipitation order changeover to P3HT first; however, the probability of PCBM's presence in the disordered regions of P3HT hinders the maximum crystallization [19].

#### 5.4.2 Grazing Incidence X-ray Diffraction (GIXRD) Measurements

In order to understand the crystalline order in the active layer of inverted OSC grazing incidence X-ray diffraction (GIXRD) measurements were carried out on cosolvent modified P3HT:PCBM films. GIXRD measurements were made using the lab source instrument as reported in the previous chapter. These measurements were recorded at three grazing incidence angles, i.e.,  $0.11^\circ$ ,  $0.13^\circ$ , and  $0.3^\circ$ , to observe the vertical phase separation through the composite film. It is seen from the data that the bending of the electromagnetic radiation such as an X-ray occurs due to the refraction in case of solid material with refractive index less than unity. So, using a fixed grazing incidence angle of  $0.11^\circ$ , i.e., smaller than the critical angle for P3HT, total reflection occurs and only a short-lived beam transverses just few nanometres beneath the surface, giving diffraction largely from the surface of the composite film. At grazing incidence angle slightly higher than the critical angle for external reflection (i.e.,  $0.13^\circ$ ); the X-ray diffuses deeper in the film giving rise the diffraction from the depth of the film. The probed depth for an organic material increases rapidly with a small increase in the incidence angle near the critical angle region. Once, we are keeping incidence angle well above the critical angle (i.e., at  $0.3^\circ$ ), it provides

diffraction from the whole volume (bulk) of the composite film [20, 21]. Thus, by varying the probe depth with the incidence angle, X-rays can be used to study the morphology of surface, underlying interfaces, and bulk material.





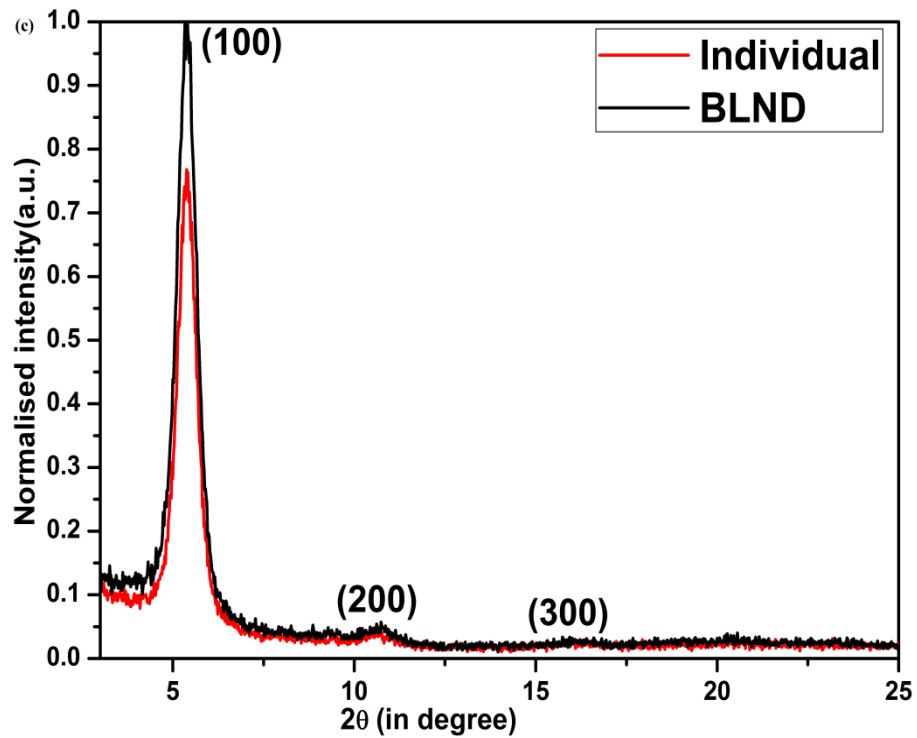


**Figure 5.2:** (a) Normalised grazing incidence X-ray diffraction (GIXRD) profiles of P3HT:PCBM composite films at grazing incidence of  $0.11^\circ$ , (b)  $0.13^\circ$ , and (c)  $0.3^\circ$

For both the BLND and individual mixed films at  $0.11^\circ$  incidence angle, three diffraction peaks were identified as (100), (200) and (300) which characterizes layered intra-chain P3HT orientation along a-axis of crystallographic plane while, (010) peak corresponds to the interchain  $\pi$ - $\pi$  stacking orientation of P3HT backbone along b-axis of crystallographic plane (Figure 5.2a) [22]. The intensities of the (100) reflection peaks at  $2\Theta = 5.4^\circ$  for BLND cosolvent modified films and for individually mixed films imply improved crystallite orientation along a-axis of the crystallographic plane in case of individually mixed film. The better P3HT crystallization is detected in case of individually mixed cosolvent modified sample which may be attributed to the small interruption by PCBM crystallites during P3HT crystallization in solvent-cosolvent mixture.

Table 5.1: Summary of interlayer distances (d) and the size of P3HT domains

S.No.	Device	Grazing incidence angle (degree)	2 $\theta$ value (degree)	Interlayer distance $d_{100}$ (Å)	FWHM	Grain size (nm)
1.	BLND	0.11 <sup>0</sup>	5.4	16.27	0.608	13.0
2.	BLND	0.13 <sup>0</sup>	5.4	16.21	0.632	12.4
3.	BLND	0.3 <sup>0</sup>	5.3	16.48	0.654	12.0
4.	Individually mixed	0.11 <sup>0</sup>	5.4	16.23	0.580	13.7
5.	Individually mixed	0.13 <sup>0</sup>	5.4	16.18	0.616	12.7
6.	Individually mixed	0.3 <sup>0</sup>	5.3	16.43	0.638	12.3

Table 5.1 presents the data of interlayer distances and crystallite sizes of P3HT domains of the (100) diffraction peak in the GIXRD patterns at three grazing incidence angles. Further implication from the study of the  $\pi$ - $\pi$  stacking (010) peak intensity emphasized that the polythiophene backbone in individually mixed cosolvent modified sample form superior  $\pi$ - $\pi$  stacked domains as compared to BLND film [23] (inset of Fig. 5.2a). So, the surface of individually mixed cosolvent modified composite film includes greater number of well crystallized P3HT domains. Also, at an incidence angle of 0.13<sup>0</sup> (Fig. 5.2b), it has been noted that individually mixed cosolvent casted film has more number of well crystallized P3HT chains. However, the differences in diffraction intensities (related to the crystallinity and number of

P3HT crystallites) that existed at the surface of BLND and individually mixed cosolvent sample film were reversed once bulk of these films was looked (Fig. 5.2c, at incidence angle of  $0.3^\circ$ ). This effect may be seen as a result of greater fraction of PCBM in the bulk of individually mixed cosolvent casted film as compared to blended cosolvent modified film.

To consider the vertical phase separation in both the cosolvent modified composite films, a comparison of P3HT diffraction peaks at  $0.11^\circ$ ,  $0.13^\circ$ , and  $0.3^\circ$  grazing incidence angles was made. By and large, the intensity of the diffraction peaks should increase with an increase in the grazing incidence angle and maximum P3HT intensity is observed at angle slightly larger than the critical angle. In individually mixed cosolvent modified composite film, the P3HT crystallization was found more at the surface than the bulk of film, as it gets more space to build up efficiently and the least hindrance from PCBM. As we go into the bulk of the film, slightly reduced P3HT diffraction peak intensities are seen which may be due to the reduced polymer crystallization or an increase in PCBM interruption. As the concentration of P3HT in both the schemes is same (number of P3HT crystallites also be the same) so, the slightly reduced intensity of the (100) reflection peak in the bulk of individually mixed cosolvent casted film may possibly be due to the lesser portion of oriented P3HT crystallites in the bulk. It reveals that there is possibly a redistribution of the P3HT through the film with more oriented P3HT crystallites at the surface and lesser of them in the bulk. However, in blended cosolvent modified films lesser number of P3HT crystallites were perceived at the surface as compared to the bulk. These revelations point to a concentration gradient in the active layer of inverted OSC primed via cosolvent addition.

Moreover, individually mixed cosolvent modified films have more number of P3HT crystallites and lesser PCBM domains at the surface, i.e., next to hole transporting layer, i.e., MoO<sub>3</sub>. Also, the bulk of these films (in the neighbourhood of electron transport layer (ETL), i.e., ZnO) consist of fewer numbers of P3HT crystallites and more PCBM domains. This upright phase separation or concentration gradient is an added advantage to inverted architecture. The complimentary concentration gradient or upright phase separation is more significant for individually mixed cosolvent modified casted film, which may consecutively benefit the OSC device. Using the Scherrer formula, we successfully worked out the size of P3HT crystallites near the surface as 13.0 and 13.7 nm for BLND and individual mixed films, respectively, while in the bulk of film, the crystallite size was found in the order of 12.0 and 12.3 nm, respectively [24]. Larger crystal size of crystallisable polymer in active layer was formed using modified cosolvent addition method. Such larger crystals are crucial for the charge transport process, which may be a contributing attribute for high photocurrent generation in OSC [25].

### **5.4.3 Surface Characteristic**

#### **5.4.3.1 Atomic Force Microscopy**

The morphological study of P3HT:PCBM composite films was made using tapping mode AFM. Fig. 5.3 (a & b) represents the topographical AFM images of individually mixed and BLND cosolvent modified films, respectively. All the films were found homogeneous and the initial optical scans did not include any micrometer sized flaws of dust, scratch, or overgrown PCBM aggregates. AFM topographic images show greater crowding at the surface of individually mixed cosolvent casted film with consistently formed crystalline P3HT phases relative to partially crystallized

broken phases in its counter film. This result is found in agreement with the GIXRD data. The continuous and well ordered P3HT domains show higher hole mobility and hence these P3HT domains are fundamental for increasing the efficiency of the OSC device [26].

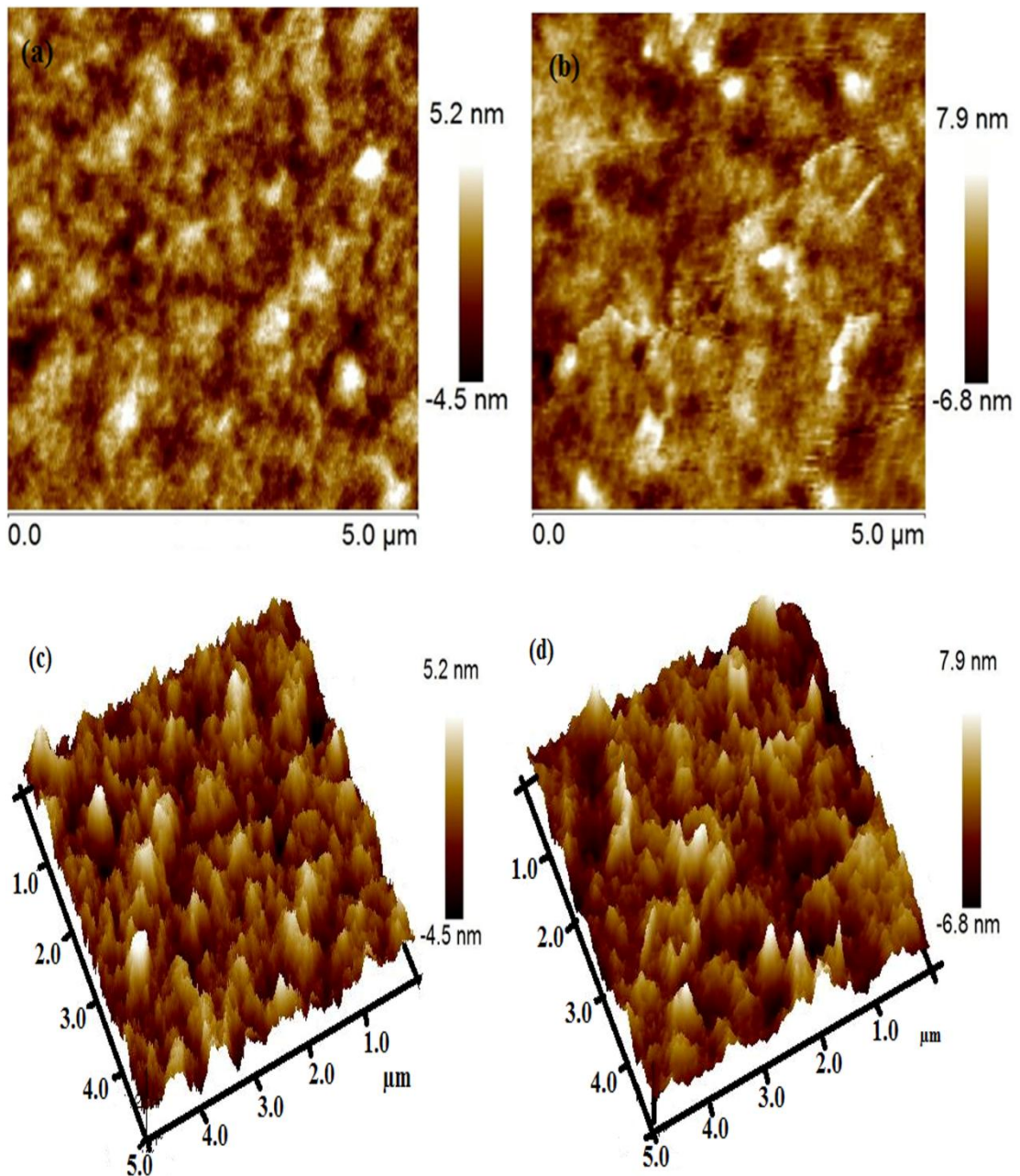


**Figure 5.3:** AFM images of P3HT:PCBM composite films modified (a) individually mixed cyclohexanone (b) blended cyclohexanone addition approaches (c) & (d) are their height images, respectively

Further, a decrease in surface roughness (1.4 nm) in case of individually mixed sample is related with well organized and unhindered P3HT crystallization as well as decrease in PCBM domains as compared to BLND film. The BLND film has higher root mean square roughness (2.0 nm) as shown in Fig. 5.3d owing to limited P3HT crystallite growth as a result of greater fraction of disordered PCBM phase at the surface [27]. Perusal of the root mean square roughness data and topographic images of BLND and individually mixed films illustrate denser and ordered P3HT crystallites with lesser PCBM segment in individually mixed cosolvent modified sample. The root mean square roughness values also agreeing with the surface morphology data taken from the GIXRD measurement. A uniform and homogenous active layer is essential for photon harvesting, as the non-uniform active layer may end up causing a short circuit or exciton recombination. Thus, this modified method of cosolvent addition is found useful for fabricating smoother and uniform films.

#### **5.4.3.2 Contact Angle Measurements**

In order to evaluate the surface properties of P3HT:PCBM thin films, water contact angles were studied (Fig. 5.4) in detail. The conventional P3HT:PCBM film has a contact angle of  $60.94^\circ$  without any cosolvent addition while an individually mixed and blended cosolvent modified films have shown the contact angle of  $83.29^\circ$  and  $62.01^\circ$ , respectively. These surface properties are also supported by GIXRD measurement data. The water contact angle of conventional P3HT:PCBM film is representing the lowest build up of hydrophobic P3HT at the surface of the film while after cosolvent addition a transformation in the surface morphology of these films is noticed [28]. Individually mixed cosolvent addition encourages the maximum crystallization in P3HT domains which are found on the surface of the film owing to

the lower surface energy of P3HT polymer [29]. This is found in agreement with the highest water contact angle monitored for individually mixed cosolvent modified film. While, in case of blend cosolvent modified film, the water contact angle ( $62.01^\circ$ ) is lesser than individually mixed cosolvent modified film because of the suppression of P3HT crystallization in the presence of PCBM.

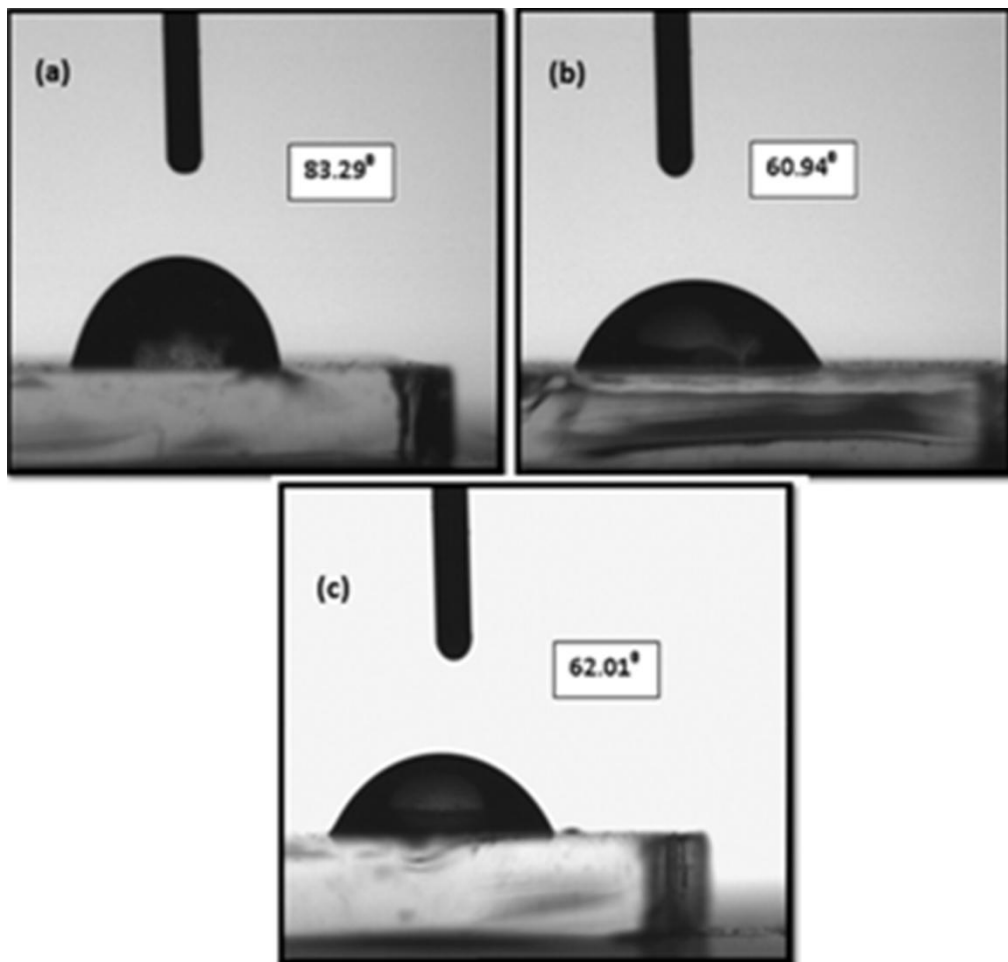


**Figure 5.4:** Water contact angle images of P3HT:PCBM films (a) individually mixed cyclohexanone modified (b) conventional and (c) BLND addition

#### 5.4.4 Photoluminescence Emission

Fig. 5.5 describes the photoluminescence (PL) emission spectra of P3HT:PCBM composite films casted using individually mixed cosolvent addition and



blended cosolvent addition. Photoluminescence measurements were made to see the possible effects of two different methods of cosolvent addition on the nanomorphology of donor-acceptor domains and charge transfer mechanism in composite layer. As we know that the photoluminescence is a measure of photoinduced charge transfer between the donor and acceptor phase, and supposed to be quenched in an intimately mixed donor-acceptor composite.

The weakly coupled H-aggregate model which is used for describing the coupling interaction in aggregates failed in case of P3HT nanowhiskers as its PL ratio ( $PL_{0-0}/ PL_{0-1}$ , i.e., ratio of PL peak intensity of zero-phonon transition to the vibrational replicas) reaching a value as high as two which is exceeding Huang-Rhys parameter (HR) limit. This implies that the allowed zero phonon (0-0) transition is not because of disorder in the structure of macromolecule but due to the intrachain excitons coupling interaction which is expected for a J-type of aggregate. This intrachain excitons coupling interaction also favour in case of P3HT aggregate formation in individually mixed cosolvent casted film, where PL spectra present larger PL 0-0/0-1 ratio (though not of the order of two but of 0.973) as compared to 0.96 in blend cosolvent modified sample. In addition to the above factor, a slight reduction in PL 0-2/0-1 intensity is also observed in case of individually mixed cosolvent casted film which suggests intramolecular interaction (through bonds coupling) in the P3HT chains.

Exciton bandwidth 'W' of aggregate being proportional to HR (PL 0-2/0-1 ratio) is slightly reduced in individually mixed film resulting in efficient charge transfer to PCBM. A further evidence of intrachain structural order (or J- aggregate formation) in individually mixed cosolvent casted film was reported by a decrease of



5 nm in stoke's shift (difference in nanometre between peak excitation and peak emission wavelength) similar to that of P3HT nanofibers [30]. So, a decrease in PL emission in individually mixed sample is owing to weaker radiative transition from the lowest lying excitons in the film.

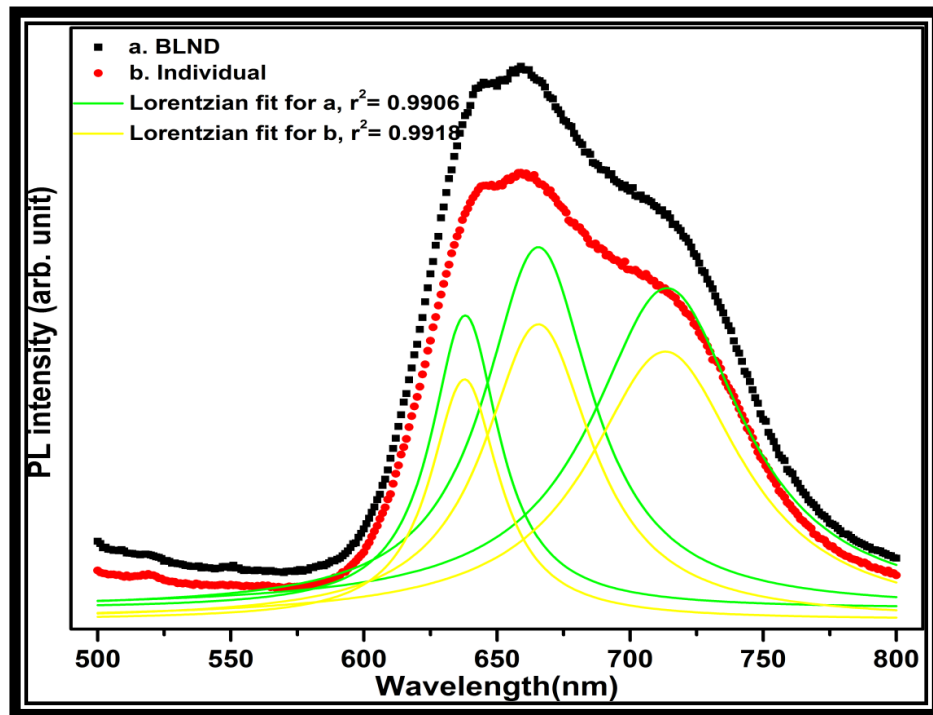


**Figure 5.5: Photoluminescence spectra of P3HT:PCBM composite films modified by individually mixed and blended cyclohexanone addition**

Reduced PL intensity in individually mixed modified film provides an indication of larger critical exciton dissociation at the interface between the domains of composite film compared to incomplete quenching or higher PL intensity in blended cosolvent modified casted film. This higher PL intensity in blended cosolvent mixed casted film shows a coarser P3HT:PCBM mixture or inconvenient phase separation between the domains of larger sizes. All the excitons generated in one polymer do not reach at the interface of the other polymer within the same film [31]. It verifies the adverse decrease of efficiency in blended cosolvent casted device,

suggesting more carrier recombination in devices and hence reduced short circuit current density ( $J_{sc}$ ). However, an individually mixed cosolvent casted film offers the precise equilibrium phase separation for efficient charge separation and transport. Phase separation is less coarser in individual mixed sample assuring close contact of donor and acceptor domains to undergo a charge transfer. Further in this case, the grain size relaxation and substantial quenching is noticed because of the novel long-range excitons quenching mechanism [32]. An unusual PL quenching is observed in case of bit larger grain sized ( $\sim 13.7$  nm) individually mixed cosolvent casted film driven by self quenching mechanism. The more ordered and planar P3HT chains formed in case of individually mixed film provide a secure dissipation pathway for the interchain excitons to discharge its energy at a diffusion length which is beyond the normal excitons diffusion length (8-10 nm) in organic polymers. Thus, the probability of photoluminescence radiative decay is diminishing [33].

#### 5.4.5 Photovoltaic Properties

Fig. 5.6b shows the current density-voltage characteristic of the devices in dark. These devices were primed with active layers modified by two different routes such as blended and individually mixed cosolvent addition method. Particulars of these two processing pathways for cosolvent addition are presented in the previous sections. The solar cell devices that have been fabricated by both the schemes demonstrated diode like characteristics. A large increase in the forward and reversed biased current at higher voltages for the solar device with an individually mixed cosolvent modified active layer in comparison to blended cosolvent modified device is due to the shrinkage in interfacial charge injection barriers between the active layer and electrodes. This shrinking of charge injection barriers is resulting because of

greater crystalline P3HT phase and lesser PCBM (hole blocker) domains near to HTL in individually mixed cosolvent modified device. Fig. 5.6a illustrates the current density-voltage characteristics of the illuminated solar devices prepared via adopting two different approaches of modification with cyclohexanone solvent in the (1:0.6) P3HT:PCBM composite layer.

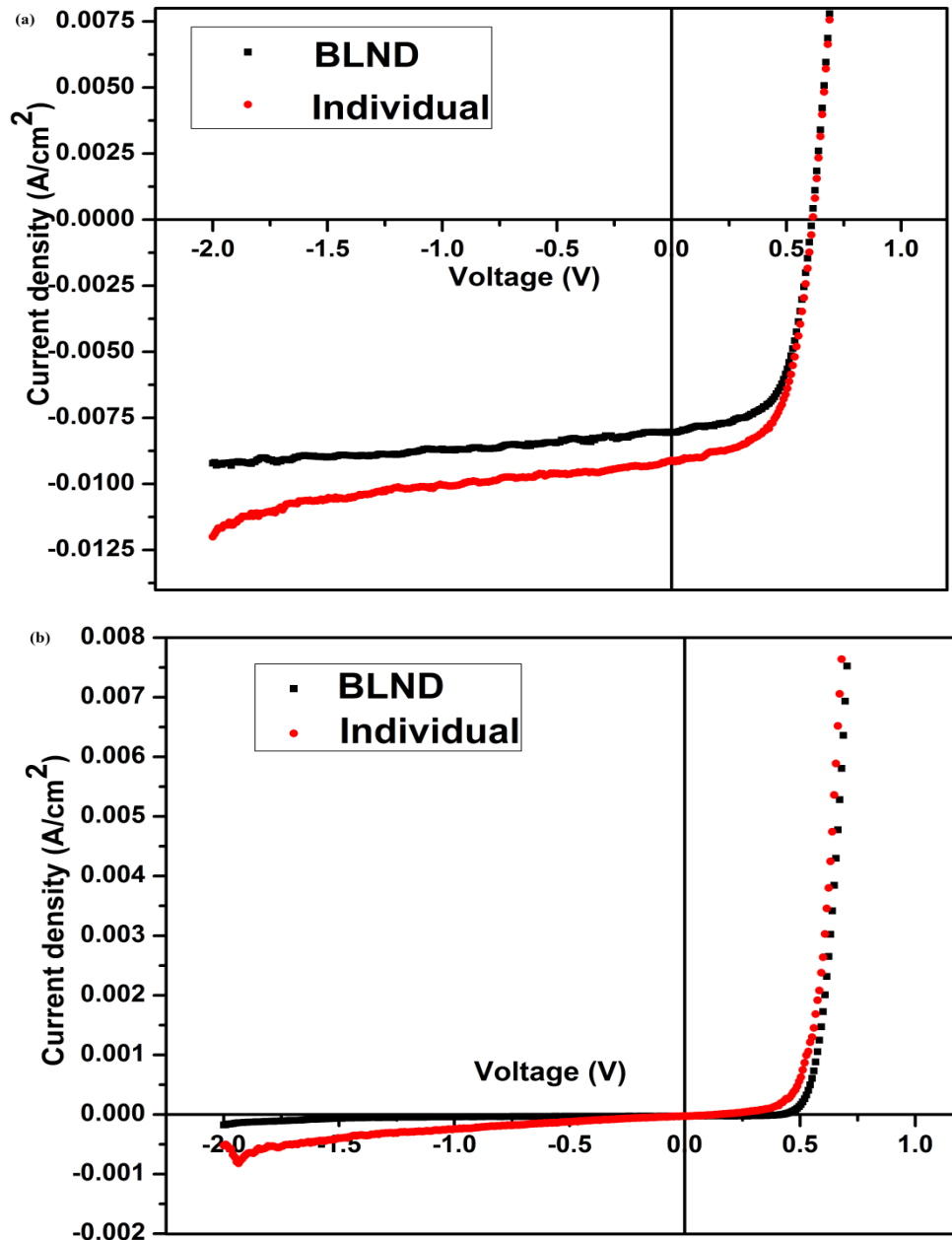
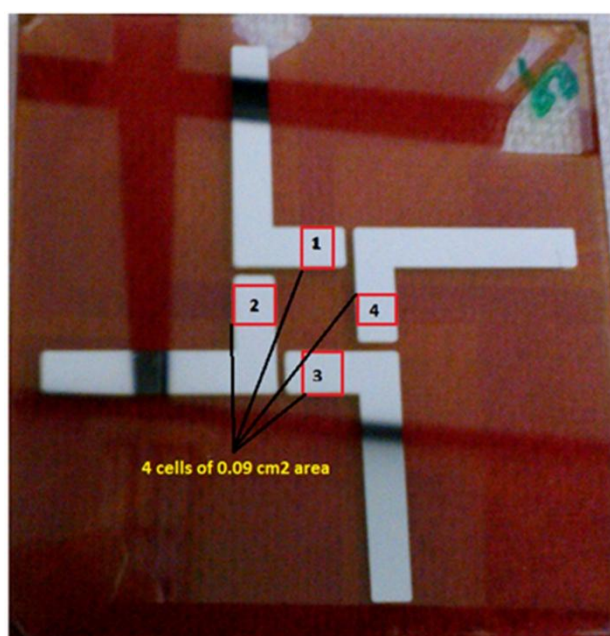


Figure 5.6: (a) Current density-voltage ( $J$ - $V$ ) characteristic of OSC devices under AM 1.5 G white light illumination (b) OSC devices tested in dark

Fig. 5.7 represents an inverted polymeric solar cell primed on 5 cm × 5 cm ITO/glass substrate comprising of 4 cells each of 0.09 cm<sup>2</sup> area. A summarized report of all the device parameters is presented in Table 5.2. It is revealed that an individually mixed cosolvent addition approach proved to be favourable for getting better device performance. A particular case of individually mixed cosolvent modified device had short circuit current density ( $J_{sc}$ ) of 9.01E-03 A cm<sup>-2</sup>, open circuit voltage ( $V_{oc}$ ) of 0.61 V and fill factor (FF) of 0.61, resulting in an efficiency of 3.39%. While on the contrary, a device modified with blended cosolvent addition had device parameters  $J_{sc}$  8.04E-03 A cm<sup>-2</sup>,  $V_{oc}$  0.61 V and FF 0.61, resulting in an efficiency of 3.01%. A 10% increase in efficiency in the devices primed with individually mixed cosolvent approach compared to blended cosolvent addition approach is a result of the apparent increase in the device current attributable to improved crystallization of P3HT in the photoactive layer avoiding PCBM interference to a great extent.



**Figure 5.7: Pictorial view of inverted organic solar cell primed on 5 cm × 5 cm ITO/glass substrate comprising 4 cells each of 0.09 cm<sup>2</sup> area**

An improved crystallinity of P3HT donor benefits the device performance in two ways. Firstly, an enhanced crystallinity brings about the greater optical absorption of solar spectrum by the photoactive layer. This improved crystallinity also result in an efficient hole transport and its collection at anode [34].

**Table 5.2: Photovoltaic device parameters for ITO/ZnO/P3HT:PCBM/MoO<sub>3</sub>/Ag polymer solar cell**

Substrate	Cell No.	Device	$V_{oc}$ (V)	$J_{sc}$ (Acm <sup>-2</sup> )	FF	%E	$R_{sh}$ ( $\Omega\text{cm}^2$ )	$R_s$ ( $\Omega\text{cm}^2$ )
1	1	BLND	0.61	8.04E-03	0.61	3.01	700	12
1	2	BLND	0.61	8.14E-03	0.62	3.09	600	12
1	3	BLND	0.62	7.94E-03	0.61	3.00	1167	12
1	4	BLND	0.62	7.62E-03	0.64	3.01	1391	12
2	1	Individual	0.61	9.01E-03	0.61	3.39	1008	12
2	2	Individual	0.61	9.16E-03	0.60	3.37	355	12
2	3	Individual	0.61	8.78E-03	0.62	3.33	750	11
2	4	Individual	0.62	8.99E-03	0.60	3.32	700	12

<sup>a</sup>Individual and BLND devices refer to the different processing conditions

Individual = individually cyclohexanone added mixed device

BLND = P3HT:PCBM blended cyclohexanone added device

<sup>b</sup>Substrate is a 5cm × 5cm ITO glass substrate with inverted layer sequence comprising 4 cells each of area 0.09 cm<sup>2</sup>

It is inferred from the data that an increase in efficiency of the device primed with individually mixed cosolvent casted active layer was attributed due to the increased size of P3HT crystallites on the surface. The Chiu et al. work also supports an enhancement in efficiency of their device via annealing, to the increased crystallite size of the components in the composite mixture to a limit of successful exciton dissociation [35].

As discussed in previous section, the P3HT crystallites of the order of 13.7 nm is sufficiently small for successful exciton dissociation permitting long distance exciton quenching relaxation which is favoured in highly crystalline and planar chains. Again, an increase in the shunt resistance of device with an individually mixed cosolvent casted active layer results in lesser recombination losses and leakage current agreeing with the smoother film observed by AFM and reflected from additional quenched PL intensity.

## **5.5 Conclusion**

Power conversion efficiency (PCE) of a distinctive device, primed with the cosolvent modified active layer was ascertained to improve  $3.01\pm 0.05\%$  to  $3.39\pm 0.05\%$  by altering the cosolvent addition method from conventional blended mixture addition to individually mixed method. This improvement in the device efficacy is related to an improved characteristic surface morphology as seen in AFM images, proven by improved crystallization of donor polymer supported by the UV-Visible, GIXRD and PL data. A fine coverage of homogenously distributed well grown P3HT crystallites is evident in an individually mixed cosolvent casted film. This morphology supports the enhanced photoabsorption and charge transport properties which benefit the device in terms of increased  $J_{sc}$  and power conversion

efficiency. GIXRD data also support more favourable upright concentration gradient in individually mixed films which eases the charge transport in the devices.

**References**

1. G. Li, R. Zhu and Y. Yang, *Nat. Photonics.*, 2012, 6, 153.
2. F. Zhang, X. Xu, W. Tang, J. Zhang, Z. Zhuo, J. Wang, J. Wang, Z. Xu and Y. Wang, *Sol. Energy Mater. Sol. Cells*, 2011, 95, 1785.
3. E. Pavlopoulou, G. Fleury, D. Deribew, F. Cousin, M. Geoghegan and G. Hadziioannou, *Org. Electron.*, 2013, 14, 1249.
4. S. K. Gupta, A. Sharma, S. Banerjee, R. Gahlot, N. Aggarwal, Deepak and A. Garg, *Sol. Energy Mater. Sol. Cells*, 2013, 116, 135.
5. G. Li, V. Shrotriya, Y. Yao, J. Huang and Y. Yang, *J. Mater. Chem.*, 2007, 17, 3126.
6. L. Li, H. Tang, H. Wu, G. Lu and X. Yang, *Org. Electron.*, 2009, 10, 1334.
7. S. Berson, R. D. Bettignies, S. Bailly and S. Guillerez, *Adv. Funct. Mater.*, 2007, 17, 1377.
8. Y. Kim, S. A. Choulis, J. Nelson, D. D. C. Bradley, S. Cook and J. R. Durrant, *J. Mater. Sci.*, 2005, 40, 1371.
9. C. W. Chu, H. Yang, W. J. Hou, J. Huang, G. Li and Y. Yang, *Appl. Phys. Lett.*, 92, 2008, 103306.
10. F. C. Chen, H. C. Tseng and C. J. Ko, *Appl. Phys. Lett.*, 2008, 92, 103316.
11. K. Kawano, J. Sakai, M. Yahiro and C. Adachi, *Sol. Energy Mater. Sol. Cells*, 2009, 93, 514.
12. J. Peet, J. Y. Kim, N. E. Coates, W. L. Ma, D. Moses, A. J. Heeger and G. C. Bazan, *Nat. Mater.*, 2007, 6, 497.
13. J. K. Lee, W. L. Ma, C. J. Brabec, J. Yuen, J. S. Moon, J. Y. Kim, K. Lee, G. C. Bazan and A. J. Heeger, *J. Am. Chem. Soc.*, 2008, 130, 3619.
14. J. H. Kim, J. H. Park, J. H. Lee, J. S. Kim, M. Sim, C. Shim and K. Cho, *J. Mater. Chem.*, 2010, 20, 7398.
15. J. S. Kim, J. H. Lee, J. H. Park, C. Shim, M. Sim and K. Cho, *Adv. Funct. Mater.*, 2011, 21, 480.
16. N. Kiriy, E. Ja'nhne, H. J. Adler, M. Schneider, A. Kiriy, G. Gorodyska, S. Minko, D. Jehnichen, P. Simon, A. A. Fokin and M. Stamm, *Nano Lett.*, 2003, 3, 707.
17. S. Malik, T. Jana and A. K. Nandi, *Macromolecules*, 2001, 34, 275.



18. D. R. Kozub, K. Vakhshouri, L. M. Orme, C. Wang, A. Hexemer and E. D. Gomez, *Macromolecules*, 2011, 44, 5722.
19. J. Liu, S. Shao, H. Wang, K. Zhao, L. Xue, X. Gao, Z. Xie and Y. Han, *Org. Electron.*, 2010, 11, 775.
20. G. Renaud, R. Lazzari and F. Leroy, *Surf. Sci. Rep.*, 2009, 64, 255.
21. N. D. Treat, M. A. Brady, G. Smith, M. F. Toney, E. J. Kramer, C. J. Hawker and M.L. Chabinyc, *Adv. Energy Mater.*, 2011, 1, 82.
22. F. C. Chen, C. J. Ko, J. L. Wu and W. C. Chen, *Sol. Energy Mater. Sol. Cells*, 2010, 94, 2426.
23. D. H. Kim, Y. D. Park, Y. Jang, S. Kim and K. Cho, *Macromol. Rapid Commun.*, 2005, 26, 834.
24. M. -S. Su, C. -Y. Kuo, M. -C. Yuan, U. -S. Jeng, C. -J. Su and K. -H. Wei, *Adv. Mater.*, 2011, 23, 3315.
25. S. Jeong, S. H. Woo, H. K. Lyu and Y. S. Han, *Sol. Energy Mater. Sol. Cells*, 2011, 95, 1908.
26. A. DeSio, T. Madena, R. Huber, J. Parisi, S. Neyshtadt, F. Deschler, E. D. Como, S. Esposito and E. Hauff, *Sol. Energy Mater. Sol. Cells*, 2011, 95, 3536.
27. K. S. Chen, H. L. Yip, C. W. Schlenker, D. S. Ginger and A. K. Y. Jen, *Org. Electron.*, 2012, 13, 2870.
28. H. Lu, B. Akgun and T. P. Russell, *Adv. Energy Mater.*, 2011, 1, 870.
29. Z. Wu, T. Song, Y. Jin and B. Sun, *Appl. Phys. Lett.*, 2011, 99, 143306.
30. M. Baghgar, J. Labastide, F. Bokel, I. Dujovne, A. McKenna, A. M. Barnes, E. Pentzer, T. Emrick, R. Hayward and M. D. Barnes, *J. Phys. Chem. Lett.*, 2012, 3, 1674.
31. R. Koeppe and N. S. Sariciftci, *Photochem. Photobiol. Sci.*, 2006, 5, 1122.
32. S. R. Scully and M. D. McGehee, *J. Appl. Phys.*, 2006, 100, 034907.
33. A. L. Ayzner, C. J. Tassone, S. H. Tolbert and B. J. Schwartz, *J. Phys. Chem. C*, 2009, 113, 20050.
34. P. W. M. Blom, V. D. Mihailetschi, L. J. A. Koster and D. E. Markov, *Adv. Mater.*, 2007, 19, 1551.
35. M.Y. Chiu, U. S. Jeng, C. H. Su, K. S. Liang and K. H. Wei, *Adv. Mater.*, 2008, 20, 2573.

# *Chapter 6*

*Ternary Solvent Mixture*

*Approach to Control the*

*P3HT:PCBM Blend*

*Morphology in Inverted*

*Organic Solar Cells*

## TERNARY SOLVENT MIXTURE APPROACH TO CONTROL THE P3HT:PCBM BLEND MORPHOLOGY IN INVERTED ORGANIC SOLAR CELLS

---

- 6.1 Introduction**
  - 6.2 Experimental**
    - 6.2.1 *Materials*
    - 6.2.2 *Device fabrication*
  - 6.3 Characterization**
  - 6.4 Results and discussion**
    - 6.4.1 *UV-Visible measurements*
    - 6.4.2 *X-ray diffraction measurements*
    - 6.4.3 *Surface morphological study*
    - 6.4.4 *Photoluminescence emission*
    - 6.4.5 *Photovoltaic characteristics*
  - 6.5 Conclusion**
- References**
- 

### 6.1 Introduction

**B**inary solvent mixtures obtained by incorporation of small quantity of a single bad solvent in the host solvent (frequently used chlorobenzene or dichlorobenzene) have been most successfully utilized for the optimization of active layer morphology in bulk heterojunction blend of donor and acceptor molecules. This solvent mixture is essentially identified in terms of relevant solubility index and vapour pressure of the secondary solvent added [1]. An addition of small amount of 1, 8-octanedithiol (OT) solvent additive into the active layer casting solution (prepared of *o*-DCB) was ascertained to produce crystallization of P3HT accompanied by an increase of photocurrent density and fill factor of fabricated OSC device [2, 3].

The ternary solvent mixture concept applied for a long time in the field of lithium ion batteries, has now been extended to the OSCs [4]. Recently, this concept of ternary solvent mixture was applied to transform the morphology of the donor-acceptor (diketopyrrolopyrrole (DPP) polymer-fullerene) combination in the OSC device. The use of ternary solvent system consisting of dichlorobenzene-chloroform-diiodooctane (DCB-CF-DIO) could successfully increase the power conversion efficiency (PCE) of the device to 6.71% owing to the growth of long-range ordered structure with coarser interfaces between the domains [5]. Moreover, the ternary mixture was helpful in improving the performance of photovoltaic devices based on DPP-PCBM blend however, it can also be extended to other donor-acceptor pair such as P3HT:PCBM blend. In addition to the above system, more such ternary solvent mixtures can be considered to modify the morphology of donor-acceptor pairs.

In the present study, we focus on the morphological changes in the P3HT:PCBM blend using a ternary solvent mixture approach. Such a ternary solvent mixture modified blend layer was then applied as an active layer of inverted organic solar cell. The effect of morphological modification on the performance of inverted OSC was evaluated in detail.

## 6.2 Experimental

### 6.2.1 Materials

Poly(3-hexylthiophene) (P3HT), [6, 6]-phenyl-C<sub>61</sub>-butyric acid methyl ester (PCBM), zinc acetate dihydrate (C<sub>4</sub>H<sub>10</sub>O<sub>6</sub>Zn), 2-methoxyethanol (C<sub>3</sub>H<sub>8</sub>O<sub>2</sub>), ethanolamine (C<sub>2</sub>H<sub>7</sub>NO), *ortho*-dichlorobenzene (*o*-DCB), cyclohexanone and toluene were purchased from Sigma Aldrich (St Louis, MO, USA). Molybdenum oxide

(MoO<sub>3</sub>) and silver (Ag) wire were procured from Central Drug House (CDH). All materials were used as received during the studies.

### 6.2.2 Device Fabrication

Patterned indium tin oxide (ITO) coated glass substrates ( $< 20 \Omega \text{ sq}^{-1}$  resistance, Moserbaer India Ltd) were cleaned prior to deposition by successive ultrasonication in boiling soap solution, deionised water, acetone, and isopropanol solution, respectively followed by UV-ozone exposure of these nitrogen dried substrates for 26 min. Bulk heterojunction inverted polymer solar cells with ITO/ZnO/P3HT:PCBM/MoO<sub>3</sub>/Ag layer structure were assembled over the cleaned patterned ITO coated glass substrates. A 30 nm thin ZnO film was spin casted for 45s at 2000 rpm from a solution made using zinc acetate dihydrate, ethanolamine and 2-methoxyethanol. The substrate was then cured at 250°C for 10 min. Further, an active layer was spin coated using a 30 mg/mL blend solution of P3HT and PCBM (1:0.6 weight ratio) dissolved in a good solvent like *ortho*-dichlorobenzene (*o*-DCB) by means of continuous stirring overnight at 50°C. The substrates were thereafter dried at 85°C for 30 min in a nitrogen glove box. A 7 nm hole transport layer (HTL) of molybdenum oxide (MoO<sub>3</sub>) layer was thermally deposited in a vacuum chamber with a deposition rate of  $0.5 \text{ \AA s}^{-1}$ . Finally, a silver (Ag) layer of 150 nm thickness was also deposited in a vacuum chamber maintained at base pressure of  $5 \times 10^{-6}$  mbar with a deposition rate of  $1.0 \text{ \AA s}^{-1}$ .

The performance of the inverted photovoltaic devices of area  $0.09 \text{ cm}^2$  was studied under a solar simulator with AM 1.5G filter. Active layer spin coating solutions were prepared using a ternary solvent mixture consisting of a good solvent (*o*-DCB) and two marginal solvents like toluene and cyclohexanone. This spin coated

active layer was compared with a P3HT:PCBM film prepared by a single good solvent. Cyclohexanone and toluene cosolvents have been selected in the present work because of their solubility index which favours more solubility of PCBM than P3HT. The total amount of cosolvent to be added to the active layer spin coating solution was optimized and found to be 5 vol %. For all such modifications, 2.5 vol % of each of these cosolvents was added and the solution was stirred for 2 h prior to spin coating.

### **6.3 Characterization**

The current density ( $J$ )–voltage ( $V$ ) characteristics were measured with a Keithley (Model 2420) source measurement unit. A solar simulator (Model SS150AAA) from Photo Emission Technology Inc. with an illumination of  $100 \text{ mW cm}^{-2}$  and AM 1.5 G filter reproduced the solar spectrum. Device preparation was carried out in a glove box from Jacomex with  $\Delta P = 3.0 \text{ mbar}$  and an oxygen level of 0.3 ppm. The absorption spectra of the P3HT:PCBM films were recorded using a Perkin Elmer 35 lambda UV–Visible spectrophotometer. Surface morphology studies were carried out using VEECO DI-3100 Nanoscope (III) atomic force microscope (AFM) in tapping mode. Grazing incidence X-ray diffraction (GIXRD) measurements were done at a grazing incidence angle of  $0.3^\circ$  (Cu- $K_\alpha$  radiation,  $\lambda = 1.54 \text{ \AA}$ ) using a Rigaku Ultima IV X-ray diffractometer. Photoluminescence measurements were carried out on a Luminescence Spectrofluorometer from Edinburgh Instruments, UK, Model: F900.

## 6.4 Results and Discussion

### 6.4.1 UV-Visible Measurements

It is known to us that the incorporation of small amount of non-solvent to the well dissolved solution of P3HT:PCBM blend stimulates the aggregation in P3HT phases which supports an increase in the absorption of photoradiation. The molecular ordering in P3HT by and large happens from the interchain  $\pi$ - $\pi$  interaction among the polymer chains reducing its unfavourable association with the added non-solvent. Such an interchain interaction is linked to a decrease in energy of the system with effective increase in the conjugation length of P3HT chain fragments. The amount of additional solvent added to initiate the growth of such ordered aggregates differs from solvent to solvent as a function of its solubility index. As the solubility of P3HT chains in the added non-solvent decreases, there is an increase in the viscosity of the solution caused by an increase of non-dissolved P3HT segments and also speeds up aggregation kinetics [6]. So, a choice of the quantity and quality of non-solvent is very important for the efficient performance of OSCs. In this study, we have chosen two non-solvents, viz, cyclohexanone and toluene. Further, 2.5 vol % of each of the non-solvent is added to the well dissolved blend solution of P3HT and PCBM in *o*-DCB. Fig. 6.1 shows the UV-Visible absorption spectra of P3HT:PCBM blend films casted using a single good solvent and ternary solvent mixture. The absorption spectra of both these films show the main absorption band at 512 nm along with two absorption shoulders in the low energy region (i.e., at 550 and 610 nm). These characteristic bands correspond to well ordered and structured chains of P3HT polymer. The main absorption peak at 512 nm is related to the crystallization process in P3HT polymer, i.e., an intra-chain transition of its random coiled conformation in

its well dissolved form to a less entangled rod like conformation. The other two absorption shoulders arise from the increased conjugation length in P3HT as a result of coiled to rod transformation and interchain  $\pi$ - $\pi$  stacking interaction among the extended P3HT chains, respectively [7].

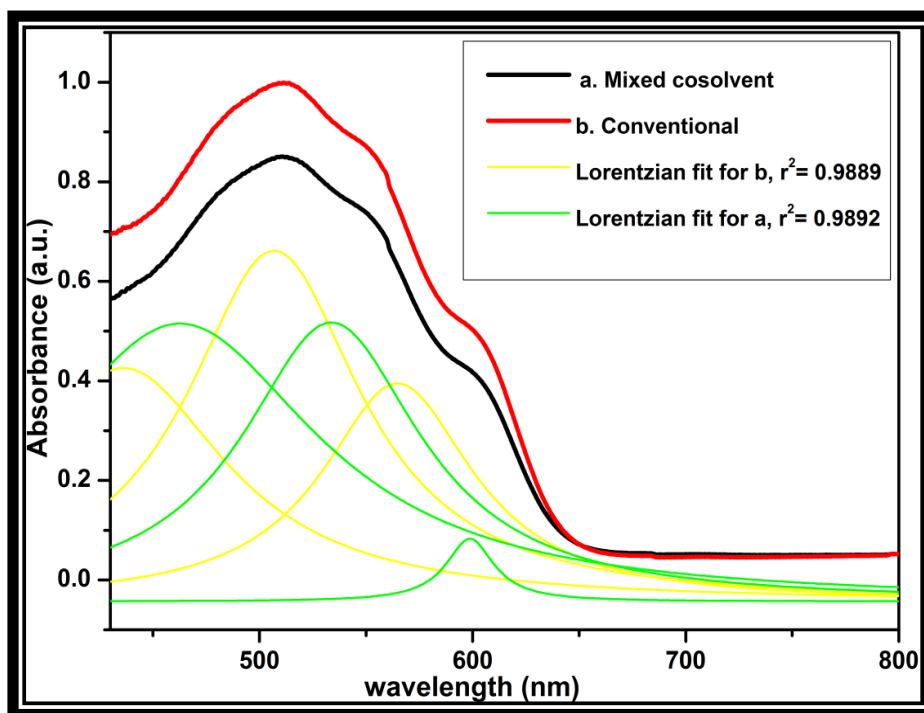


**Figure 6.1: UV-Visible absorption spectra of P3HT:PCBM blend films**

It is seen from the spectra that the increased intensities of the absorption peaks in the conventional P3HT:PCBM (using single good solvent *o*-DCB) film correspond to greater number of more ordered aggregates as compared to more disordered P3HT domains in the mixed cosolvent casted film. This may possibly be attributed to the presence of two non-solvents which must have complicated the crystallization process in mixed cosolvent film. The *o*-DCB solvent (P3HT ( $S_{P3HT}$ ) and PCBM ( $S_{PCBM}$ ) solubility of 14.7 and 42.1 mg/mL, respectively) dissolves both the components of mixture whereas, the added cosolvents (toluene and cyclohexanone) offer greater solubility to one of the component (PCBM) of blended mixture. An evaluation of



these two cosolvents suggests lesser solubility of P3HT chains in cyclohexanone cosolvent (P3HT ( $S_{P3HT}$ ) and PCBM ( $S_{PCBM}$ ) solubility of 0.2 and 23.6 mg/mL) as compared to the toluene solvent (P3HT ( $S_{P3HT}$ ) and PCBM ( $S_{PCBM}$ ) solubility of 0.7 and 15.6 mg/mL). Accordingly, a variety of solvophobic-solvophilic interactions arise between the P3HT chains and non-solvents. A competition continues among the non-solvents for P3HTs interface which results in insufficiently crystallized P3HT domains. This insufficient crystallization of polymer domains has led to less efficient photon absorption and poor device performance ultimately.

#### 6.4.2 X-ray Diffraction Measurements

The GIXRD measurements were carried out to study the molecular orientation and crystallinity modifications in P3HT:PCBM blend films with ternary solvent mixture modification.

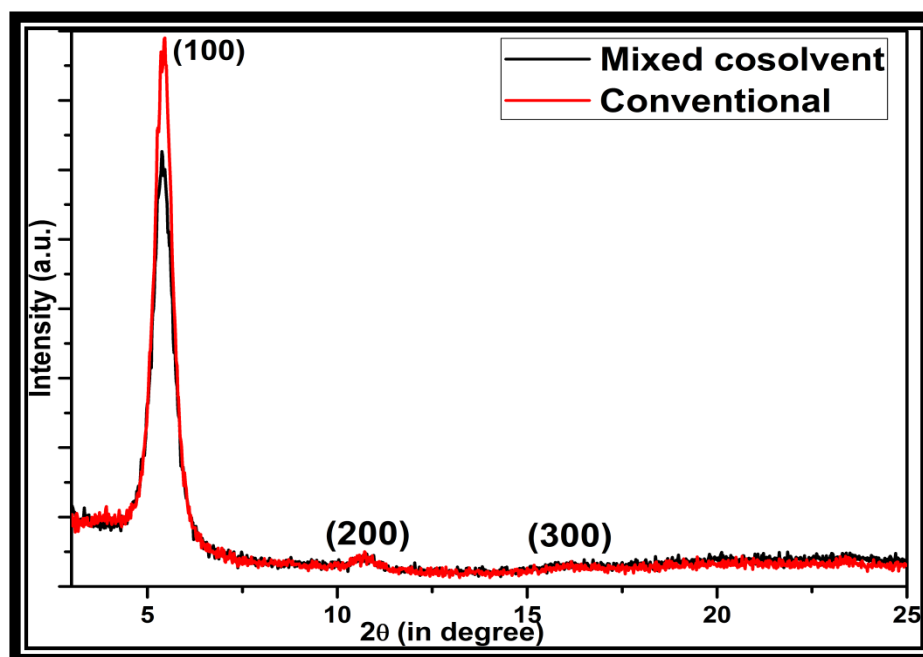


**Figure 6.2: GIXRD intensities of P3HT:PCBM films**

Fig. 6.2 shows a comparison between the out of plane grazing incidence diffraction patterns of P3HT:PCBM blend films casted of a single good solvent and

ternary solvent mixture. The higher reflection intensities were achieved from the bulk of the blend films by using grazing incidence angle at  $0.3^\circ$ . Both the P3HT:PCBM blend films show characteristic reflection peaks at  $5.3^\circ$  (100) and analogous higher order weak peaks at  $10.6^\circ$  (200) and  $16.1^\circ$  (300). These (h00) peaks are distinctive of lamella stacking of P3HT chains in an edge on orientation with their polymer backbone oriented parallel to the substrate and side chains perpendicular to the substrate. A decrease in diffraction intensity of the (100) peak in mixed cosolvent casted P3HT:PCBM film attributes the disoriented crystals along the (100) plane normal to the substrate. However, the increased intensity of the (100) reflection peak from the conventional film reveals the larger fraction of (h00) oriented crystallites normal to the substrate [8]. The presence of two competing cosolvents (cyclohexanone and toluene) having different interaction with P3HT are responsible for the formation of disoriented crystals in mixed cosolvent solution.

**Table 6.1: Interlayer distances (d) and P3HT crystallite sizes using different solvent mixtures**

S.No.	Device	Grazing incidence angle (in degree)	$2\theta$ value (in degree)	Interlayer distance $d_{100}(\text{\AA})$	FWHM	Grain size (nm)
1.	Mixed Cosolvent	$0.3^\circ$	5.3	16.43	0.655	12.0
2.	Conventional	$0.3^\circ$	5.4	16.37	0.585	13.4

Table 6.1 presents the interlayer distances and crystallite sizes of P3HT domains which were calculated for (100) diffraction peak in the GIXRD patterns of two blend films. The crystallite size was found to be 12.0 and 13.4 nm in the mixed cosolvent casted P3HT:PCBM film and conventional film, respectively. A better

crystallization in the unmodified film as compared to ternary solvent modified film is related with an extensive development of P3HT crystals along the (100) molecular axis.

#### **6.4.3 Surface Morphological Study**

Surface morphology of an active layer of OSC was evaluated using AFM. Fig. 6.3 shows the AFM topographic images and three dimensional (3D) images of P3HT:PCBM films casted without any cosolvent and with mixture of two cosolvents. The dark regions in the images are attributed to the PCBM clusters while brighter phases signify P3HT aggregates.

The casting solvent was found to have a profound effect on the morphology of film and hence, on the performance of the device. AFM topographic images reveal well-mixed and uniform phases in the conventional film owing to co-precipitation of both the components of mixture at the same point of time during the spin coating resulting in a smoother film. In the mixed cosolvent casted film, PCBM remains soluble and P3HT gets the choice of movement to form aggregates in the solution causing final demixing and phase separation in the casted film, resulting in a relatively rougher surface [9]. This aggregate formation in the modified film may not be regular and randomly structured due to the presence of two opposite non-solvents with different solubility.

The root mean square (rms) roughness values determined from the AFM 3D surface image analysis are 2.1 and 4.5 nm for conventional P3HT:PCBM film and mixed cosolvent casted P3HT:PCBM film, respectively. Such high surface roughness of the mixed cosolvent casted film signifies irregular and disordered arrangement of P3HT phases in mixed cosolvent film. A non-homogenous active layer can result in

short circuit or exciton recombination in OSC devices. Thus, a detailed examination of proper solvent combination is required for successful utilization of this concept of ternary solvent mixture in active layer preparation of inverted OSC devices.

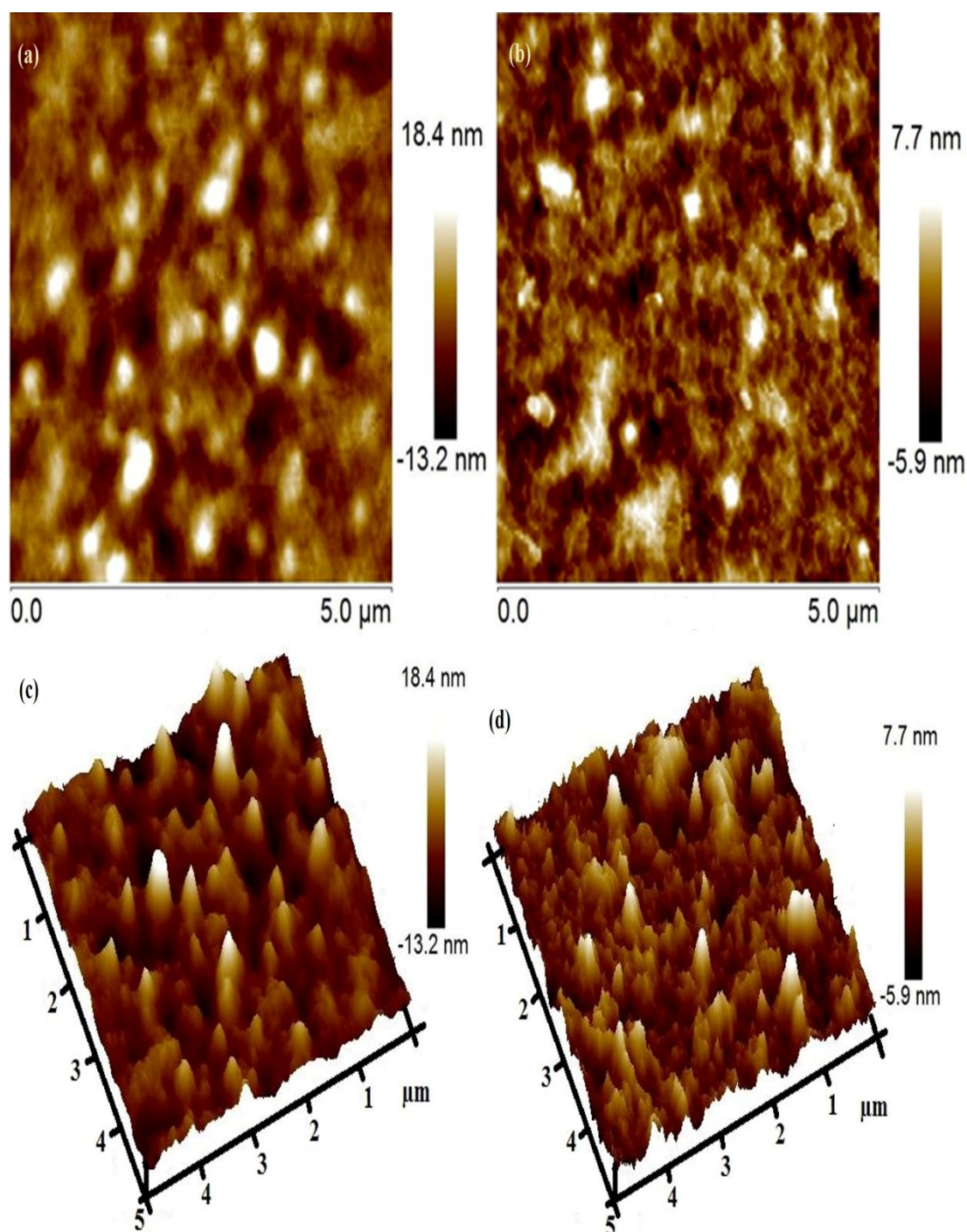


**Figure 6.3:** AFM topographic images of P3HT:PCBM films in tapping mode (a) ternary solvent mixture (b) single good solvent and (c) & (d) 3D images of these films, respectively

#### 6.4.4 Photoluminescence Emission

The optical excitation in molecular material without charge separation exhibits continuous emission of light for relaxation from excited to ground state which is recognized as the process of photoluminescence (PL). So, photoluminescence emission measurement in the P3HT:PCBM blend can provide an information on the size of P3HT domains or the distance of successive donor-acceptor interfaces from the point of photogenerated excitons. These excitons dissociation in organic semiconductors are limited by their small diffusion length of the order of 8-10 nm. The effect of solvent on the nanomorphology and phase separation of donor-acceptor domains in the P3HT:PCBM film was studied by means of PL measurement. Fig. 6.4 demonstrates the photoluminescence (PL) emission spectra of P3HT:PCBM blend films casted from solutions modified by mixed cosolvent addition and without any cosolvent modification. PL spectra were taken by exciting the blend film at the wavelength of maximum absorption (i.e., at 512 nm). PL emission is supposed to be quenched by effective charge transfer between the donor and acceptor molecules when they are in close contact [10].

A strong PL emission (incomplete quenching) from conventional P3HT:PCBM film suggests an insufficient or small interface area between the donor-acceptor phases for exciton dissociation. The co-precipitation of P3HT and PCBM results in a mixed structure without enough phase separation in the conventional film. This smaller interface region between the two components of the mixture might have resulted in exciton recombination even before their separation and hence more radiative emission is seen. However, a slightly red shifted spectrum with more distinguishable vibrational shoulders and decreased (quenched) PL emission in mixed

cosolvent casted film signifies more efficient charge separation between phase separated domains of PCBM clusters and P3HT aggregates. The weakly coupled H-aggregate model framework was found to be in agreement with the PL emission in P3HT films owing to coupled intermolecular interactions among the H-type aggregates. The PL spectrum of P3HT:PCBM films shows characteristic peaks of zero-phonon transitions (0-0) and vibrational replicas (0-1, 0-2). This zero phonon transition is characteristic of interchain exciton coupling of H-aggregates [11].

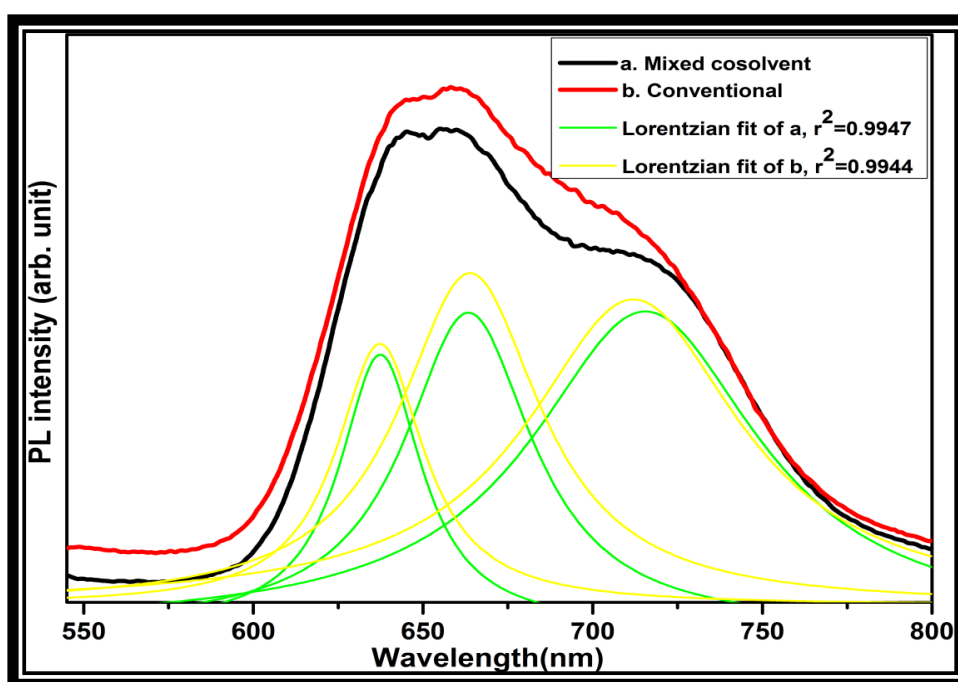


**Figure 6.4:** PL emission spectra of P3HT:PCBM films

Here, we compare the emission spectra of conventional P3HT:PCBM and ternary solvent mixture modified films. The PL ratio (PL 0-0/0-1) was found to be 1.0 in mixed cosolvent casted films as compared to 0.98 in conventional P3HT:PCBM films. This increase in PL ratio (and also the relaxation in symmetry forbidden zero phonon transition) can be accounted by an increase in the energetic disorder in mixed film. An increase in the relative intensity of zero-phonon transition cannot be related

to the intrachain excitons coupling in case of J-type aggregates as the intensity of side band (0-2) with respect to (0-1) (i.e., of the order of 0.73) also increases in mixed cosolvent casted film as compared to a value of 0.70 in conventional film. So, the formation of H-type aggregate with disorder induced relaxation in (0-0) transition is accounted in mixed cosolvent casted film [12]. An aggregate exciton bandwidth 'W' being inversely proportional to PL 0-0/0-1 ratio is also reduced in an individually mixed film resulting in efficient charge transfer to PCBM. So, PL quenching in mixed cosolvent casted film may be attributed to non-radiative (thermal loss) transition of excitons in the film.

#### 6.4.5 Photovoltaic Characteristics

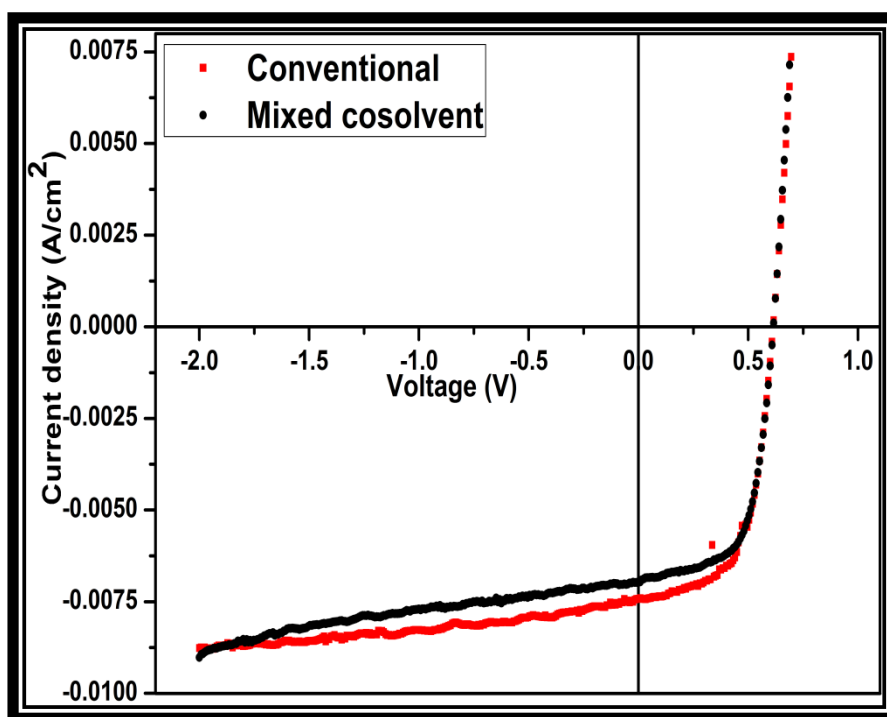


**Figure 6.5: Current density ( $J$ )-Voltage ( $V$ ) plot of P3HT:PCBM solar cells**

Fig. 6.5 shows the current density ( $J$ )-voltage ( $V$ ) curves for inverted P3HT:PCBM bulk heterojunction solar cells with photoactive layer spin coated from blend solutions modified by mixed cosolvent addition and without any cosolvent



modification. The photovoltaic parameters of the OSC devices have been presented in Table 6.2. The photovoltaic device with an active layer casted of the ternary solvent mixture (*o*-DCB-cyclohexanone-toluene) exhibited relatively poor device performances (power conversion efficiency (PCE) of 2.64±0.07) with short circuit current density ( $J_{sc}$ ) of 6.96E-03 A cm<sup>-2</sup>, open circuit voltage ( $V_{oc}$ ) of 0.61 V and fill factor (FF) of 0.63 when compared to a similar device without any cosolvent modification. A relatively better performance was found in unmodified or conventional devices (PCE of 2.74±0.05%) which can be attributed to the improved value of  $J_{sc}$  (7.41E-03 A cm<sup>-2</sup>). This indicates that the PCE of a typical inverted solar cell based on P3HT:PCBM blend is mostly dominated by  $J_{sc}$  factor. Further, a small increase in FF for ternary solvent mixture casted device was not enough to overcome the increased  $J_{sc}$  in the conventional device [13].

**Table 6.2: Photovoltaic parameters of inverted organic solar cell based on P3HT:PCBM active layer**

Substrate	Device	$V_{oc}$ (V)	$J_{sc}$ (Acm <sup>-2</sup> )	FF	%E	$R_{sh}$ ( $\Omega$ cm <sup>2</sup> )	$R_s$ ( $\Omega$ cm <sup>2</sup> )
1.	Mixed cosolvent	0.61	6.96E-03	0.63	2.68	454	13
2.	Conventional	0.61	7.41E-03	0.61	2.77	1123	14

It is well known that the factors contributing to the  $J_{sc}$  are light absorption, exciton dissociation and transport of separated charges to the respective electrodes. Disordered and unsuitably oriented P3HT domains formed in case of mixed cosolvent casted device owing to a competition among the cosolvents for P3HTs interface must have resulted in a decrease in light absorption and poor charge transport. These two



unfavourable factors have contributed to the decrease in  $J_{sc}$  and hence a decrease in efficiency of OSC device.

The solvent mixture method is known to yield extensively crystallized and oriented P3HT domains in the blend film as compared to a single good solvent [14]. However, in the present case of the ternary solvent mixture, the process of crystallization was complicated and disordered crystal formation was noticed. So, a more comprehensive study on the choice of cosolvents, its amount and other processing parameters are required for proper control over the crystallization kinetics and final morphology of the blend layer.

### 6.5 Conclusion

A mixture of three different functional solvents like *o*-DCB, toluene and cyclohexanone was utilized for an active layer preparation of inverted OSC based on bulk heterojunction blend of P3HT:PCBM. The PCE of the ternary solvent mixture modified photovoltaic device was found to be  $2.64\pm 0.07\%$  as compared to a PCE value of  $2.74\pm 0.05\%$  observed in case of unmodified device. This drop in performance of the ternary solvent modified device can be attributed to the decreased  $J_{sc}$  which may be because of the reduced light absorption and hindered charge transport through the disordered domains of P3HT. AFM images depict a rougher surface of the ternary solvent modified active layer and this rough surface can be one of the reasons for decrease in shunt resistance or leakage pathway in OSC device. PL measurement reveals quenching of the PL emission owing to the non-radiative transition (thermal loss) of energetically disordered excitons in mixed cosolvent modified film.

**References**

1. K. Kawano, J. Sakai, M. Yahir and C. Adachi, *Sol. Energy Mater. Sol. Cells*, 2009, 93, 514.
2. H. -Y. Chen, H. Yang, G. Yang, S. Sista, R. Zadoyan, G. Li and Y. Yang, *J. Phys. Chem. C*, 2009, 113, 7946.
3. Y. Yao, J. Hou, Z. Xu, G. Li and Y. Yang, *Adv. Funct. Mater.*, 2008, 18, 1783.
4. D. Peramunage, D. M. Pasquariello and K. M. Abraham, *J. Electrochem. Soc.*, 1995, 142, 1789.
5. L. Ye, S. Zhang, W. Ma, B. Fan, X. Guo, Y. Huang, H. Ade and J. Hou, *Adv. Mater.*, 2012, 24, 6335.
6. Y. D. Park, H. S. Lee, Y. J. Choi, D. Kwak, J. H. Cho, S. Lee and K. Cho, *Adv. Funct. Mater.*, 2009, 19, 1200.
7. J. S. Kim, J. H. Lee, J. H. Park, C. Shim, M. Sim and K. Cho, *Adv. Funct. Mater.*, 2011, 21, 480.
8. S. -J. Kang, Y. -S. Kim, W. B. Kim, D. -Y. Kim and Y. -Y. Noh, *ACS Appl. Mater. Interfaces*, 2013, 5, 9043.
9. M. N. Yusli, T. W. Yun and K. Sulaiman, *Mater. Lett.*, 2009, 63, 2691.
10. R. Koeppe and N. S. Sariciftci, *Photochem. Photobiol. Sci.*, 2006, 5, 1122.
11. X. M. Jiang, R. Osterbacka, O. Korovyanko, C. P. An, B. Horovitz, R. A. J. Janssen and Z. V. Vardeny, *Adv. Funct. Mater.*, 2002, 12, 587.
12. N. Banerji, S. Cowan, E. Vauthey and A. J. Heeger, *J. Phys. Chem. C*, 2011, 115, 9726.
13. P. W. M. Blom, V. D. Mihailetschi, L. J. A. Koster and D. E. Markov, *Adv. Mater.*, 2007, 19, 1551.
14. J. -H. Kim, J. H. Park, J. H. Lee, J. S. Kim, M. Sim, C. Shim and K. Cho, *J. Mater. Chem.*, 2010, 20, 7398.



# *Chapter 7*

*Conclusion & Future Scope*

**7.1 Conclusion****7.2 Future scope**

---

**7.1 Conclusion**

An inverted organic solar cell with a layer sequence comprising glass/ITO/ZnO/P3HT:PCBM/MoO<sub>3</sub>/Ag was successfully prepared. An active layer of inverted OSC device was prepared using four different solvent combinations. Study of these solvent mixtures revealed a better role of ortho-dichlorobenzene-cyclohexanone solvent mixture to produce optimal polymer crystallization and phase separation for efficient performance of inverted solar cell.

The concept of solvent induced crystallization of donor polymer, i.e., P3HT was then effectively extended to an active blend of inverted OSCs. An improvement in its efficiency from  $2.74\pm 0.05\%$  in unmodified device to  $3.01\pm 0.05\%$  in cyclohexanone cosolvent modified device was achieved with an optimized concentration of cyclohexanone cosolvent with ageing period of 2 h. This improvement is related to an increase in current density and fill factor of the device. An increase in P3HT crystallinity is observed with cyclohexanone addition which leads to an efficient photoabsorption. The commensurate vertical concentration gradient in P3HT fractions of the blend is possibly responsible for efficient hole transport and betterment of the photovoltaic parameters in the inverted OSC device.

The P3HT:PCBM composite films prepared using simple marginal solvent such as cyclohexanone addition in poly(3-hexylthiophene):[6,6]-phenyl C<sub>61</sub>-butyric acid methyl ester (P3HT:PCBM) solution were not found to be effectively crystallized. So, two steps individually mixed method was adopted with cyclohexanone addition to P3HT solution in first step and subsequently mixing of PCBM solution in second. This modified method presents an improvement in the efficiency to  $3.39\pm 0.05\%$  which is attributable to improved crystallization of P3HT donor. This improved crystallization of modified film is found because of negligible interruption caused by PCBM domains during the crystallization of P3HT.

Further, an introduction of newer concept of ternary solvent mixture for active layer preparation led to a decrease in efficiency to  $2.64\pm 0.07\%$  in the inverted OSC device when it was compared with a device fabricated without any cosolvent modification. However, a comprehensive study of ternary solvent mixture method is further needed to explore the possibility of improvement in efficiency of inverted photovoltaic device which can replace the existing silicon technology in the energy harvesting sector by considering various parameters such as the choice of cosolvents, its amount and processing etc.

## **7.2 Future Scope**

One may possibly carry forward this work in future to realize better efficiency in inverted organic solar cells by extending the concept of ternary solvent mixture approach to other donor-acceptor including low band gap materials. Additionally, more of such ternary solvent mixtures can be explored to modify the morphology of donor-acceptor pairs. Although a lot of work has already been carried out in this area however, researchers have not reached to optimum blend morphology for commercialization of organic solar cells which still remains a challenge. So, we anticipate a better prospect for organic solar cells market in the near future especially in a developing country like ours (India) with optimized morphology of the photoactive blend for maximum possible harvesting of solar radiation.



**Sarita S Nair**

**S**arita S Nair received her Masters of Science degree in chemistry (Inorganic) from Hansraj college, University of Delhi (India) in 2008 and Bachelors of Science degree in chemistry from Gargi college, University of Delhi (India) in 2006. She worked for two years in Indian Oil Corporation Ltd. R&D Centre, Faridabad as Project Associate. She is currently pursuing her doctoral research work on “Development and Efficiency Studies of Organic Solar Cells” with Prof. D. Kumar in the Department of Applied Chemistry and Polymer Technology at Delhi Technological University, Delhi.

Her area of interests includes conducting polymers, its composites and more importantly its application in the area of organic solar cells. She has to her credit four publications in international journals of repute. She has presented her work in more than ten National and International conferences.

### **Papers Published in SCI Journals of Repute**

(1) A manuscript titled “A Study on the Effect of Co-solvent Addition Pathway on the Optical and Morphological Properties of P3HT: PCBM Composite Films” by **Sarita S Nair**, D Kumar, Amitava Majumdar, has been published in the journal “Advances in Polymer Technology”. DOI 10.1002/adv.21445

(2) A manuscript titled “Study of the Processing Pathway for Co-Solvent Addition in Active Layer Preparation of Inverted Organic Solar Cell” by **Sarita S Nair**, D Kumar, Abhishek Sharma, Amitava Majumdar, has been published in “Polymer Engineering and Science” journal. DOI 10.1002/pen.24014

(3) A manuscript titled “Effect of Co-solvents on the Photovoltaic Performance of an Inverted Organic Solar Cell” by **Sarita S Nair**, D Kumar, Amitava Majumdar is accepted for publication in “Polymer Engineering and Science” journal.

### **Papers Communicated in International Journals of Repute**

(1) A manuscript titled “Morphology Control in the Bulk Heterojunction Blend of Inverted Organic Solar Cell via Co-solvent Addition” by **Sarita S Nair**, D Kumar, Amitava Majumdar is under review in “E-Polymers” journal.

(2) A manuscript titled “Ternary Solvent Mixture Approach to Control the Active Layer Blend Morphology in Inverted Organic Solar Cells” by **Sarita S Nair**, D Kumar, Amitava Majumdar is under review in “International Journal of Polymeric Materials & Biomaterials”

### **Papers Not Included in the Thesis Work**

(1) A manuscript titled “Electrochemical Studies of DNA Doped Polypyrrole Films” by **Sarita S Nair**, D Kumar has been published in “Advanced Science Letters” journal. Adv. Sci. Lett. 20, 1274-1280 (2014)



(2) A manuscript titled “Investigations on Functioning of Conducting Fabrics for Application in Wearable Clothes” by Sudha, **Sarita S Nair**, Devendra Kumar has been published in *International Journal of Research in Advent Technology*, Vol.2, No.5, May 2014, E-ISSN: 2321-9637

### **Papers Presented in National/International Conferences**

1. Presented a paper titled “Virtual study of pani-graphite oxide and pani-graphene composite as an electrode material for energy applications” **Sarita S Nair**, Priyanka, D. Kumar in *International conference on Advancements in Polymeric materials- innovation in materials and product development*, March 01-03,2013 at CIPET Lucknow, India.

2. Presented a paper titled “Influence of PANI morphology towards the performance of PANI-graphite oxide composite as an electrode material” **Sarita S Nair**, D. Kumar in the *National Symposium on Emerging Areas in Polymer/Fiber/Textile Research (Young Researcher’s Symposium-2013)*, March 07-09, 2013 at IIT Delhi, India.

3. Presented a poster titled “Morphology control in BHJ blend of inverted organic solar cell via co-solvent addition” **Sarita S Nair**, D. Kumar, Abhishek Sharma, Nikhil Aggarwal in *3rd FAPS Polymer Congress and Macro-2013 International conference*, May 15-18, 2013 at Indian Institute of Science Bangalore.

4. Poster titled “Reviving the processing pathway for co-solvent addition in BHJ blend of inverted organic solar cell” **Sarita S Nair**, D Kumar has been accepted in the *4th International Symposium on Organic and Inorganic Electronic Materials and Related Nanotechnologies (EM-NANO 2013)*, 17-20, June, 2013 at Kanazawa, Japan.

5. Presented a paper titled “Inverted polymeric solar cells based on P3HT: PCBM: A comparative study of different co-solvents” **Sarita S Nair**, D. Kumar in *International conference on Advanced Polymeric materials- ICAPM2013*, October 11-13,2013 at Mahatma Gandhi University, Kerala (India).

6. Presented a poster titled “pH responsive drug release from Dependal-M loaded polyacrylamide hydrogels” **Sarita S Nair**, Raman Dwivedi, D Kumar\* in *ijwbme2013 Indo-japan workshop on Biomolecular Electronics*, Dec 11-13, 2013 at Delhi Technological University, Delhi.

7. Poster titled “ Synthesis and characterization of polypyrrole-zno nanocomposite” **Sarita S Nair**, **Raman Dwivedi**, D Kumar was presented in *ijwbme2013 Indo-japan workshop on Biomolecular Electronics*, Dec 11-13, 2013 at Delhi Technological University, Delhi.

8. Presented a poster titled “Inverted polymeric solar cells based on P3HT: PCBM: a study of processing pathway for co-solvent addition” **Sarita S Nair**, D. Kumar in *International conference on Polymers-Visions & Innovations- APA2014*, February 19-21,2014 at India Habitat Centre, New Delhi (India).

9. Poster titled “Electrochemical aspects of polypyrrole-graphene based composite ” **Sarita S Nair**, **Raman Dwivedi**, D Kumar was presented in *International conference on Polymers-Visions & Innovations- APA2014*, February 19-21,2014 at India Habitat Centre, New Delhi (India).

10. Presented a paper titled “Electrochemical studies of DNA doped polypyrrole films” **Sarita S Nair**, D. Kumar in *National conference on Nanotechnology and Renewable Energy- NCNRE2014*, April 28-29,2014 at Jamia Millia Islamia, New Delhi (India).

11. Presented a poster titled “Morphology control in the active layer of inverted organic solar cell via co-solvent addition” **Sarita S Nair**, D. Kumar, Amitava Majumdar in *National conference on Nanotechnology and Renewable Energy-NCNRE2014*, April 28-29,2014 at Jamia Millia Islamia, New Delhi (India).